Advanced Control Algorithms For Satellite Attitude Maneuver

A project report submitted

in partial fulfillment for the award of the degree of

Bachelor of Technology

in

Electronics & Communication Engineering (Avionics)

by

Debajyoti Chakrabarti

Department of Avionics

Indian Institute of Space Science and Technology

Thiruvananthapuram, India

May, 2019

Certificate

This is to certify that the project report titled ***Advanced Control Algorithms For Satellite Attitude Maneuver*** submitted by **Debajyoti Chakrabarti**, to the Indian Institute of Space Science and Technology, Thiruvananthapuram, in partial fulfillment for the award of the degree of **Bachelor of Technology** in **Electronics & Communication Engineering (Avionics)**, is a bonafide record of the research work carried out by him/her under my supervision. The contents of this report, in full or in parts, have not been submitted to any other Institute or University for the award of any degree or diploma.

Dr. N. Selvaganesan
Associate Professor
Department of Avionics
IIST

Dr. Manoj B. S.
Head of the Department
Department of Avionics
IIST

Place: Thiruvananthapuram
Date: May, 2019

Declaration

I declare that this project report titled ***Advanced Control Algorithms For Satellite Attitude Maneuver*** submitted in partial fulfillment for the award of the degree of **Bachelor of Technology** in **Electronics & Communication Engineering (Avionics)** is a record of original work carried out by me under the supervision of **Dr. N. Selvaganesan**, and has not formed the basis for the award of any degree, diploma, associateship, fellowship, or other titles in this or any other Institution or University of higher learning. In keeping with the ethical practice in reporting scientific information, due acknowledgments have been made wherever the findings of others have been cited.

Place: Thiruvananthapuram
Date: May, 2019

Debajyoti Chakrabarti
(SC15B084)

This project report is dedicated to my parents, grandparents (thamma, dadu, dida), my brother Partha Sarkar and my sisters Anushka Chakraborty, Swarnali Chatterjee

Acknowledgements

First I would like to thank Almighty God for giving me blessings towards the completion of this project work.

I would never be able to complete this project work without help and support from these kind people around me. To begin with, I would like to express my deepest gratitude to my guide **Dr. N. Selvaganesan**, Associate Professor, Department of Avionics, IIST, for his constant support and guidance throughout this project work. His technical and editorial advice has been extremely important for the completion of the project.

I would like to take this opportunity to express my special thanks to **Shri. M. V. Dekhane**, Satish Dhawan Professor, IIST, for sharing his technical experience in the form of valuable advice whenever I have approached him for clearing doubts regarding my project. His precious suggestions during midterm evaluation has provided proper direction in my project and finally complete the project successfully. I also convey my sincere gratitude to my professors **Dr. Harsha Simha M. S.**, Assistant Professor, IIST and **Dr. H. Priyadarsanam**, Associate Professor, IIST, for their cordial support, valuable information and guidance in my project.

I would also like to give special thanks to **Mr. P. Satish Kumar**, Ph.D Research Scholar, IIST. Without thanking him, my acknowledgement would have remained incomplete. He is the person who has always remained behind me in spite of his busy work schedule, from explaining basic theories to solving coding error. I also express my special gratitude to **Rejitha Raveendran**, M.Tech alumni (2017), IIST. Her M.Tech thesis work on 'Satellite Attitude Control' has been the main source of motivation and guidance of this project.

I convey my special vote of thanks to the **High Performance Computing Facility (HPC)** group at IIST for their help and support. I would also like to acknowledge my institute especially **Department of Avionics**, for providing me such an excellent research environment to complete the project. Last but no means least, I thank my parents, my friends for their good wishes and unequivocal support throughout this project.

Debajyoti Chakrabarti

Abstract

'Attitude Determination and Control System' of a satellite, can be regarded as one of the major subsystems of satellite design, as satellite needs to be oriented properly depending on various purposes like: solar panel operation or pointing antenna towards Earth and many other applications. Attitude of an object means orientation of body frame of reference with respect to external reference frame. Among the various methods of attitude representation, in this work quaternion based representation method is chosen due to its simplicity. The dynamics and kinematics of satellite is formulated as a non linear model and reaction wheel assembly is chosen as actuator which provides the necessary torque to control the satellite attitude. The main objective of this work is to control and stabilize the satellite at desired attitude and angular velocity by attitude correction maneuver as per the requirement. To achieve the objective, various linear and non linear form of integer and fractional order control laws are proposed in this work. In case of linear control laws, PD controller and PD^{β} controller are tuned for the linearized satellite model to meet the desired specifications. On the other hand, non linear control laws are proposed to achieve better disturbance rejection and robustness towards system parameter uncertainty. The proposed non linear control laws in this work are: PD Sliding Mode Control, PD Sliding Mode Control with Modified Reaching Law, PD^{β} Sliding Mode Control and PD^{β} Sliding Mode Control with Modified Reaching Law. All the controller parameters are tuned using optimization technique and numerical simulations are carried out for the defined satellite model with these controllers. Further, disturbance rejection and robustness towards parameter uncertainty analysis are carried out for the satellite attitude control system with all controllers.

Contents

List of Figures

List of Tables

Abbreviations

ADCS	Attitude Determination and Control System
CMG	Control Moment Gyro
ECI	Earth Centred Inertial
ECEF	Earth Centred Earth Fixed
DCM	Direction Cosine Matrix
FC	Fractional Calculus
FOC	Fractional Order Controller
IAE	Integral Absolute Error
ITAE	Integral Time Absolute Error
ISE	Integral Square Error
PD	Proportional-Derivative
PI	Proportional-Integral
SMC	Sliding Mode Control
LTI	Linear Time Invariant

Nomenclature

$\mathbb{R}$	Set of real numbers
$\mathbb{R}_+$	Set of positive real numbers
$\mathbb{R}^n$	n-dimensional space of real numbers
ϕ	Roll angle
θ	Pitch angle
ψ	Yaw Angle
q	Quaternions
ω	Angular velocity of satellite
J	Moment of Inertia tensor of satellite
h_w	Angular momentum of reaction Wheel assembly
ω_w	Angular velocity of reaction wheel
τ_w	Time constant of reaction wheel
T_w	Torque provided by flywheel assembly
T_c	Control torque provided to satellite
T_d	Disturbance torque
$G_i(s)$	Transfer function of linearized satellite model along ith axis
$G_{op}(S)$	Open loop trasnfer function
Arg	Argument of transfer function
ω_{gc}	Gain crossover frequency
ϕ_m	Phase margin
$D^\beta\{.\}$	Fractional derivative operator of order β
Sat	Saturation function
u_{eq}	Equivalent control law
$u_{discont}$	Discontinuous control law
S	Sliding surface
t_{reach}	Reaching time towards sliding surface
α	Power coefficient of power rate type reaching law

Chapter 1

Introduction

1.1 Scope of Project

Attitude of a satellite is the orientation of satellite with respect to external frame of reference. Attitude of satellite must be stabilized and controlled for several purposes. For example, solar panels needs to be pointing towards Sun, or antenna of communication satellite should point towards ground station. For all these purpose, each satellite has 'Attitude determination & control' (ADCS) subsystem, which has two jobs to perform:(i) To determine attitude of a satellite moving in a orbit, (ii) Control the orientation of satellite according to the mission requirement.

Now a satellite in orbit, is subjected to various disturbance torques. For low Earth orbit (LEO), aerodynamic torque, torque due to gravity (gravity gradient torque) and torque due to Earth's magnetic field are dominant. For higher orbits (for example, geostationary orbit) torque due to solar radiation pressure is to be considered. Although forces associated with these disturbance torques are not significant to perturb the orbit, but these torques are sufficient to change the attitude of satellite. Therefore, attitude needs to be corrected. Here comes the role of ADCS. In fact, ADCS turns out to be one of the important subsystems of satellite. Figure 1.1. shows ADCS block diagram.

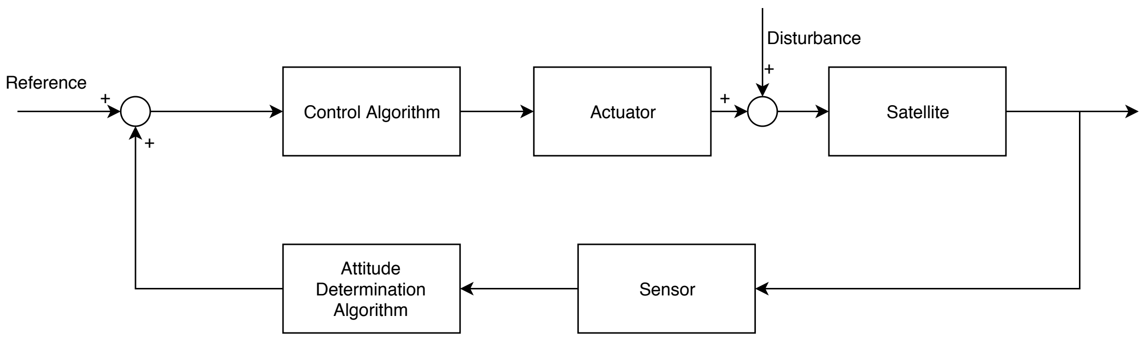

Figure 1.1: Block diagram of Attitude Determination & Control System

ADCS operates by determining the current orientation of satellite w.r.t external reference. External references includes the Sun, stars, Earth's horizon and local magnetic field. Sun sensor, star sensor, gyroscope, magnetometer, horizon sensor are the commonly used sensors for attitude determination process. Information from sensors are feed to attitude determination algorithm, which calculates the current attitude of satellite.
Now comes the attitude control part, which can be of two types: (i) Passive Attitude Control (ii) Active Attitude Control. Passive attitude control uses the disturbance torques aforesaid for attitude correction, which may not be exact or sufficient always. Therefore active attitude control is preferred. In active attitude control, attitude information from sensors are compared to the reference values, and accordingly control torque signal is generated, which is fed to the actuator. Commonly used actuators in satellite are Magneto torquer, Momentum exchange device (Reaction wheel (RW), Momentum wheel), Control moment gyro (CMG) and Reaction jet thrusters. Magneto torquers are normally used in nano satellites due to its low weight, less power consumption and low cost. But it works on the principle of interaction with Earth's magnetic field. Therefore it is more effective in LEO, also it cannot provide large torque. Therefore cases which demands large torque, for satellite in higher orbit, other actuators need to be used. Reaction wheel & momentum wheel are widely used for that purpose. Another option used normally, is CMG. One advantage with CMG is that they have actuation property almost 100 times more than RW s, but they don't ensure precision pointing or can even under go 'Gimbal lock'.
Based on the above discussion, a satellite model has been considered with RW assembly as actuator in this project. Different control algorithms (both linear and non linear) have been proposed in this work to determine which control algorithm gives the best performance in terms of performance indices defined, and this is the scope of this work.

1.2 Literature Review and Motivations

Modelling of spacecraft based on various methods of attitude representation and the modern spacecraft control techniques are presented in [4] and [7]. Various reference frames are discussed in [2]. The satellite attitude is defined using quaternion, Euler angle and direction cosine matrix methods. In the quaternion concepts, quaternion algebra, geometry and rotation using quaternions have been well established [8], [5]. The applications and working of different actuators like reaction wheel, reaction thrusters, momentum wheel and magneto torquer in satellite attitude control is given in [9], [1] and [10]. The dynamics of reaction wheel is described in [11], [12] and the concepts of momentum based actuators for satellite attitude control is discussed in [13].

Modelling and controller design for a spacecraft with different actuator dynamics have been presented in [14]. The synthesis aspects of the simulation model developed for the attitude control system of a small satellite that uses micro jet engine as actuator is presented in [15]. The guidance and control approach for a spacecraft having 3D orbit transfer mission is proposed in [16]. In this method the genetic algorithm is employed to find optimal variation of guidance command and gas thrusters are used as an actuator to apply the required torque. This method can be used to design optimal estimators with prescribed eigenvalues. A feedback control law for linear systems based on a minimum energy regulator problem with fixed terminal state constraints has been presented in [17] and [18]. A numerical convex optimization technique for the analysis and design of linear control systems has been described in [19]. In [20], different control laws for the three axis stabilization of a magnetically actuated satellite system have been presented.

Sliding mode control theory and design approach principle are explained in [21] and [22]. In [23], a sliding mode controller is proposed using modified Rodriguez parameters. A robust Sliding Mode Controller (SMC) for spacecraft attitude control problem is proposed in [24] and the spacecraft attitude is represented using Gibbs vector of Rodriguez parameter. The stability of the designed controller is analysed with direct method of Lyapunov stability. Two optimal sliding mode controllers are proposed in [25] using integral sliding mode concepts. For the optimal control part, the state dependent Riccati equation is used and Lyapunov function approach is used to solve the infinite-time nonlinear optimal problem. In [26] and [27], the design of conventional and different advanced sliding mode controller for different mechanical systems, their analysis and MATLAB simulations have been described. A sliding mode control for the attitude control of a communication satellite has been proposed in [28], using Euler angle representation. The large angle maneuver problem of a spacecraft is treated in [10] using the concept of variable structure control theory. In [29] the attitude control of a geosynchronous communication satellite with thrust jets by using SMC technique is presented. The attitude tracking control problem of a spacecraft with external disturbances and inertia uncertainties are addressed in [30]. In [31], the attitude and speed control of geostationary satellites using PD and SMC is presented.

To prevent the chattering in the SMC quasi-sliding mode controller is presented in [32]. A nonlinear integral sliding mode controller scheme for a second order nonlinear system is presented in [33] and the stability cum robustness is proved by Lyapunov stability theory and LaSalle invariance principle. A SMC with integral augmented sliding surface has been proposed in [34] and [35] to improve the performance and robustness of an electromechanical system. The attitude control of a spacecraft using eigen axis maneuver in presence of parameter uncertainty and external disturbances have been proposed in [36]. In [37], the comparison of performances of a linear control and SMC for attitude control of the spacecraft with reaction wheels are presented. In [38], two nonlinear controllers for satellite attitude control using Euler angle formulation are presented. First technique is a robust recursive nonlinear method related to integral back-stepping and feedback linearisation. Second one is a learning control that updates the control input by learning laws without the computation of the system parameters and inverse dynamics of the system. A tracking controller is proposed in [39] to stabilize the attitude of a micro satellite via integrator back stepping and quaternion feedback.

Fractional order calculus and computations, definitions and properties of fractional calculus, time domain analysis and filter approximation techniques have been explained in [40]. A Fractional Order Sliding Mode Control (FOSMC) for pico satellite using reduced quaternion model in presence of gravity gradient disturbance torque is proposed in [41] and [42]. FOSMC is proposed with different sliding surfaces using modified Rodriguez parameter [43]. A fractional regulator for spacecraft attitude stabilization is introduced in [44] and comparative study between fractional and optimal control law have also been established. A FOSMC with two subsliding manifolds is presented in [45] for the deployment of tethered space systems with external disturbances and unmodelled dynamics. In [46], all the major modules comprising the FOMCON toolbox, the analysis of fractional order systems, identification, controller design, tuning and optimization are presented.[47] develops a fractional-order (FO) power rate type reaching law for sliding mode control (SMC) of nonlinear integer order systems with disturbance and uncertainty. The paper [48] provides stability analysis of finite dimensional fractional differential systems. Alleviation of chattering by power rate exponential reaching law(PRERL) has been proposed in [6]. In [1] Stability of fractional-order nonlinear dynamic systems is studied using Lyapunov direct method with the introductions of Mittag-Leffler stability and generalized Mittag-Leffler stability notions. In [49], stability of fractional order (FO) systems is investigated in the sense of the Lyapunov stability theory.

From the literature survey it can be observed that various robust control algorithms have been proposed for satellite attitude control system. Among the robust, non linear control algorithms, significant amount of research work has been done on Sliding mode based control algorithms as indicated in the literature survey. Among all of these works, some of the research works have proposed a hybridization of linear control law in sliding mode algorithm, to take advantages of both linear and non linear control law. All these works have contributed a hybrid control structure, which is combination of linear control law and sliding mode control law. But none of these literature surveyed, provides a sliding mode based control law, where linear control law has been incorporated in the sliding surface of the sliding mode controller so as to take the advantage of linear control law in the sliding surface formulation. Considering the advantages of fractional controllers over integer controllers, many research works have already been done on satellite attitude control using fractional order sliding mode controller. But their is a wide scope yet to be explored in this domain. In the context of satellite attitude control, analysis of different sliding mode based control laws (both integer and fractional order) and comparison of them in terms of their disturbance rejection and robustness property , is also a research work yet to be carried out as per the literature concerned. Also design of a sliding mode based control law , which is chattering free at the same time ensures robustness, is another an important research direction in the context of satellite attitude control. All of these aforesaid research ideas and existing problems have worked as main source of motivation behind this research project.

1.3 Objective of the Project

Based on the literature review, motivations and the scope of the project, objective of this work is defined as following:

- Study ,understand and compare various attitude representation techniques and choose one of them for attitude representation of satellite.

- Study and implement satellite model with reaction wheel as actuator.
- Tuning of integer order and fractional order controllers for satellite attitude stabilization.
- Tuning of sliding mode and fractional sliding mode based non linear control laws for satellite attitude stabilization.
- Stability analysis of sliding mode based non linear controller.
- Validation of all the tuned controllers on satellite model, followed by the analysis of disturbance rejection property and robustness property of the controllers.

1.4 Outline of the Project

- Chapter 1 explains the scope of the project, literature survey and outline of the project.
- Chapter 2 describes basic concept and notations related two attitude control of satellite. It also contains description of various reference frames commonly used for satellite. This chapter also deals with various attitude representation methods and their advantages, disadvantages.
- Chapter 3 provides detailed mathematical modelling of kinematics and dynamics of satellite. Reaction wheel is also modelled in this chapter.
- Chapter 4 gives the detailed description of linear controllers (PD,PD^{β}) design through optimization method.
- Chapter 5 explains design of non linear controllers (PD-SMC, PD-SMC with modified reaching law, $PD^{\beta} - SMC$, $PD^{\beta} - SMC$ with modified reaching law) in details. Also tuning method of parameters of each of the controller via optimization, is discussed in this chapter.
- Chapter 6 comprises of simulation results obtained by testing both linear and non linear controllers (tuned in chapter 4 & 5) on the mathematical model of satellite(designed in chapter 3). Simulation results of different controllers are analyzed and compared on the basis of performance indices specified.

- Chapter 7 draws the concluding remarks on the basis of the detailed analysis made in chapter 6. Future recommendations in this domain, are also provided in this chapter.

Chapter 2

Basic Concepts & Notations

2.1 Introduction

Attitude of a satellite is the orientation of a pre-defined body fixed coordinate frame with respect to an external frame of reference. *Attitude determination and control* (ADCS) is the process of measuring the satellite's orientation w.r.t the reference frame(attitude determination) and thereafter correcting it according to the requirement(attitude control).

ADCS requires (i) Frame of Reference, (ii) Attitude representation method, to be defined properly before the attitude determination and correction process.

In this chapter, we first discuss different reference frames in the context of satellite attitude control and then we discuss various methods of representation of satellite attitude.

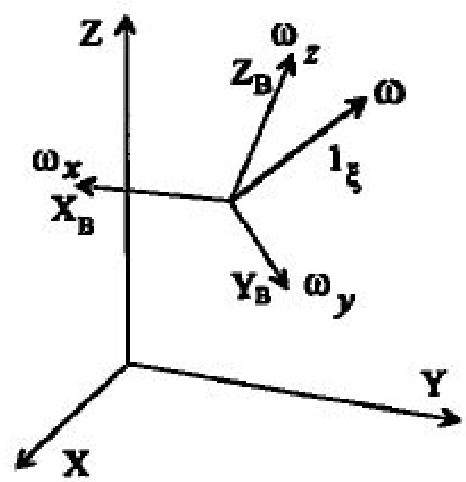

Figure 2.1: Vector measurement in two different frames [1]

2.2 Frame of Reference

Measurement of any vector requires a frame of reference. There may be several frames present to measure a vector. Although the components of vector may change w.r.t. different frames, but its length remains same in all frames. In the the figure 2.1. ω is the vector to be measured. There are two frames considered in the figure namely, $X - Y - Z$ frame and $X_B - Y_B - Z_B$ frame. Also it can be seen from figure that w.r.t 2^{nd} frame, the components of ω are $\omega_X, \omega_Y, \omega_Z$ respectively. With respect to this work on attitude control of satellite, we discuss briefly some of the reference frames [2] [4], which are normally used to describe the position and orientation of a satellite in orbit, listed as following:

- Earth Centred Inertial (ECI) frame
- Earth Centred Earth fixed Fixed (ECEF) frame
- Orbit frame
- Body frame

2.2.1 Earth Centred Inertial (ECI) Frame

This is basically inertial, non rotating frame. This frame is also called as *Conventional Inertial System* (CIS), *Geocentric Equatorial System*[2]. Below figure 2.2. shows the ECI frame, with x_i axis pointing towards Vernal Equinox. y_i axis is $90°$ from X axis towards east along the equatorial plane. z_i axis is along axis of rotation of Earth.

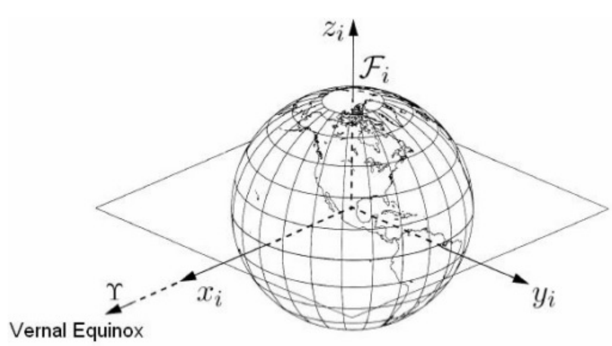

Figure 2.2: ECI frame [2]

2.2.2 Earth Centred Earth Fixed (ECEF) Frame

ECEF frame, as the name suggests, is fixed at the centre of Earth. That means it can rotate along with the rotation of Earth. This frame is also called as *International Terrestrial Reference Frame*. Here X axis is from centre of Earth to Greenwich meridian on the equatorial plane, Z axis is same as ECI frame i.e. axis of rotation of Earth. Y axis completes the right hand triad. Figure 2.3. shows ECEF frame of reference. Here object position can be represented by latitude(ϕ), longitude(λ) and altitude(h).

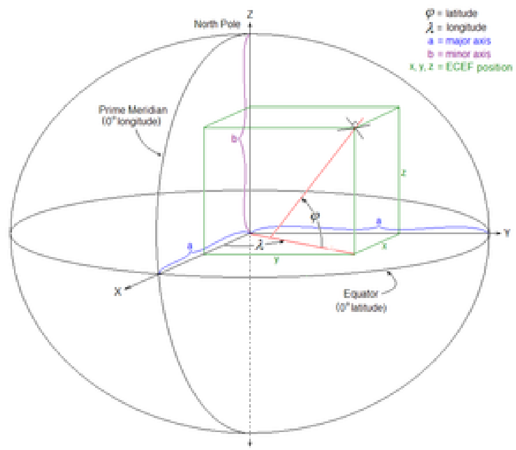

Figure 2.3: ECEF frame [2]

Apart from these main coordinate frames, there are few other frames noteworthy, *Topocentric Horizon Coordinate Frame* (SEZ system), *Topocentric Equitorial Frame*.

2.2.3 Orbit Frame

This frame is same as *Roll-Pitch-Yaw* frame. In case of orbit frame [3], origin lies at the centre of mass of satellite. X_o axis is tangential to the orbit (is in velocity direction for circular orbits), Z_o axis is in nadir direction (centre of Earth) and Y_o axis is to complete right hand coordinate system (negative normal to orbit). An orbit frame is shown in figure 2.4. There are few variations of this type of frame. For example, RSW or *Gaussian Coordinate frame*, NTW frame, *Equinoctial Frame* (EQW).

2.2.4 Body Frame

Body frame is attached to satellite's centre of mass, shown in figure 2.5. As discussed in the beginning, body frame is fixed on the body (satellite). Whenever satellite undergoes

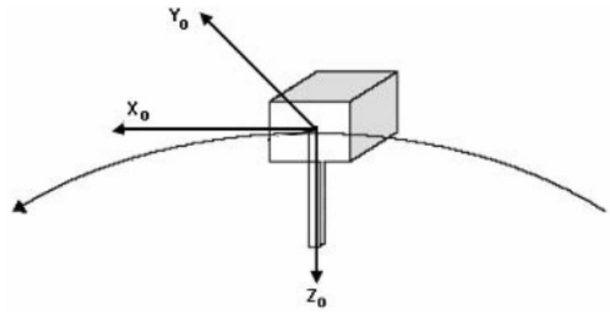

Figure 2.4: Orbit frame [3]

attitude maneuver, body frame also changes its orientation according. When there is zero roll, pitch and yaw angles, only then body frame X_b, Y_b axes coincide with orbit frame's X_o, Y_o axes respectively. Z axis of body frame i.e. Z_b points towards nadir always.

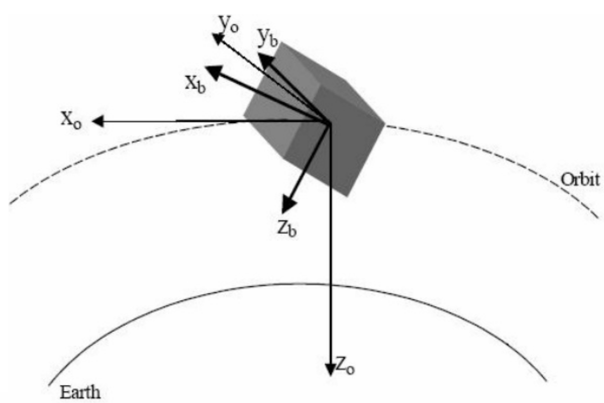

Figure 2.5: Body frame [3]

2.3 Attitude Representation Methods

There are several ways existing in literature on representation of attitude of a spacecraft/satellite. We discuss some of the methods in this section, which are commonly used for attitude representation. They are listed below:

- Direction Cosine Matrix (DCM)
- Euler Angles
- Quaternions

2.3.1 Direction Cosine Matrix (DCM)

Direction cosine Matrix (DCM) describes the relationship between two frames. Given a vector in one frame, it can be transformed to other frame using DCM.
Consider the following figure 2.6, In this figure, axes $1, 2, 3$ are orthogonal unit vectors

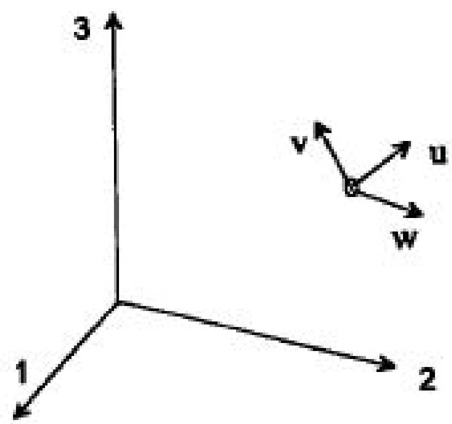

Figure 2.6: Coordinate System of $1, 2, 3$ inertial frame and u, v, w body frame [4]

defining a right handed triad and the triad is chosen as inertial reference frame (I). Another orthogonal triad attached to the center of mass is considered namely u, v, w; this is called as the body frame (B). Then we can define a matrix C_I^B as following,

$$C_I^B = \begin{bmatrix} u_1 & u_2 & u_3 \\ v_1 & v_2 & v_3 \\ w_1 & w_2 & w_3 \end{bmatrix} \tag{2.1}$$

In the matrix u_1, u_2, u_3 are components of unit vector u along three axes of the reference frame,$u = [u_1, u_2, u_3]^T$. Similarly w, v 's components are there in the matrix [4].The matrix C_I^b is called the *Direction Cosine Matrix* (DCM), also called as the *Attitude Matrix,Coordinate Transformation Matrix* , having the property of mapping vector from one frame to other. Here the notation C_I^B implies that this DCM is used to transform a vector from inertial frame to body frame i.e. $C_I^B : I \mapsto$B.
Now consider vector $\vec{a}$ has components $[a_1, a_2, a_3]^T$ in the inertial reference frame, and

denote it by a_I. Then it can be shown,

$$C_I^B a_I = \begin{bmatrix} u_1 & u_2 & u_3 \\ v_1 & v_2 & v_3 \\ w_1 & w_2 & w_3 \end{bmatrix} \begin{bmatrix} a_1 \\ a_2 \\ a_3 \end{bmatrix} = \begin{bmatrix} u.a \\ v.a \\ w.a \end{bmatrix} \begin{bmatrix} a_u \\ a_v \\ a_w \end{bmatrix} = a_B \tag{2.2}$$

a_B is the vector $\vec{a}$ mapped in body frame from inertial frame.
DCM C_I^B or simply C has *orthonormal* property, this means

$$\begin{aligned} C^{-1} &= C^T \\ \implies CC^T &= C^T C = I \end{aligned} \tag{2.3}$$

where I is identity matrix.

The main disadvantage with equations involving DCM is that we have to ensure orthonormal property, which is sometimes difficult while doing numerical computation with finite precision computer. Also another disadvantage with differential equations involving DCM is that for a DCM of size 3×3 , 9 differential equations need to be solved, which may be computationally expensive in some applications for example space application. Nevertheless DCM is one of the commonly used attitude representation Method.

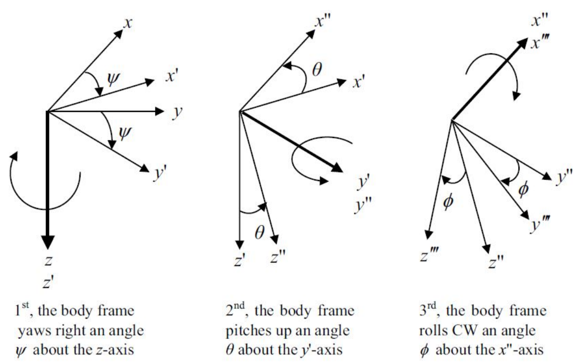

Figure 2.7: Euler Angle Sequence [5]

2.3.2 Euler Angles

Euler angle method is one of the commonly used method to represent attitude. Transformation from any reference frame (say A) to other (say B) can be broken into three successive rotations about three specified axes by the amount represented by Euler angles, such that no two successive rotations are about the same axes [5].

In the figure 2.7. $Z-Y-X$ rotation sequence is followed. First ψ amount rotation is done about Z(yaw) axis to form $X'Y'Z'$ frame. As rotation is about Z axis, hence Z & Z' are same. Next θ amount rotation is carried about Y'(pitch) axis to get $X''Y''Z''$ frame (again note Y' & Y'' are same). Finally rotation is done about roll axis/ X'' axis by angle ϕ, and the required frame orientation (B) is achieved. Rotation matrices of corresponding Euler angles are as following:

$$R_{X"}(\phi) = \begin{bmatrix} 1 & 0 & 0 \\ 0 & cos\phi & sin\phi \\ 0 & -sin\phi & cos\phi \end{bmatrix} \tag{2.4}$$

$$R_{Y'}(\theta) = \begin{bmatrix} cos\theta & 0 & -sin\theta \\ 0 & 1 & 0 \\ sin\theta & 0 & cos\theta \end{bmatrix} \tag{2.5}$$

$$R_{Z}(\psi) = \begin{bmatrix} cos\psi & sin\psi & 0 \\ -sin\psi & cos\psi & 0 \\ 0 & 0 & 1 \end{bmatrix} \tag{2.6}$$

Therefore overall DCM for transforming from frame I to frame B is given by,

$$\begin{aligned} C_A^B &= R_{X"}(\phi) R_{Y'}(\theta) R_Z(\psi) \\ &= \begin{bmatrix} c\psi c\theta & s\psi c\theta & -s\theta \\ c\psi s\theta s\phi + s\psi c\phi & s\psi s\theta s\phi + c\psi c\phi & c\theta s\phi \\ c\psi s\theta c\phi + s\psi s\phi & s\psi s\theta c\phi - c\psi s\phi & c\theta c\phi \end{bmatrix} \end{aligned} \tag{2.7}$$

where c- means cosine and s- means sine.
Similarly there are other different combinations by which rotation can be performed.Among all these sequences, two distinct types of rotations can be defined.

- Successive rotation about each of the three axes X, Y, Z . There are six such combinations:1-2-3,1-3-2,2-1-3,2-3-1,3-1-2,3-2-1.(1 means X axis,2 means Y axis, 3 means Z axis).Each of them are called *Proper Euler Angles*.

- First and third rotation about same axis and second rotation about remaining of the two axes. Again there are six such cases: 1-2-1,1-3-1,2-1-2,2-3-2,3-1-3 and 3-2-3. Here each combinations are called *Tait-Brian Angles*.

The main disadvantage of Euler angle representation is: **Gimbal Lock** or **Singularity Problem**. This problem occurs when pitch angle becomes $90°$. In that case roll and yaw rotations cannot be distinguished. Another problem with Euler angles is that equations involved are trigonometric in nature. Hence difficulty arises while solving equations involving Euler angles using numerical methods. Still Euler angles are widely used because of their less computational load (they need only 3 elements to be computed where DCM has 9 elements for example).

2.3.3 Quaternions

Quaternions are another way to represent attitude of satellite. Concept of quaternions can be followed from *Euler's Rotation Theorem*, which is as following:

Theorem 2.1. *In three-dimensional space, any displacement of a rigid body such that a point on the rigid body remains fixed, is equivalent to a single rotation about some axis that runs through the fixed point.*

The corresponding axis is known as *Euler axis* [4] and the angle of rotation is *Euler angle* (this different from euler angle sequence defined previously).
Therefore quaternion is formulated as,

$$q = \begin{bmatrix} e_1 \sin\theta/2 \\ e_2 \sin\theta/2 \\ e_3 \sin\theta/2 \\ \cos\theta/2 \end{bmatrix} \tag{2.8}$$

where $\hat{e} = [e_1, e_2, e_3]^T$ is axis of rotation, θ denotes the angle of rotation.
In the above formulation, first three parts constitute the vector component of quaternion and the last component is the scalar component.
Using vector notation, quaternions can be denoted in the following way:

$$\begin{aligned} q &= q_4 + \vec{q} \\ q &= q_4 + \hat{\imath}q_1 + \hat{\jmath}q_2 + \hat{k}q_3 \end{aligned} \tag{2.9}$$

where $\vec{q} = \hat{\imath}q_1 + \hat{\jmath}q_2 + \hat{k}q_3$ is vector part of the quaternion, q_4 is the scalar part of it. Unit vectors $\hat{\imath}, \hat{\jmath}, \hat{k}$ are along body axes and they satisfy following equalities:

$$
\begin{aligned}
i^2 &= j^2 = k^2 = -1 \\
ij &= -ji = k \\
jk &= -kj = i \\
ki &= -ik = j
\end{aligned}
\tag{2.10}
$$

if q is a unit quaternion, then it satisfies the following relation:

$$q_1^2 + q_2^2 + q_3^2 + q_4^2 = 1 \tag{2.11}$$

2.3.4 Few operations on Quaternions

Here few quaternion related operations are briefly described, which will be used throughout this work.

2.3.4.1 Conjugate of a Quaternion

Conjugate of a quaternion q is given by,

$$
\begin{aligned}
q^* &= q_4 - \vec{q} \\
&= q_4 - \hat{i}q_1 - \hat{j}q_2 - \hat{k}q_3
\end{aligned}
\tag{2.12}
$$

2.3.4.2 Norm of Quaternion

Norm of quaternion q is defined by,

$$\|q\| = \sqrt{qq^*} = \sqrt{q^*q} = \sqrt{q_1^2 + q_2^2 + q_3^2 + q_4^2} \tag{2.13}$$

If $\|q\| = 1$, then the quaternion is called *unit qauternion*.

2.3.4.3 Inverse of Quaternion

Quaternion inverse, denote by q^{-1}, is defined as below,

$$q^{-1} = \frac{q^*}{\|q\|^2} \tag{2.14}$$

In case of unit quaternion, $q^{-1} = q^*$.

2.3.4.4 Quaternion Multiplication

Quaternion multiplication is different from normal multiplication in the sense that quaternion multiplication is not commutative, so if q, p are two quaternions, then $q \otimes p \neq p \otimes q$. Consider 2 quaternions, q & p. Therefore definition of quaternion multiplication is given by,

$$q \otimes p = q_4 p_4 - \vec{q}.\vec{p} + q_4\vec{p} + p_4\vec{q} + \vec{q} \times \vec{p} \tag{2.15}$$

Above eqn. (2.15) can also be written as,

$$q \otimes p = \begin{bmatrix} q_4 p_{1:3} + p_4 q_{1:3} + q_{1:3} \times p_{1:3} \\ q_4 p_4 - q_{1:3}^T p_{1:3} \end{bmatrix} \tag{2.16}$$

where $1 : 3$ implies 3 axis components. For example, $q_{1:3} = [q_1, q_2, q_3]^T$. Above eqn. (2.16) can be used to construct the matrix form of quaternion multiplication. Therefore matrix formulation of quaternion multiplication is given by,

$$q \otimes p = Q(q)p = \bar{Q}(p)q \tag{2.17}$$

where

$$Q(q) = \begin{bmatrix} q_4 & q_3 & -q_2 & q_1 \\ -q_3 & q_4 & q_1 & q_2 \\ q_2 & -q_1 & q_4 & q_3 \\ -q_1 & -q_2 & -q_3 & q_4 \end{bmatrix} \tag{2.18}$$

and $\bar{Q}$ is given by,

$$\bar{Q}(p) = \begin{bmatrix} p_4 & -p_3 & p_2 & p_1 \\ p_3 & p_4 & -p_1 & p_2 \\ -p_2 & p_1 & p_4 & p_3 \\ -p_1 & -p_2 & -p_3 & p_4 \end{bmatrix} \tag{2.19}$$

2.3.5 Conversion between Attitude Representations

Now after discussing various methods of attitude representation, we now discuss conversion from one attitude representation to other.

2.3.5.1 Quaternion to Euler Angles

Given a quaternion q and considering particular rotation sequences, Euler angles can be computed as below[5] (here yaw-pitch-roll sequence taken):

$$\phi = tan^{-1}\Big(\frac{m_{23}}{m_{33}}\Big) \tag{2.20}$$

$$\theta = sin^{-1}(-m_{13}) \tag{2.21}$$

$$\psi = tan^{-1}\Big(\frac{m_{12}}{m_{11}}\Big) \tag{2.22}$$

where

$$\begin{aligned} m_{11} &= 2q_1^2 + 2q_4^2 - 1 \\ m_{12} &= 2q_1q_2 + 2q_3q_4 \\ m_{13} &= 2q_1q_3 - 2q_2q_4 \\ m_{23} &= 2q_2q_3 + 2q_1q_4 \\ m_{33} &= 2q_3^2 + 2q_4^2 - 1 \end{aligned} \tag{2.23}$$

2.3.5.2 Quaternion to Direction Cosine Matrix

For a given quaternion q, DCM can be obtained as below:

$$C = \begin{bmatrix} 2q_1^2 + 2q_4^2 - 1 & 2q_1q_2 + 2q_3q_4 & 2q_1q_3 - 2q_2q_4 \\ 2q_1q_2 - 2q_3q_4 & 2q_2^2 + 2q_4^2 - 1 & 2q_2q_3 + 2q_1q_4 \\ 2q_1q_3 + 2q_2q_4 & 2q_2q_3 - 2q_1q_4 & 2q_3^2 + 2q_4^2 - 1 \end{bmatrix} \tag{2.24}$$

where DCM C is defined as,

$$C = \begin{bmatrix} C_{11} & C_{12} & C_{13} \\ C_{21} & C_{22} & C_{23} \\ C_{31} & C_{32} & C_{33} \end{bmatrix}$$

2.3.5.3 Euler Angles to Qauternion

For a given set of Euler angles(ϕ, θ, ψ) and given rotation sequence (here again yaw-pitch-roll sequence chosen), corresponding quaternion can be obtained as,

$$\begin{aligned} q_1 = & \quad sin\frac{\phi}{2}cos\frac{\theta}{2}cos\frac{\psi}{2} - cos\frac{\phi}{2}sin\frac{\theta}{2}sin\frac{\psi}{2} \\ q_2 = & \quad cos\frac{\phi}{2}sin\frac{\theta}{2}cos\frac{\psi}{2} + sin\frac{\phi}{2}cos\frac{\theta}{2}sin\frac{\psi}{2} \\ q_3 = & \quad cos\frac{\phi}{2}cos\frac{\theta}{2}sin\frac{\psi}{2} - sin\frac{\phi}{2}sin\frac{\theta}{2}cos\frac{\psi}{2} \\ q_4 = & \quad cos\frac{\phi}{2}cos\frac{\theta}{2}cos\frac{\psi}{2} + sin\frac{\phi}{2}sin\frac{\theta}{2}sin\frac{\psi}{2} \end{aligned} \tag{2.25}$$

2.3.5.4 Direction Cosine Matrix to Quaternion

For the DCM given in 2.1., corresponding quaternion can be calculated as,

$$\begin{aligned} q_1 &= (C_{23} - C_{32})/(4q_4) \\ q_2 &= (C_{31} - C_{13})/(4q_4) \\ q_3 &= (C_{12} - C_{21})/(4q_4) \\ q_4 = \frac{1}{2}&\sqrt{C_{11} + C_{22} + C_{33} + 1} \end{aligned} \tag{2.26}$$

2.4 Summary

In this chapter, basic definitions and representation methods related to 'attitude determination & control' is discussed. Under this, various frames which are normally used for satellite, are discussed. Also, different attitude representation methods for satellite are presented in this chapter.

Chapter 3

Mathematical Modelling of Satellite

3.1 Introduction

In the previous chapter, various frame of reference and attitude representation methods of satellite are discussed. The mathematical model of satellite is discussed in this chapter. Based on this modelling, attitude controller of satellite will be designed in the next chapter.

3.2 Mathematical Modelling of Satellite

Mathematical model of a satellite, from the attitude control point of view, has two parts namely, *kinematics* & *Dynamics*.

3.2.1 Kinematics

Kinematics is concerned about the orientation of a satellite without reference to any force/torque which has caused it. Kinematic model is described using time derivative of attitude as a function of angular velocity.

In this section, kinematics is described using DCM differential equation, differential equation involving Euler angles and quaternion differential equation.

3.2.1.1 Direction Cosine Matrix

Consider two reference frames A and B as shown in Figure 3.1. which are in motion relative to each other. Let $\vec{\omega} \equiv \vec{\omega}_A^B$ be the angular velocity vector of the reference frame B with respect to the reference frame A. Then the time dependent angular velocity vector $\vec{\omega}$

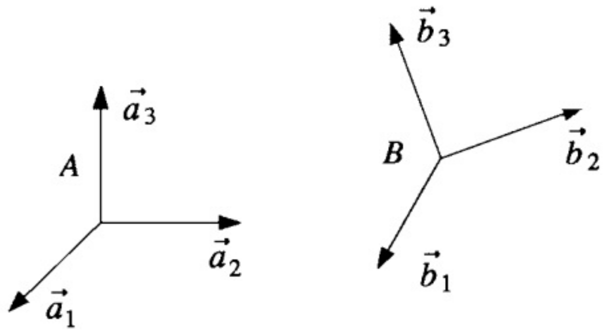

Figure 3.1: Two reference frames A & B [4]

can be represented in reference frame B as,

$$\vec{\omega} = \omega_1 \vec{b_1} + \omega_2 \vec{b_2} + \omega_3 \vec{b_3} \tag{3.1}$$

Basis vectors of B can be represented using Direction Cosine Matrix $C \equiv C_A^B$ as,

$$\begin{bmatrix} \vec{b_1} \\ \vec{b_2} \\ \vec{b_3} \end{bmatrix} = C \begin{bmatrix} \vec{a_1} \\ \vec{a_2} \\ \vec{a_3} \end{bmatrix} \tag{3.2}$$

$$\begin{bmatrix} \vec{a_1} \\ \vec{a_2} \\ \vec{a_3} \end{bmatrix} = C^{-1} \begin{bmatrix} \vec{b_1} \\ \vec{b_2} \\ \vec{b_3} \end{bmatrix} = C^T \begin{bmatrix} \vec{b_1} \\ \vec{b_2} \\ \vec{b_3} \end{bmatrix} \tag{3.3}$$

As the two reference frames are in motion relative to each other, the Direction Cosine Matrix is a function of time. Taking the time derivative of eqn. (3.3) with respect to A frame,

$$\begin{aligned} \begin{bmatrix} 0 \\ 0 \\ 0 \end{bmatrix} &= \dot{C^T} \begin{bmatrix} \vec{b_1} \\ \vec{b_2} \\ \vec{b_3} \end{bmatrix} + C^T \begin{bmatrix} \dot{\vec{b_1}} \\ \dot{\vec{b_2}} \\ \dot{\vec{b_3}} \end{bmatrix} \\ &= \dot{C^T} \begin{bmatrix} \vec{b_1} \\ \vec{b_2} \\ \vec{b_3} \end{bmatrix} + C^T \begin{bmatrix} \vec{\omega} \times \vec{b_1} \\ \vec{\omega} \times \vec{b_2} \\ \vec{\omega} \times \vec{b_3} \end{bmatrix} \\ &= \dot{C^T} \begin{bmatrix} \vec{b_1} \\ \vec{b_2} \\ \vec{b_3} \end{bmatrix} - C^T \begin{bmatrix} 0 & -\omega_3 & \omega_2 \\ \omega_3 & 0 & -\omega_1 \\ -\omega_2 & \omega_1 & 0 \end{bmatrix} \begin{bmatrix} \vec{b_1} \\ \vec{b_2} \\ \vec{b_3} \end{bmatrix} \end{aligned} \tag{3.4}$$

where,

$$\dot{C} = \begin{bmatrix} \dot{C_{11}} & \dot{C_{12}} & \dot{C_{13}} \\ \dot{C_{21}} & \dot{C_{22}} & \dot{C_{23}} \\ \dot{C_{31}} & \dot{C_{32}} & \dot{C_{33}} \end{bmatrix} \tag{3.5}$$

Now we define a skew-symmetric matrix Ω as,

$$\Omega = \begin{bmatrix} 0 & -\omega_3 & \omega_2 \\ \omega_3 & 0 & -\omega_1 \\ -\omega_2 & \omega_1 & 0 \end{bmatrix} \tag{3.6}$$

Then eqn. (3.4) becomes

$$\begin{aligned} \left[\dot{C}^T - C^T\Omega\right] \begin{bmatrix} \vec{b_1} \\ \vec{b_2} \\ \vec{b_3} \end{bmatrix} &= \begin{bmatrix} 0 \\ 0 \\ 0 \end{bmatrix} \\ \dot{C}^T - C^T\Omega &= 0 \end{aligned} \tag{3.7}$$

$$\dot{C}^T = C^T\Omega \tag{3.8}$$

Taking transpose on both sides,

$$\begin{aligned} \left(\dot{C}^T\right)^T &= \left(C^T\Omega\right) \\ \dot{C} &= \Omega^T C \end{aligned} \tag{3.9}$$

Since Ω is a skew-symmetric matrix,

$$\dot{C} + \Omega C = 0 \tag{3.10}$$

Eqn. (3.10) is the Kinematic Equation of the satellite using Direction Cosine Matrix. The Differential Equation for each element of C can be written as,

$$\begin{aligned} \dot{C_{11}} &= \omega_3 C_{21} - \omega_2 C_{31} \\ \dot{C_{12}} &= \omega_3 C_{22} - \omega_2 C_{32} \\ \dot{C_{13}} &= \omega_3 C_{23} - \omega_2 C_{33} \\ \dot{C_{21}} &= \omega_1 C_{31} - \omega_3 C_{11} \\ \dot{C_{22}} &= \omega_1 C_{32} - \omega_3 C_{12} \end{aligned}$$

$$
\begin{aligned}
\dot{C_{23}} &= \omega_1 C_{33} - \omega_3 C_{13} \\
\dot{C_{31}} &= \omega_2 C_{11} - \omega_1 C_{21} \\
\dot{C_{32}} &= \omega_2 C_{12} - \omega_1 C_{22} \\
\dot{C_{33}} &= \omega_2 C_{13} - \omega_1 C_{23}
\end{aligned}
\tag{3.11}
$$

The components of angular velocity ω_1, ω_2 and ω_3 can be expressed in terms elements of Direction cosine Matrix as,

$$
\begin{aligned}
\omega_1 &= \dot{C_{21}} C_{31} + \dot{C_{22}} C_{32} + \dot{C_{23}} C_{33} \\
\omega_2 &= \dot{C_{31}} C_{11} + \dot{C_{32}} C_{12} + \dot{C_{33}} C_{13} \\
\omega_3 &= \dot{C_{11}} C_{21} + \dot{C_{12}} C_{22} + \dot{C_{13}} C_{23}
\end{aligned}
\tag{3.12}
$$

3.2.1.2 Euler Angles

Euler angles can also be used to describe the kinematics of satellite. To derive that we consider orientation of frame B w.r.t frame A.
Consider the rotation sequence of $C_1(\phi) \leftarrow C_2(\theta) \leftarrow C_3(\psi)$ from A to B with two intermediate frames A_1 and A_2 as,

$$
\begin{gathered}
C_3(\psi) : A_1 \leftarrow \text{A} \\
C_2(\theta) : A_2 \leftarrow A_1 \\
C_1(\phi) : B \leftarrow A_2
\end{gathered}
$$

where $C_1(\phi)$, $C_2(\theta)$ and $C_3(\psi)$ are rotation matrices corresponding to roll, pitch and yaw axes,

$$
C_1(\phi) = \begin{bmatrix} 1 & 0 & 0 \\ 0 & cos\phi & sin\phi \\ 0 & -sin\phi & cos\phi \end{bmatrix}
\tag{3.13}
$$

$$
C_2(\theta) = \begin{bmatrix} cos\theta & 0 & -sin\theta \\ 0 & 1 & 0 \\ sin\theta & 0 & cos\theta \end{bmatrix}
\tag{3.14}
$$

$$
C_3(\psi) = \begin{bmatrix} cos\psi & sin\psi & 0 \\ -sin\psi & cos\psi & 0 \\ 0 & 0 & 1 \end{bmatrix}
\tag{3.15}
$$

$\dot{\theta}_3$, $\dot{\theta}$ and $\dot{\phi}$ represents the time derivatives of Euler angles. Then the angular velocity of reference frame B with respect to reference frame A, $\vec{\omega}_A^B$ (or simply $\vec{\omega}$) can be written as,

$$\begin{aligned}\begin{bmatrix}\omega_1\\\omega_2\\\omega_3\end{bmatrix} &= \begin{bmatrix}\dot{\phi}\\0\\0\end{bmatrix} + C_1(\phi)\begin{bmatrix}0\\\dot{\theta}\\0\end{bmatrix} + C_1(\phi)C_2(\theta)\begin{bmatrix}0\\0\\\dot{\psi}\end{bmatrix} &(3.16)\\ &= \begin{bmatrix}1 & 0 & -sin\theta\\0 & cos\phi & sin\phi cos\theta\\0 & -sin\phi & cos\phi cos\theta\end{bmatrix}\begin{bmatrix}\dot{\phi}\\\dot{\theta}\\\dot{\psi}\end{bmatrix} &(3.17)\end{aligned}$$

The inverse relation gives

$$\begin{bmatrix}\dot{\phi}\\\dot{\theta}\\\dot{\psi}\end{bmatrix} = \frac{1}{cos\theta}\begin{bmatrix}cos\theta & sin\phi sin\theta & cos\phi sin\theta\\0 & cos\phi cos\theta & -sin\phi cos\theta\\0 & sin\phi & cos\phi\end{bmatrix}\begin{bmatrix}\omega_1\\\omega_2\\\omega_3\end{bmatrix} \tag{3.18}$$

Eqn. (3.18) is the Kinematic differential equation using Euler angles for the sequence of rotation $C_1(\phi) \leftarrow C_2(\theta) \leftarrow C_3(\psi)$.

If ω_1, ω_2 and ω_3 are known, then the orientation of reference frame B w.r.t to frame A can be determined by solving the Eqn. (3.18). The *singularity problem/ gimbal lock problem* will arise when θ=$\frac{\pi}{2}$ in the kinematic equation. As the sequence of rotation changes the Kinematic differential equation also change accordingly.

3.2.1.3 Quaternions

Here we derive the kinematic differential equation interms of quaternions. By substituting eqn. (3.11) into eqn. (3.12) we get,

$$\begin{aligned}\omega_1 &= 2(\dot{q}_1q_4 + \dot{q}_2q_3 - \dot{q}_3q_2 - \dot{q}_4q_1)\\ \omega_2 &= 2(\dot{q}_2q_4 + \dot{q}_3q_1 - \dot{q}_1q_3 - \dot{q}_4q_2)\\ \omega_3 &= 2(\dot{q}_3q_4 + \dot{q}_1q_2 - \dot{q}_2q_1 - \dot{q}_4q_3)\end{aligned} \tag{3.19}$$

Differentiating eqn. (2.11),

$$0 = 2(\dot{q}_1q_1 + \dot{q}_2q_2 - \dot{q}_3q_3 - \dot{q}_4q_4) \tag{3.20}$$

Combining equations (3.19) and (3.20) ,

$$\begin{bmatrix} \omega_1 \\ \omega_2 \\ \omega_3 \\ 0 \end{bmatrix} = 2 \begin{bmatrix} q_4 & q_3 & -q_2 & -q_1 \\ -q_3 & q_4 & q_1 & -q_2 \\ q_2 & -q_1 & q_4 & -q_3 \\ q_1 & q_2 & q_3 & q_4 \end{bmatrix} \begin{bmatrix} \dot{q}_1 \\ \dot{q}_2 \\ \dot{q}_3 \\ \dot{q}_4 \end{bmatrix} \tag{3.21}$$

or

$$\begin{bmatrix} \dot{q}_1 \\ \dot{q}_2 \\ \dot{q}_3 \\ \dot{q}_4 \end{bmatrix} = \frac{1}{2} \begin{bmatrix} q_4 & -q_3 & q_2 & q_1 \\ q_3 & q_4 & -q_1 & q_2 \\ -q_2 & q_1 & q_4 & q_3 \\ -q_1 & -q_2 & -q_3 & q_4 \end{bmatrix} \begin{bmatrix} \omega_1 \\ \omega_2 \\ \omega_3 \\ 0 \end{bmatrix} \tag{3.22}$$

It can be rewritten as

$$\begin{bmatrix} \dot{q}_1 \\ \dot{q}_2 \\ \dot{q}_3 \\ \dot{q}_4 \end{bmatrix} = \frac{1}{2} \begin{bmatrix} 0 & \omega_3 & -\omega_2 & \omega_1 \\ -\omega_3 & 0 & \omega_1 & \omega_2 \\ \omega_2 & -\omega_1 & 0 & \omega_3 \\ -\omega_1 & -\omega_2 & -\omega_3 & 0 \end{bmatrix} \begin{bmatrix} q_1 \\ q_2 \\ q_3 \\ q_4 \end{bmatrix} \tag{3.23}$$

The $\vec{q}$ and $\vec{\omega}$ are defined as

$$\vec{q} = \begin{bmatrix} q_1 \\ q_2 \\ q_3 \end{bmatrix} \qquad \vec{\omega} = \begin{bmatrix} \omega_1 \\ \omega_2 \\ \omega_3 \end{bmatrix} \tag{3.24}$$

Rewriting the Kinematic differential equation (3.23) as following:

$$\dot{\vec{q}} = \frac{1}{2}\left(q_4\vec{\omega} - \vec{\omega} \times \vec{q}\right) \tag{3.25}$$

$$\dot{q}_4 = -\frac{1}{2}\vec{\omega}^T\vec{q} \tag{3.26}$$

Combining equations (3.25) and (3.26),

$$\begin{bmatrix} \dot{\vec{q}} \\ \dot{q}_4 \end{bmatrix} = \frac{1}{2} \begin{bmatrix} q_4\vec{\omega} - \vec{\omega} \times \vec{q} \\ -\omega^T\vec{q} \end{bmatrix} \tag{3.27}$$

Therefore eqn. (3.27) is quaternion differential equation describing the kinematics of satellite.

Remark 3.1. *Through out this work, quaternion differential equation(3.27) has been used to represent kinematcis of satellite.*

3.2.2 Dynamics

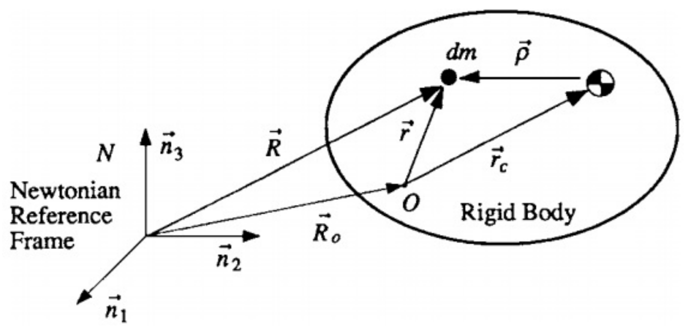

Figure 3.2: Rigid body motion relative to Newtonian reference frame

Dynamic equation gives the angular velocity of the spacecraft [3]. Dynamics is described using *Euler Moment Equation*, which we will derive next. Consider a rigid body which is in motion relative to a Newtonian reference inertial frame N, as shown in Figure 3.2. The equation of rotational motion of the body is given as,

$$\int \vec{r} \times \ddot{\vec{R}} dm = \vec{M}_o = \vec{T}_o \tag{3.28}$$

$dm \rightarrow$ infinitesimal mass element
$\vec{r} \rightarrow$ position vector of the mass element dm relative to O
$\vec{R} \rightarrow$ position vector of dm from the origin of the inertial frame.
$\ddot{\vec{R}} \rightarrow$ inertial acceleration of dm
$\vec{M}_o \rightarrow$ total external moment about the point O

Let $\vec{r_c}$ be the position vector of the center of mass about the point O, $\vec{\rho}$ be the position vector of dm relative to the center of mass and m be the mass of the rigid body.
Then

$$\int \vec{r} dm = m\vec{r_c} \tag{3.29}$$

$$\int \vec{\rho} dm = 0 \tag{3.30}$$

since $\vec{R}$=$\vec{R_o}$+$\vec{r}$

$$\dot{\vec{h_0}} + m\vec{r_c} \times \ddot{\vec{R_0}} = \vec{M_0} \tag{3.31}$$

where $\vec{h_o}$ is the relative angular momentum about the point O and is given by,

$$\vec{h_o} = \int \vec{r} \times \dot{\vec{r}} dm \tag{3.32}$$

The absolute angular momentum is defined as,

$$\vec{H_o} = \int \vec{r} \times \dot{\vec{R}} dm \tag{3.33}$$

Combining equations (3.28) and (3.33), we get

$$\dot{\vec{H_o}} + m\dot{\vec{R_o}} \times \dot{\vec{r_c}} = \vec{M_o} \tag{3.34}$$

If the reference point O is inertially fixed or at the center of mass of the rigid body, then Equation 3.34 becomes,

$$\dot{\vec{H_o}} = \vec{M_o} \qquad \dot{\vec{h_o}} = \vec{M_o} \tag{3.35}$$

Consider a rigid body with a body fixed frame B with its origin at the center of mass of the rigid body as in Figure 3.3. $\vec{R_c}$ denotes the position vector of the center of mass from the origin of the inertial frame N and $\vec{R}$ is the position vector of dm from the inertial origin. Let $\vec{\omega} \equiv \vec{\omega}_N^B$ be the angular velocity of the rigid body with respect to the inertial frame N.

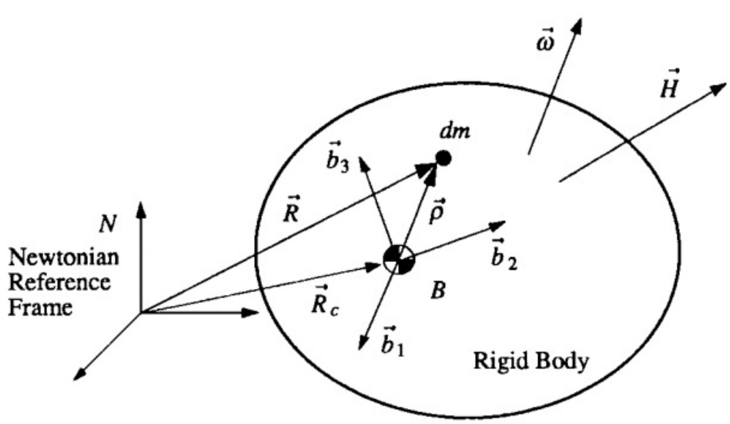

Figure 3.3: Rigid body with a body fixed frame with origin at the center of mass [4]

The angular momentum vector $\vec{H}$ of the rigid body about the center of mass is defined as,

$$\begin{aligned}
\vec{H} &= \int \vec{\rho} \times \dot{\vec{R}} dm \\
&= \int \vec{\rho} \times \big(\dot{\vec{R}}_c + \dot{\vec{\rho}}\big) dm \\
&= \int \vec{\rho} \times \dot{\vec{R}}_c dm + \int \vec{\rho} \times \dot{\vec{\rho}} dm \\
&= \int \vec{\rho} dm \times \dot{\vec{R}}_c + \int \vec{\rho} \times \dot{\vec{\rho}} dm
\end{aligned} \tag{3.36}$$

$$\dot{\vec{\rho}} = \Big(\frac{d\rho}{dt}\Big)_N = \Big(\frac{d\rho}{dt}\Big)_B + \vec{\omega} \times \vec{\rho} \tag{3.37}$$

Substituting equations (3.30) and 3.37 in 3.36, then we get

$$\vec{H} = \int \vec{\rho} \times \big(\vec{\omega} \times \vec{\rho}\big) dm \tag{3.38}$$

where $\vec{\rho}$ and $\vec{\omega}$ are given as,

$$\vec{\rho} = \rho_1 \vec{b_1} + \rho_2 \vec{b_2} + \rho_3 \vec{b_3} \tag{3.39}$$

$$\vec{\omega} = \omega_1 \vec{b_1} + \omega_2 \vec{b_2} + \omega_3 \vec{b_3} \tag{3.40}$$

Using eqn. (3.36), the angular momentum can be written as,

$$\vec{H} = \big(J_{11}\omega_1 + J_{12}\omega_2 + J_{13}\omega_3\big)\vec{b_1} + \big(J_{21}\omega_1 + J_{22}\omega_2 + J_{23}\omega_3\big)\vec{b_2} + \big(J_{31}\omega_1 + J_{32}\omega_2 + J_{33}\omega_3\big)\vec{b_3} \tag{3.41}$$

where J is Moment of Inertia tensor of rigid body.

$$J_{11} = \int \big({\rho_2}^2 + {\rho_3}^2\big) dm$$

$$J_{22} = \int \big({\rho_1}^2 + {\rho_3}^2\big) dm$$

$$J_{33} = \int \big({\rho_1}^2 + {\rho_2}^2\big) dm$$

$$J_{12} = J_{21} = -\int \rho_1 \rho_2 dm$$

$$
\begin{aligned}
J_{13} = J_{31} = -\int \rho_1\rho_3 dm \\
J_{23} = J_{32} = -\int \rho_2\rho_3 dm
\end{aligned} \tag{3.42}
$$

The angular momentum vector can be expressed as,

$$\vec{H} = H_1\vec{b_1} + H_2\vec{b_2} + H_3\vec{b_3} \tag{3.43}$$

$$\begin{bmatrix} H_1 \\ H_2 \\ H_3 \end{bmatrix} = \begin{bmatrix} J_{11} & J_{12} & J_{13} \\ J_{21} & J_{22} & J_{23} \\ J_{31} & J_{32} & J_{33} \end{bmatrix} \begin{bmatrix} \omega_1 \\ \omega_2 \\ \omega_3 \end{bmatrix} \tag{3.44}$$

$$H = J\omega \tag{3.45}$$

According to eqn.(3.35), the angular momentum of a rigid body about its center of mass is given as,

$$\vec{M} = \dot{\vec{H}} \tag{3.46}$$

$\vec{H} \rightarrow$ Angular momentum vector of a rigid body about its center of mass
$\vec{M} \rightarrow$ External moment acting along the body about its center of mass.

$$\dot{\vec{H}} = \left(\frac{dH}{dt}\right)_N = \left(\frac{dH}{dt}\right)_B + \vec{\omega} \times \vec{H} \tag{3.47}$$

Therefore rotational dynamics equation about the center of mass of a rigid body,also called as *Euler Moment Equation*, is given by,

$$\vec{M} = \left(\frac{dH}{dt}\right)_B + \vec{\omega} \times \vec{H} \tag{3.48}$$

Let $\vec{M}$, $\vec{H}$ and $\vec{\omega}$ can be expressed in terms of the basis vectors of the body fixed frame as,

$$
\begin{aligned}
\vec{M} &= M_1\vec{b_1} + M_2\vec{b_2} + M_3\vec{b_3} \\
\vec{H} &= H_1\vec{b_1} + H_2\vec{b_2} + H_3\vec{b_3} \\
\vec{\omega} &= \omega_1\vec{b_1} + \omega_2\vec{b_2} + \omega_3\vec{b_3}
\end{aligned}
$$

Substituting these into eqn.(3.48),

$$\begin{bmatrix} M_1 \\ M_2 \\ M_3 \end{bmatrix} = \begin{bmatrix} \dot{H}_1 \\ \dot{H}_2 \\ \dot{H}_3 \end{bmatrix} + \begin{bmatrix} 0 & -\omega_3 & \omega_2 \\ \omega_3 & 0 & -\omega_1 \\ -\omega_2 & \omega_1 & 0 \end{bmatrix} \begin{bmatrix} H_1 \\ H_2 \\ H_3 \end{bmatrix} \tag{3.49}$$

since

$$\begin{bmatrix} H_1 \\ H_2 \\ H_3 \end{bmatrix} = \begin{bmatrix} J_{11} & J_{12} & J_{13} \\ J_{21} & J_{22} & J_{23} \\ J_{31} & J_{32} & J_{33} \end{bmatrix} \begin{bmatrix} \omega_1 \\ \omega_2 \\ \omega_3 \end{bmatrix}$$

therefore

$$\begin{bmatrix} M_1 \\ M_2 \\ M_3 \end{bmatrix} = \begin{bmatrix} J_{11} & J_{12} & J_{13} \\ J_{21} & J_{22} & J_{23} \\ J_{31} & J_{32} & J_{33} \end{bmatrix} \begin{bmatrix} \dot{\omega}_1 \\ \dot{\omega}_2 \\ \dot{\omega}_3 \end{bmatrix} + \begin{bmatrix} 0 & -\omega_3 & \omega_2 \\ \omega_3 & 0 & -\omega_1 \\ -\omega_2 & \omega_1 & 0 \end{bmatrix} \begin{bmatrix} J_{11} & J_{12} & J_{13} \\ J_{21} & J_{22} & J_{23} \\ J_{31} & J_{32} & J_{33} \end{bmatrix} \begin{bmatrix} \omega_1 \\ \omega_2 \\ \omega_3 \end{bmatrix} \tag{3.50}$$

Let

$$\Omega = \begin{bmatrix} 0 & -\omega_3 & \omega_2 \\ \omega_3 & 0 & -\omega_1 \\ -\omega_2 & \omega_1 & 0 \end{bmatrix}$$

Then Equation 3.50 becomes

$$J\dot{\omega} + \Omega J\omega = M \tag{3.51}$$

or

$$J\dot{\omega} + \omega \times J\omega = M \tag{3.52}$$

Eqn. (3.52) is the **Dynamic equation of a satellite**, where M is the total external moment acting on the satellite. That is equivalent to the total external torque acting on it. i.e., $M \equiv T$. Then eqn. (3.52) becomes,

$$J\dot{\omega} + \omega \times J\omega = T \tag{3.53}$$

In case of principal axis reference frame, the Euler's rotational equation of the motion of satellite(3.53) become,

$$\begin{aligned} J_1\dot{\omega}_1 - \big(J_2 - J_3\big)\omega_2\omega_3 &= T_1 \\ J_2\dot{\omega}_2 - \big(J_3 - J_1\big)\omega_3\omega_1 &= T_2 \\ J_3\dot{\omega}_3 - \big(J_1 - J_2\big)\omega_1\omega_2 &= T_3 \end{aligned} \tag{3.54}$$

These are the three coupled nonlinear ordinary differential equations for state variables ω_1, ω_2, ω_3 of a rigid body, in which J_1, J_2 and J_3 are the principal moments of inertia.

Consider the case, where reaction wheel is used as actuator. Let $h_w \rightarrow$ the angular momentum of the reaction wheel
Then the dynamic equation given in (3.53) becomes,

$$J\dot{\omega} + \omega \times (J\omega + h_w) + \dot{h_w} = T \tag{3.55}$$

Now external torque 'T', as described in eqns. (3.53),(3.55), can be broken into two parts namely,

1. External control torque acting on satellite(T_e)
2. External disturbance torque(T_d)

Therefore eqn. (3.55) can be modified as,

$$J\dot{\omega} + \omega \times (J\omega + h_w) + \dot{h_w} = T_e + T_d \tag{3.56}$$

3.3 Modelling of Reaction Wheels

A reaction wheel is an electromechanical device composed of an electric motor that drives a disc or wheel. The wheel is designed to have a large moment of inertia for the mass it contain. The motor is integrated within the wheel structure [50].

Reaction wheel based attitude control is governed by the principle of Law of Conservation of Angular Momentum. i.e. "When the external torque acting on a system about a given axis is zero, the angular momentum of the system about that axis remains constant". Therefore in a closed system, angular momentum can be exchanged between objects, but total angular momentum before and after exchange remains constant.

In satellites, reaction wheels are simple disks or rotors that are spun by an electric motor. When the motor applies a torque to speed up or slow down the rotor, it produces a reacting torque on the body of the satellite. Since the satellite is a closed system, the total angular momentum of the system i.e. the angular momentum of the satellite body plus reaction wheel remains constant.

Thus, any change in the angular momentum of the reaction wheel results in an equal and opposite change in the angular momentum of the satellite body.

3.3.1 Configurations of Reaction Wheel

There are various configurations of reaction wheels for satellite attitude control. Three reaction wheel and four reaction wheel configurations are the commonly used configuration for reaction wheel mounting.

3.3.1.1 Three Reaction Wheel

In this configuration, Reaction wheels are mounted along the principal axis direction so that it can contribute momentum along its mounting axis. For an example, if a wheel is mounted along x-axis direction, it will contribute momentum change only in the x direction. This model is simple, however if wheel failure happens the body loses its controllability about the mounting axis. Also zero momentum condition can achieved only by providing zero momentum to each of the reaction wheel.

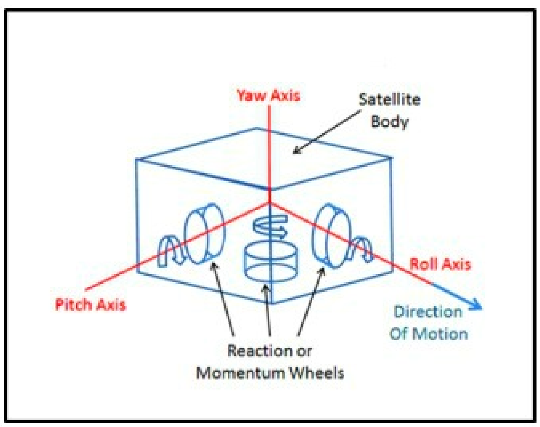

Figure 3.4: Three Reaction Wheel Configuration [3]

3.3.1.2 Four Reaction Wheel

In this configuration, wheels are mounted in pyramidal/tetrahedral configuration with respect to satellite body axis. In a four reaction wheel configuration each wheel will contribute momentum for all the three body axis.Figure 3.5. shows reaction wheel assembly of 4 wheels in pyramidal configuration. The main advantage of four reaction wheel configuration over the three reaction wheel configuration is zero momentum can be achieved

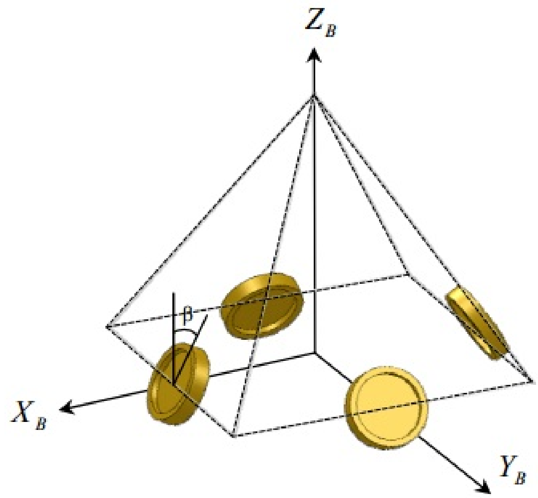

Figure 3.5: Four Reaction Wheel Configuration [3]

with all the four wheels are rotated in same speed but in opposite direction, alternately. It is possible to handle the reaction wheel failure efficiently in this configuration, and such configuration of reaction wheels increases the reliability and avoid saturation related issues.

3.3.2 Reaction Wheel as Actuator

In this project, Reaction wheel is selected as the actuator [3]. The reaction wheel has a simple structure and hence it is the most commonly used actuator for spacecraft. Also, for accurate attitude control systems and moderately fast maneuvers, Reaction Wheels are well suited because they allow continuous and smooth control. The disturbing torques related with reaction wheels are comparatively very low. Reaction wheels provide torques about three body axes.

3.3.2.1 Reaction wheel aligned with satellite coordinate system

Assume that the axis of the reaction wheels are aligned with the satellite body coordinate system. Let J_w denotes the moment of inertia of the reaction wheel, ω_w is the angular velocity of the wheel, h_w is the angular momentum of the wheel and h_{sbc} be the angular momentum of the wheel measured in satellite body coordinates. Then the torque produced by the reaction wheel is given by,

$$\dot{h}_{sbc} = \frac{d\big(J\omega_w\big)}{dt} = T_w \tag{3.57}$$

Therefore the control torque on the satellite is given by,

$$Tc = -\dot{h}_{sbc} = -\frac{d(J\omega_w)}{dt} \tag{3.58}$$

3.3.2.2 Reaction wheel aligned in other direction

When the reaction wheel is aligned with some other direction other than the axis of the satellite body coordinate system then the angular momentum vector of the wheel with respect to satellite coordinate system can be find out using a rotation from wheel coordinates to satellite body coordinates.

$$\begin{bmatrix} h_1 \\ h_2 \\ h_3 \end{bmatrix}_{sbc} = \begin{bmatrix} a_{11} & a_{12} & a_{13} \\ a_{21} & a_{22} & a_{23} \\ a_{31} & a_{32} & a_{33} \end{bmatrix} \begin{bmatrix} h_{w1} \\ h_{w2} \\ h_{w3} \end{bmatrix} \tag{3.59}$$

In vector form,

$$h_{sbc} = A_w h_w \tag{3.60}$$

where the matrix A_w is called transformation matrix or distribution matrix. The number of columns of the distribution matrix is the number of reaction wheel in the satellite system. If the reaction wheel assembly consists of four wheels then,

$$h_{sbc} = \begin{bmatrix} h_1 \\ h_2 \\ h_3 \end{bmatrix}_{sbc} = \begin{bmatrix} a_{11} & a_{12} & a_{13} & a_{14} \\ a_{21} & a_{22} & a_{23} & a_{24} \\ a_{31} & a_{32} & a_{33} & a_{34} \end{bmatrix} \begin{bmatrix} h_{w1} \\ h_{w2} \\ h_{w3} \\ h_{w4} \end{bmatrix} \tag{3.61}$$

3.3.3 Actuator Dynamics

Reaction Wheels consist of a DC motor with a flywheel. It is assumed that each reaction wheel has a torque limit and an angular momentum limit. That leads to an additional problem regarding with saturation. Let T_w be the torque provided by the flywheel assembly and T_c be the output torque provided by the reaction wheel actuator. Then the dynamic relation between T_w and T_c is given by the equation

$$\begin{aligned} \tau_w \ddot{h} &= -\dot{h} + T_w \\ T_c &= -\dot{h} \\ h(t) &= \int_0^t \dot{h}(\tau) d\tau + h(0) \end{aligned} \tag{3.62}$$

where τ_w is the time constant of reaction wheel and h_{sbc} is denoted by h for simplicity. In Laplace domain, the control torque can be written as,

$$T_c(s) = -\frac{1}{1 + s\tau_w} T_w(s) \tag{3.63}$$

Remark 3.2. *In this work, satellite model considered consists of 3 reaction wheels aligned along satellite body coordinates and this reaction wheel assembly is used as actuator, which provides necessary control torque on the satellite. So, $h = h_w$ can be considered.*

Therefore $T_e = 0$ in this problem and $T_c = -\dot{h}_w$ is the only control torque (internal) acting on the satellite. Hence modified attitude dynamics of satellite with control torque applied from reaction wheel assembly is as following,

$$J\dot{\omega} + \omega \times (J\omega + h_w) = T_c + T_d \tag{3.64}$$

3.4 Combined Nonlinear Model

Combining equations (3.64),(3.27),(3.62) overall non linear model of angular motion of satellite is obtained. The model is given as below:

$$\frac{d}{dt}\begin{bmatrix} \omega \\ q \\ q_4 \\ h_w \\ \dot{h}_w \end{bmatrix} = \begin{bmatrix} J^{-1}(-\omega \times (J\omega + h_w) + T_c + T_d) \\ -\frac{1}{2}\omega \times q + \frac{1}{2} q_4 I_{3\times 3}\omega \\ -\frac{1}{2}\omega^T q \\ -T_c \\ -\frac{1}{\tau_w}\dot{h}_w + \frac{1}{\tau_w} T_w \end{bmatrix} \tag{3.65}$$

In the above eqn. vector notation ‘ $\rightarrow'$ has been dropped from the vector quantities and same notation has been continued throughout the remaining part of this project. So, q means here vector part of a quaternion i.e. $q = [q_1, q_2, q_3]^T$ for example.

3.5 Linearization of Mathematical Model

For design of linear controllers, proposed in the next chapter , mathematical model of the satellite is to be linearized about the chosen operating point.

To linearize satellite model, the non linear model (3.65) is considered with state vector x defined as, $x = [\omega, q, h_w, \dot{h}_w]^T$.

Let the steady state point of operation of the system be denoted by $\bar{x} = [\bar{\omega}, \bar{q}, \bar{h}_w, \bar{\dot{h}}_w]^T$ and deviation from operating point is denoted by Δ before variables namely $\Delta x = [\Delta\omega, \Delta q, \Delta h_w, \Delta\dot{h}_w]^T$. Then state space model of linearized satellite model is given as below [50],

$$\Delta\dot{x}(t) = A(t)\Delta x(t) + B_u(t)\Delta T_w(t) + B_d\Delta T_d(t) \tag{3.66}$$

where jacobian matrices $A_{ij} = \frac{\partial f_i}{\partial x_j}$ and $B_{ij} = \frac{\partial f_i}{\partial u_j}$ (in this work u denotes T_w which equals to $[T_{w1}, T_{w2}, T_{w3}]^T$ and f is given by,

$$f = \begin{bmatrix} J^{-1}(-\omega \times (J\omega + h_w) + T_c + T_d) \\ -\frac{1}{2}\omega \times q + \frac{1}{2}q_4 I_{3\times3}\omega \\ -\frac{1}{2}\omega^T q \\ -T_c \\ -\frac{1}{\tau_w}\dot{h}_w + \frac{1}{\tau_w}T_w \end{bmatrix} \tag{3.67}$$

Using (3.67), matrices A, B_u, B_d are calculated as,

$$A = \begin{bmatrix} J^{-1}A_w & 0_{3\times3} & J^{-1}A_h & -J^{-1} \\ \frac{1}{2}I_{3\times3} & 0_{3\times3} & 0_{3\times3} & 0_{3\times3} \\ 0_{3\times3} & 0_{3\times3} & 0_{3\times3} & 0_{3\times3} \\ 0_{3\times3} & 0_{3\times3} & 0_{3\times3} & -\frac{1}{\tau_w}I_{3\times3} \end{bmatrix} \tag{3.68}$$

and

$$B_u = \begin{bmatrix} 0_{3\times3} \\ 0_{3\times3} \\ 0_{3\times3} \\ -\frac{1}{\tau_w}I_{3\times3} \end{bmatrix}, B_d = \begin{bmatrix} J^{-1} \\ 0_{3\times3} \\ 0_{3\times3} \\ 0_{3\times3} \end{bmatrix}$$

The inertia matrix of satellite J is given by,

$$J = \begin{bmatrix} J_{11} & 0 & 0 \\ 0 & J_{22} & 0 \\ 0 & 0 & J_{33} \end{bmatrix} \tag{3.69}$$

Remark 3.3. *Throughout this work, satellite body coordinate system is considered to be aligned along principal axis*

In eqn. (3.68),

$$A_w = \begin{bmatrix} 0 & \omega_3(J_{33} - J_{22}) - h_{w3} & \omega_2(J_{33} - J_{22}) + h_{w2} \\ \omega_3(J_{11} - J_{33}) + h_{w3} & 0 & \omega_1(J_{11} - J_{33}) - h_{w1} \\ \omega_2(J_{22} - J_{11}) - h_{w2} & \omega_1(J_{22} - J_{11}) + h_{w1} & 0 \end{bmatrix} \tag{3.70}$$

, and

$$A_h = \begin{bmatrix} 0 & \omega_3 & -\omega_2 \\ -\omega_3 & 0 & \omega_1 \\ \omega_2 & -\omega_1 & 0 \end{bmatrix} \tag{3.71}$$

The above expressions of state matrices A, B_u, B_d are to be evaluated at the chosen operating point namely, $\bar{x} = [\bar{\omega}, \bar{q}, \bar{h_w}, \bar{\dot{h_w}}]^T$.

3.5.1 Linearization Parameters

Parameters	Value
$\bar{q}$	$[0\ \ 0\ \ 0\ \ 1]$
$\bar{w}$	$[0.02\ \ -0.07\ \ 0.05]$
$\bar{h_w}$	$[0\ \ 0\ \ 0]$
$\bar{\dot{h}}_w$	$[0.02\ \ -0.07\ \ 0.05]$
Inertia matrix of satellite	$diag[50, 75, 100]$
Time constant of the reaction wheel	100 ms

Table 3.1: Parameters for Linearization

3.5.2 Transfer Function Representation

The linearized satellite model with reaction wheel assembly has $T_w = [T_{w1}, T_{w2}, T_{w3}]^T$ as input torque and vector part of quaternion $q = [q_1, q_2, q_3]^T$ as output. Therefore the whole model of satellite system consists 3 inputs and 3 outputs, when formulated in laplace domain, linearized systems contains 9 transfer functions namely, T_{w1} input q_1 output, T_{w2} input q_1 output, T_{w2} input q_1 output, T_{w1} input q_2 output, T_{w2} input q_2 output,T_{w3} input q_2 output, T_{w1} input q_3 output,T_{w2} input q_3 output, T_{w3} input q_3 output. Out of these 9 transfer functions, the transfer functions T_{w1} input q_1 output, T_{w2} input q_2 output, T_{w3} input q_3 output are direct axis transfer functions in the sense that these transfer functions have input and output along same axis. While remaining transfer functions are cross axis transfer functions i.e. input and output are along different axes. For the given linearization parameters , magnitude of cross axis transfer functions are negligible. Hence only 3 controllers to be designed for 3 direct axis transfer functions. They are given as below,

- For T_{w1} input and q_1 output, corresponding transfer function is,

$$G_1(s) = \frac{0.1}{s^3 + 10s^2} \tag{3.72}$$

- For T_{w2} input and q_2 output, corresponding transfer function is,

$$G_2(s) = \frac{0.06667}{s^3 + 10s^2} \tag{3.73}$$

- For T_{w3} input and q_4 output, corresponding transfer function is,

$$G_3(s) = \frac{0.05}{s^3 + 10s^2} \tag{3.74}$$

3.6 Summary

In this chapter, the non linear of satellite is developed, which consists of two parts: Kinematics and Dynamics. Different methods have been proposed to formulate the kinematics of satellite. Conservation of angular momentum has been used to model the attitude dynamics of satellite. Finally the non linear model of satellite is linearized around the equilibrium point. Further three axis transfer functions for the satellite model, have been derived from the linearized model.

Chapter 4

Linear Controller Design

4.1 Introduciton

There are different methods existing for controlling the attitude of satellite. They can be broadly classified as: *Passive Attitude Control* technique and *Active Attitude Control* technique. *Spin stabilization, Gravity gradient stabilization, Aerodynamic stabilization, Solar pressure stabilization* comes under passive attitude control technique. Therefore passive attitude control is based on external disturbance torques acting on satellite, where as Active attitude control is based on feedback control theory. 'Attitude Determination & Control' (ADCS) subsystem is designed under this category.

The main disadvantage of passive attitude control methods is that, this type of control methods have poor accuracy and inflexibility to condition/ environment change. Also stability is not guaranteed in these methods as environment and other effect can induce induce unwanted attitude maneuver in passively stabilized body. Additional damping system is needed to augment such effect. Therefore, active stabilization method also known as *three axis attitude control* has been chosen in this work.

Now the single axis transfer function of the linearized satellite model, is of the form $G(s) = \frac{1}{Js^2}$ (J being the satellite's moment of inertia). The transfer function has two poles at the origin. Therefore PI based control laws can lead the system to instability. Hence in this work, PD based control laws are proposed namely,

- PD control law
- PD^{β} control law
- PD Sliding Mode Control Law
- PD Sliding Mode Control Law with Modified Reaching law

- PD^β Sliding Mode Control Law

- PD^β Sliding Mode Control Law with Modified Reaching law

Among all these controllers, linear controllers(PD and PD^β) are the topics of discussion of this chapter. Rest are discussed in the next chapter.

4.2 Generalized Block Diagram Representation

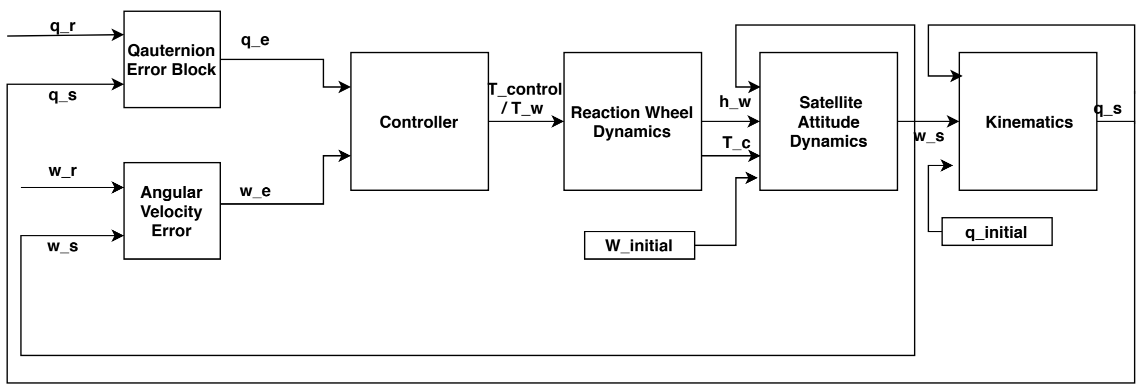

Figure 4.1: Block Diagram of Linear Attitude Control System

Block diagram 4.1. depicts the general structure of the linear attitude control system of satellite. Internal structure of controller block will vary depending on whether it is integer order or fractional order controller.In the block diagram 4.1., Reaction wheel dynamics, Satellite Dynamics and Kinematics blocks are developed based on the equations formulated in previous chapter. $T_{control}$ is the output of controller, which is also the torque acting on the reaction wheel rotor(T_w). h_w denotes angular momentum of reaction wheel assembly and T_c is the torque applied on satellite from reaction wheel assembly, as described in previous chapter.Angular velocity and quaternion Initial conditions are provided to satellite dynamics block and kinematics block using $\omega_{initial}$ and q_{intial} blocks respectively.
Considering above block diagram,we now define followings , which will be used throughout this project.

- Error quaternion (q_{er}) is a 4×1 vector defined as below,
  Let q_s and q_r be the measured and reference satellite quaternions. Then error quater-

nion is defined as[**?**],

$$q_{er} = q_s^{-1} \otimes q_r = \begin{bmatrix} q_{s4} & q_{s1} & q_{s2} & q_{s3} \\ -q_{s1} & q_{s4} & q_{s3} & -q_{s2} \\ -q_{s2} & -q_{s3} & q_{s4} & q_{s1} \\ -q_{s3} & q_{s2} & -q_{s1} & q_{s4} \end{bmatrix} \begin{bmatrix} q_{r4} \\ q_{r1} \\ q_{r2} \\ q_{r3} \end{bmatrix} = \begin{bmatrix} q_{e1} \\ q_{e2} \\ q_{e3} \\ q_{e4} \end{bmatrix} \tag{4.1}$$

Where $\otimes$ denotes quaternion multiplication.
Vector part of error quaternion(shown in block diagram) is denoted by q_e, which equals to $[q_{e1}, q_{e2}, q_{e3}]^T$.

- Angular velocity error(ω_e) is defined as,

$$\omega_e = \omega_r - \omega_s = \begin{bmatrix} \omega_{e1} \\ \omega_{e2} \\ \omega_{e3} \end{bmatrix} \tag{4.2}$$

Where $\omega_r = \begin{bmatrix} \omega_{rx} \\ \omega_{ry} \\ \omega_{rz} \end{bmatrix}$ reference angular velocity and $\omega_s = \begin{bmatrix} \omega_{sx} \\ \omega_{sy} \\ \omega_{sz} \end{bmatrix}$ satellite angular velocity.

4.3 Control Design Approach

Before designing the linear controller laws, we consider the fact that operation of satellite is dependent on power generated by on-board batteries and solar panels. Hence it is always preferable to minimize power consumed by the ADCS , for precise operation of satellite up to the specific period of time. Therefore, Control Effort ($\|\vec{u}(t)\|_2^2$) Minimization has been chosen as objective while designing linear the controller.
$\|\vec{u}(t)\|_2^2$ is defined as below,

$$\begin{aligned} \|\vec{u}(t)\|_2^2 &= \|\vec{u}_1(t)\|_2^2 + \|\vec{u}_2(t)\|_2^2 + \|\vec{u}_3(t)\|_2^2 \\ &= \int_0^\infty |\vec{u}_1(t)|^2 dt + \int_0^\infty |\vec{u}_2(t)|^2 dt + \int_0^\infty |\vec{u}_3(t)|^2 dt \end{aligned} \tag{4.3}$$

where $\vec{u}(t)$ is the output of the controller acting in close loop (same as $T_{control}$ or T_w in figure 4.1). Hence, We formulate the general optimization problem for linear controller design as following,

minimize $\quad \|\vec{u}(t)\|_2^2$
subject to $\quad$ Conditions specified below, from (4.4) to (4.6)

Frequency domain approach has been used in this work to set up the constraints of the optimization problem discussed above. 3 frequency domain specifications are discussed here in general namely, *phase margin specification*, *Isodamping condition* and *gain crossover frequency specification*.

Suppose the plant transfer function be $G(s)$ and the controller transfer function be $G_c(s)$. Then all three frequency domain specifications mentioned above can be listed as,

4.3.1 Phase Margin Specification

$$Arg[G(j\omega_{gc})G_c(j\omega_{gc})] + \pi < \phi_m \tag{4.4}$$

where ϕ_m is the specified upper limit of the required phase margin, ω_{gc} is the required gain crossover frequency

4.3.2 Gain Crossover Frequency Specification

At gain crossover frequency ω_{gc}, open loop transfer function $G(s)G_c(s)$ satisfies following condition,

$$|G(j\omega_{gc})G_c(j\omega_{gc})| = 1 \tag{4.5}$$

4.3.3 Isodamping Condition

This condition also termed as 'robustness to gain variations' is given as below,

$$\left.\frac{d(Arg[G(j\omega)G_c(j\omega)])}{d\omega}\right|_{\omega=\omega_{gc}} = 0 \tag{4.6}$$

This condition satisfies phase flatness around gain crossover frequency, hence ensuring robustness against gain changes and overshoot of time domain response remains same.

Remark 4.1. *Number of specifications to be used for controller design, will be decided depending on the structure of the controller.*

4.4 Proportional Derivative Controller (PD)

Mathematical of model satellite, as given by eqn. (3.65) is non linear in in nature, where as PD controller is a linear controller. Therefore linearized model of satellite has to be taken into account.

4.4.1 Formulation of Optimization Problem

Let, the PD control structure for the linearized satellite model be,

$$G_{ci}(s) = K_{pi}(1 + K_{di}s) \qquad \forall i = 1(.)3 \tag{4.7}$$

where $i \implies$ any of the 3 axes.
Consider, $G_i(s)$ be the direct axis transfer function along any particular axis 'i'(Same design procedure is followed for all 3 axes). Then open loop transfer function is,

$$G_{op}(s) = K_{pi}(1 + K_{di}s)G_i(s) \tag{4.8}$$

For design of PD controller (4.7), having two parameters (K_{pi}, K_{di}), phase margin specification and gain crossover frequency specification are only considered. Hence equations (4.4) & (4.5) are evaluated for this open loop dynamics (4.8).

- From eqn. (4.4),

$$Arg[G_i(j\omega_{gc})] + Arg[G_{ci}(j\omega_{gc})] + pi < \phi_m \tag{4.9}$$

Now $Arg[G_{ci}(j\omega_{gc})] = \tan^{-1}(K_{di}\,\omega_{gc})$. Say $Arg[G_i(j\omega_{gc})]$ is denoted by $\angle G_i\Big|_{\omega_{gc}}$. Then from eqn. (4.9), phase margin specification is evaluated as,

$$\begin{aligned}
&\angle G_i\Big|_{\omega_{gc}} + \tan^{-1}(K_{di}\,\omega_{gc}) + \pi < \phi_m \\
&\implies \tan^{-1}(K_{di}\,\omega_{gc}) < \phi_m - \pi - \angle G_i\Big|_{\omega_{gc}} \\
&\implies \tan^{-1}(K_{di}\,\omega_{gc}) < A \\
&\implies K_{di}\,\omega_{gc} - \tan(A) < 0
\end{aligned} \tag{4.10}$$

Therefore, the phase margin constraint is simplified for PD controller as follows,

$$K_{di}\,\omega_{gc} - \tan(A) < 0 \tag{4.11}$$

where

$$A = \phi_m - \pi - \angle G_i\Big|_{\omega_{gc}} \tag{4.12}$$

- Now consider eqn. (4.5),

$$|G_i(j\omega_{gc})||G_{ci}(j\omega_{gc})| = 1 \tag{4.13}$$

Again $|G_{ci}(j\omega_{gc})| = K_{pi}\sqrt{1 + (K_{di}\omega_{gc})^2}$ (for $K_{pi} > 0$).

Therefore eqn. (4.13) simplifies to,

$$|G_i(j\omega_{gc})|K_{pi}\sqrt{1 + (K_{di}\,\omega_{gc})^2} - 1 = 0 \tag{4.14}$$

Hence optimization problem for design of PD controller, is constructed as following,

$$\begin{aligned} \text{minimize} \quad & \|\vec{u}(t)\|_2^2 \\ \text{subject to} \quad & K_{di}\,\omega_{gc} - \tan(A) < 0 \\ & |G_i(j\omega_{gc})|K_{pi}\sqrt{1 + (K_{di}\,\omega_{gc})^2} - 1 = 0 \quad \forall i = 1(.)3 \text{ \&A given in (4.25)} \end{aligned}$$

Remark 4.2. *Optimization problems are set up for all 3 axes separately.Gain values of 3 axis PD controller(K_{pi}, K_{di}) are to be obtained by solving those optimization problems.*

4.4.2 Control Law Design

Before solving the optimization problem constructed above, the parameters ω_{gc} and ϕ_m need to be chosen properly.

ω_{gc} is related to system bandwidth and ϕ_m related to damping of time domain response. Hence ω_{gc} should be less than resonance frequency of lowest bending mode and slosh mode, at the same time ω_{gc} should be large enough to have adequate bandwidth for system response [51].

Again ϕ_m should be chosen depending on the damping required in time domain response. In this work, ω_{gc} and ϕ_m are set as follows,

$$\omega_{gc} = 1\ rad/s \text{ and } \phi_m = 80^\circ$$

Finally optimization problem is solved (for each axis) using above values of ω_{gc} and ϕ_m.

PD control law for non linear satellite attitude dynamics model, is formulated as below[4],

$$T_{control} = 2K_P\, q_e + K_D\, \omega_e \tag{4.15}$$

Where $K_P = diag\{K_{p1}, K_{p2}, K_{p3}\}$ and $K_D = diag\{K_{D1}, K_{D2}, K_{D3}\}$
('Diag' means principal diagonal of a diagonal matrix)
and $K_{Di} = K_{pi}K_{di}\ \forall\ i = 1(.)3$. Other terms in eqn. (4.15) are explained previously.

4.5 Fractional Proportional Derivative Controller (PD^{β})

Fractional controllers are those which are described using fractional integrals and derivative operators. In various literature, fractional controllers are claimed to be superior compare to their integer order counterpart, in terms of performance indices. This project aims to verify those claims. First we briefly introduce Fractional Calculus concept. Followed by that, fractional control law is designed.

4.5.1 Fractional Calculus

In fractional calculus the generalization of fractional integral and derivative of order β with initial condition t_0 is [52],

$${}_{t_0}D_t^{\beta} = \begin{cases} \frac{d^{\beta}}{dt^{\beta}} & Re(\beta) > 0 \\ 1 & Re(\beta) = 0 \\ \int_{t_0}^{t} d\tau^{\beta} & Re(\beta) < 0 \end{cases} \tag{4.16}$$

Generally there are three common definitions followed in fractional calculus.

Definition 4.1. *The Caputo fractional derivative of the order α of a continuous function $f : R^{+} \to R$ is defined as,*

$$D^{\beta} f(t) = \begin{cases} \frac{1}{\Gamma(m-\beta)} \int_0^t \dfrac{f^{(\beta)}(\tau)}{(t-\tau)^{\beta-m+1}} d\tau & m-1 < \beta < m \\ \frac{d^m}{dt^m} f(t) & \beta = m \end{cases} \tag{4.17}$$

where m is the smallest integer bigger than β,
$\Gamma(x) = \int_0^{\infty} e^{-x} x^{n-1} dx$ *be the Gamma function.*

Definition 4.2. *Riemann-Liouville fractional integration of order β is defined as,*

$$J^{\beta}f(t) = \frac{1}{\Gamma(\beta)}\int_{a}^{t} f(\tau)(t-\tau)^{\beta-1}d\tau \tag{4.18}$$

where $\beta > 0$ and $t > a$.

Definition 4.3. *Riemann-Liouville fractional derivative of order β is defined as,*

$$D^{\beta}f(t) = \begin{cases} \frac{1}{\Gamma(n-\beta)}\frac{d^n}{dt^n}\int_a^t \dfrac{f(\tau)}{(t-\tau)^{\beta+1-n}}d\tau & n-1 < \beta < n \in N \\ \frac{d^n}{dt^n}f(t) & n = \beta \end{cases} \tag{4.19}$$

Throughout this work, Caputo's definition has been used to define fractional derivative terms.

4.5.2 Formulation of Optimization Problem

Consider the structure of PD^{β} fractional controller is of the form,

$$G_{cfi}(s) = K_{pi}(1 + K_{di}s^{\beta_i}) \qquad \forall\, i = 1(.)3 \tag{4.20}$$

Here s^{β} implies laplace form of fractional derivative of order β, with $0 < \beta < 1$. Hence open loop transfer function is given by,

$$G_{op}(s) = K_{pi}(1 + K_{di}s^{\beta_i})G_i(s) \tag{4.21}$$

Where $G_i(s)$ is one of the direct axis transfer functions as described in (4.8)
It is to be noted that same design procedure is to be followed for all 3 axes.
Now in case of PD^{β} controller, there are 3 parameters to be designed namely, K_p, K_d and β. Therefore, all 3 frequency domain conditions, (4.4)-(4.6) are considered.

- From eqn. (4.4) we can write,

$$Arg[G_i(j\omega_{gc})] + Arg[G_{cfi}(j\omega_{gc})] + pi < \phi_m \tag{4.22}$$

Now $Arg[G_{cfi}(j\omega_{gc})] = \tan^{-1}\dfrac{\sin\frac{(1-\beta_i)\pi}{2} + K_{di}\,\omega_{gc}^{\beta_i}}{\cos\frac{(1-\beta_i)\pi}{2}} - \dfrac{(1-\beta_i)\pi}{2}$ [52]
Hence from (4.22), the phase margin specification simplifies to,

$$
\begin{aligned}
&\angle G_i\Big|_{\omega_{gc}} + \tan^{-1}\frac{\sin\frac{(1-\beta_i)\pi}{2} + K_{di}\,\omega_{gc}^{\beta_i}}{\cos\frac{(1-\beta_i)\pi}{2}} - \frac{(1-\beta_i)\pi}{2} + \pi < \phi_m \\
\implies &\tan^{-1}\frac{\sin\frac{(1-\beta_i)\pi}{2} + K_{di}\,\omega_{gc}^{\beta_i}}{\cos\frac{(1-\beta_i)\pi}{2}} - \frac{(1-\beta_i)\pi}{2} < \phi_m - \angle G_i\Big|_{\omega_{gc}} \\
\implies &\tan^{-1}\frac{\sin\frac{(1-\beta_i)\pi}{2} + K_{di}\,\omega_{gc}^{\beta_i}}{\cos\frac{(1-\beta_i)\pi}{2}} - \frac{(1-\beta_i)\pi}{2} < A \\
\implies &\tan^{-1}\frac{\sin\frac{(1-\beta_i)\pi}{2} + K_{di}\,\omega_{gc}^{\beta_i}}{\cos\frac{(1-\beta_i)\pi}{2}} < \frac{(1-\beta_i)\pi}{2} + A \\
\implies &\frac{\sin\frac{(1-\beta_i)\pi}{2} + K_{di}\,\omega_{gc}^{\beta_i}}{\cos\frac{(1-\beta_i)\pi}{2}} < \tan(B) \\
\implies &K_{di}\,\omega_{gc}^{\beta_i} + \sin\frac{(1-\beta_i)\pi}{2} - \cos\frac{(1-\beta_i)\pi}{2}\tan(B) < 0
\end{aligned} \tag{4.23}
$$

where

$$B = \frac{(1-\beta_i)\pi}{2} + A \tag{4.24}$$

and A given by,

$$A = \phi_m - \pi - \angle G_i\Big|_{\omega_{gc}} \tag{4.25}$$

- Next consider the gain cross over condition (4.5),

$$|G_i(j\omega_{gc})||G_{cfi}(j\omega_{gc})| = 1 \tag{4.26}$$

Again magnitude of G_{cfi} at gain cross over frequency ω_{gc} is given by,

$|G_{cfi}(j\omega_{gc})| = K_{pi}\sqrt{(1 + K_{di}\,\omega_{gc}^{\beta_i}\cos\frac{\beta_i\pi}{2})^2 + (K_{di}\,\omega_{gc}^{\beta_i}\sin\frac{\beta_i\pi}{2})^2}$, for $K_{pi} > 0$.
Therefore eqn. (4.26) simplifies to,

$$|G_i(j\omega_{gc})|K_{pi}\sqrt{(1 + K_{di}\,\omega_{gc}^{\beta_i}\cos\frac{\beta_i\pi}{2})^2 + (K_{di}\,\omega_{gc}^{\beta_i}\sin\frac{\beta_i\pi}{2})^2} - 1 = 0 \tag{4.27}$$

- Finally consider the isodamping condition (4.6),

$$\frac{dArg[G_i(j\omega)]}{d\omega}\Big|_{\omega=\omega_{gc}} + \frac{dArg[G_{cfi}(j\omega)]}{d\omega}\Big|_{\omega=\omega_{gc}} = 0$$

$$\implies \frac{d\angle G_i}{d\omega}\Big|_{\omega_{gc}} + \frac{d\angle G_{cfi}}{d\omega}\Big|_{\omega_{gc}} = 0 \tag{4.28}$$

Now $\angle G_{cfi}\Big|_{\omega_{gc}} = \tan^{-1}\frac{\sin\frac{(1-\beta_i)\pi}{2} + K_{di}\,\omega_{gc}^{\beta_i}}{\cos\frac{(1-\beta_i)\pi}{2}} - \frac{(1-\beta_i)\pi}{2}$, which gives,

$$\frac{d\angle G_{cfi}}{d\omega}\Big|_{\omega_{gc}} = \frac{K_{di}\,\beta_i\,\omega_{gc}^{\beta_i-1}}{\cos\frac{(1-\beta_i)\pi}{2}(1+\tan^2 B)} \tag{4.29}$$

Hence using (4.29), isodamping condition(4.28) reduces to,

$$\frac{d\angle G_i}{d\omega}\Big|_{\omega_{gc}} + \frac{K_{di}\,\beta_i\,\omega_{gc}^{\beta_i-1}}{\cos\frac{(1-\beta_i)\pi}{2}(1+\tan^2 B)} = 0 \tag{4.30}$$

Therefore the optimization problem for PD^{β} controller design is formulated as following,

minimize $\quad \|\vec{u}(t)\|_2^2$

subject to $\quad K_{di}\,\omega_{gc}^{\beta_i} + \sin\frac{(1-\beta_i)\pi}{2} - \cos\frac{(1-\beta_i)\pi}{2}\tan(B) < 0$

$$|G_i(j\omega_{gc})|K_{pi}\sqrt{(1+K_{di}\,\omega_{gc}^{\beta_i}\cos\frac{\beta_i\pi}{2})^2 + (K_{di}\,\omega_{gc}^{\beta_i}\sin\frac{\beta_i\pi}{2})^2} - 1 = 0$$

$$\frac{d\angle G_i}{d\omega}\Big|_{\omega_{gc}} + \frac{K_{di}\,\beta_i\,\omega_{gc}^{\beta_i-1}}{\cos\frac{(1-\beta_i)\pi}{2}(1+\tan^2 B)} = 0$$

4.5.3 Control Law Design

For design of PD^{β} control law, above optimization problem needs to be solved.
In the optimization problem, The parameters ω_{gc} and ϕ_m are chosen same as the values chosen for PD controller.
We solve the optimization problems for 3 axes separately and K_p, K_d, β values obtained for each axis separately. Finally these gain values are used to construct fractional control law of the non linear satellite model as following,

$$T_{control} = 2K_P\,q_e + K_D\,D^{\beta-1}\omega_e \tag{4.31}$$

Where D^{β} is the fractional derivative operator and operator $D^{\beta} = [D^{\beta_1}, D^{\beta_2}, D^{\beta_3}]^T$ operates element wise on ω_e.
Also $K_P = diag\{K_{p1}, K_{p2}, K_{p3}\}$ and $K_D = diag\{K_{D1}, K_{D2}, K_{D3}\}$
where $K_{Di} = K_{pi}K_{di}, \forall\, i = 1(.)3$

4.6 Summary

In this chapter, linear controllers namely PD and PD^{β} are designed for satellite attitude control. Linearized model of satellite has been used for that purpose. For a particular control law, separate controllers have been designed for all the three direct axis transfer functions of the linearized satellite model. Parameters of each of the controllers are tuned using optimization method. Gain cross over frequency, phase margin and Isodamping conditions are used as constraints for tuning the controllers.

Chapter 5

Non Linear Controller Design

5.1 Introduction

Design approach for linear controllers is simple. But the problem with linear controllers, specifically for plants with non linear dynamics is that, design of linear controllers does not ensure the robustness condition. Also the linear controllers are designed for particular operating point. Hence they cannot provide satisfactory performance over a wide range of operating points, which is very crucial for dynamic systems like satellite or launch vehicle , where operating point changes with time.

All these problems can be overcome by nonlinear controllers. In this work, non linear controllers have been designed to verify the superiority of non linear controllers over the linear controllers.

Sliding mode based nonlinear controllers have been aproached in this work. The main advantages of sliding mode (discussed later) control laws are, *robustness towards parameter uncertainity* & *disturbance rejection* and *order reduction* during sliding phase (hence better assurance over the convergence of states towards origin).

From the satellite attitude control point of view, these properties of sliding mode control, exactly matches with the design requirement of ADCS i.e. satellite can operate without being affected by external disturbance torques, and satellite can withstand parameter variations (robustness).

In this work, 4 sliding mode based non linear control laws have been proposed. They are as following,

- PD Sliding Mode Control (PD-SMC)

- PD SMC with Modified Reaching Law

- Fractional PD Sliding Mode Control (PD^{β}-SMC)
- PD^{β}-SMC with Modified Reaching Law

5.2 Generalized Block Diagram Representation

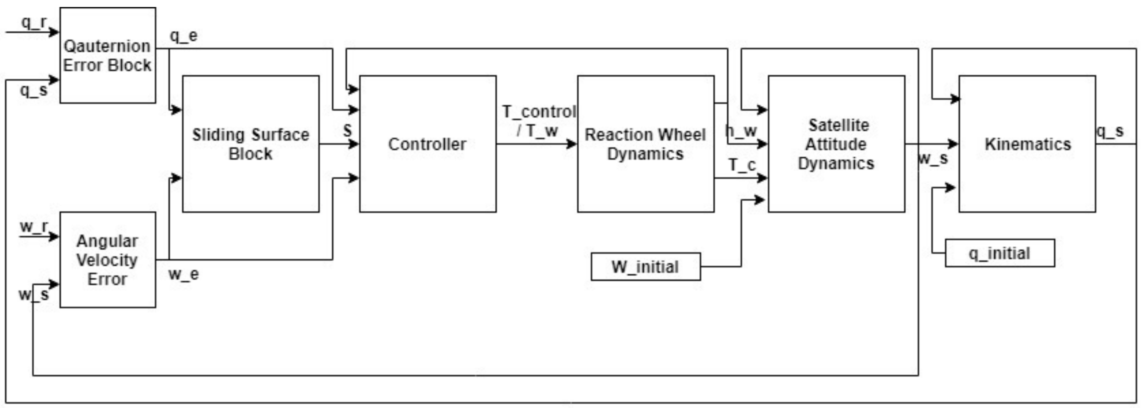

Figure 5.1: Block Diagram of Non Linear Attitude Control System

Block diagram 5.1. represents the generalized structure of the nonlinear attitude control system of satellite. Depending on the sliding surface and control law chosen, internal structures of sliding surface block and controller will vary. Apart from sliding surface block and controller block, other blocks in fig. 5.1, are same as in fig. 4.1. Therefore other blocks are not explained here again.

5.3 Brief Review on Sliding Mode Control

As the nonlinear control laws to be designed in this work are sliding mode based, therefore a brief introduction on sliding mode control is provided here [3].

Sliding Mode Control (SMC) is a nonlinear control that brings the system states into a surface known as sliding surface or sliding manifold, where the system states stay for all the time. Sliding manifold is a surface, where once the system states have reached there then it will converge to the desired states. SMC is a discontinuous control and the control signal switches from one structure to another based on the current position in the state space from the sliding surface(hence SMC is also termed as *variable structure control technique*.

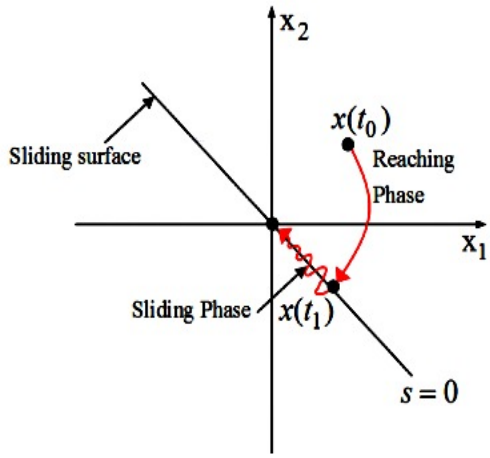

Figure 5.2: Sliding surface with sliding phases [3]

The phase trajectory of the SMC is having two phases: *Reaching phase* and *Sliding phase*, which is shown Figure 5.2. The trajectories that are starting from outside of the sliding surface are tends towards the sliding surface. This phase is known as reaching phase. After reaching the sliding surface the trajectory starts to move along the sliding surface towards the desired states. This phase is called sliding phase.

5.3.1 SMC Law Design

Design of sliding mode control comprises of two components [53]:

- Design of surface known sliding surface such that reduced ordered sliding motion satisfies design specifications imposed by the designer.
- Synthesis of control law, discontinuous about the sliding surface such that trajectories of the closed loop motion are directed towards surface, in other words control law must be such that sliding surface is attractive.

5.3.2 Advantages of Sliding Mode Control

- SMC has the ability to nullify the effect of certain kind parameter variations implicit in the input channel(known as *matched uncertainty*) and hence the SMC is robust.
- Also SMC has the capability to reject disturbance while sliding on the surface.
- Another advantage of sliding mode control is that reduction in order of the system while system is in sliding motion, which gives a better assurance on convergence of system states towards origin of sliding surface,

5.3.3 Chattering Effect

Although the advantages described above, make the sliding mode technique highly acceptable among the existing robust control methods, this method has flaw from the practical implementation point of view. In practical case, system states after reaching the sliding surface, will not stop but overshoot it. This behaviour is termed as *chattering*. There are mainly two reasons behind chattering:

- Un-modelled part in the dynamics(also known as parasitic dynamics)

- Finite Sampling time:
  In ideal case, sliding mode requires infinite sampling frequency. But in reality due to switching non idealities, system works on finite sampling time, which causes this chattering phenomenon.

5.3.3.1 Chattering Avoidance

We consider here switching operation to be the source of chattering. From the mathematical point of view signum function used for switching causes chattering.The chattering leads to low control accuracy, high wear of moving mechanical parts and wastage of energy. So chattering phenomenon should be avoided. The commonly used method to avoid chatter is *Boundary Layer Control*, which is basically to replace the signum function in the control signal with saturation function, which is given by:

$$sat(S,\phi) = \begin{cases} 1, & for \;\; S > \phi \\ \frac{S}{\phi}, & for \;\; |S| \leq \phi \\ -1, & for \;\; S < \phi \end{cases} \tag{5.1}$$

where ϕ is the thickness of boundary layer, S be the sliding surface.

As the value of ϕ approaches to zero, the saturation function become signum function. As ϕ reduces the chattering effect will increase. For high value of ϕ, chattering effect gets eliminated but it occurs in cost of loss of robustness property. Therefore boundary layer thickness should be chosen with care.
Now we discuss one by one all the non linear control laws mentioned at the beginning of these chapter.

5.4 Proportional Derivative Sliding Mode Controller (PD-SMC)

The name of this control law being $PD - SMC$ is followed from the fact that PD control law is incorporated in design of sliding surface to avail the advantages with PD control law. Aim of this work is to check that claim from the behaviour of the closed loop system.

Design of $PD - SMC$ consists of two phases namely,
(i)Design of Sliding Surface
(ii) Design of control law that stabilizes the system.
The objective of control law design is to attain desired quaternions and angular velocity, i.e. to make q_e, ω_e to zero.

5.4.1 Sliding Surface Design

As described before, choice of sliding surface(S) is followed from PD control law for 3 axis satellite attitude control [4],

$$S = 2K_P\, q_e + K_D\, \omega_e \tag{5.2}$$

where K_P, K_D are gain values of PD controller, S consists of 3 components namely,$[S_1, S_2, S_3]^T$.

5.4.2 Control Law Design

Followed by the theory of sliding mode control, $PD - SMC$ Control law can be broken into two parts,
(i) Equivalent control law(u_{eq})
(ii) Discontinuous Control Law($u_{discont}$)
Hence overall control torque is expressed as following,

$$T_{control} = u_{eq} + u_{discont} \tag{5.3}$$

Firstly, continuous part of control torque i.e. u_{eq} is designed, followed by design of $u_{discont}$.

5.4.2.1 Equivalent Control Design (u_{eq})

For design of u_{eq}, we use the fact that during sliding phase, discontinuous part of control law (function of sliding surface ‘S’) becomes 0, as during sliding phase $S = 0$. Therefore

only the equivalent control law acts during sliding phase.
From above discussion we can conclude that during sliding phase $\dot{S} = 0$. It implies that,

$$\dot{S} = 2K_P\, \dot{q}_e + K_D\, \dot{\omega}_e = 0 \tag{5.4}$$

Now followed by (3.27), we can write,

$$\dot{q}_{er} = \begin{bmatrix} \dot{q}_e \\ \dot{q}_{e4} \end{bmatrix} = \frac{1}{2} \begin{bmatrix} q_{e4}\omega_e - \omega_e \times q_e \\ -\omega_e^T q_e \end{bmatrix} \tag{5.5}$$

From above equation relation between $\dot{q}_e$ and ω_e can be written as,

$$\begin{aligned} \dot{q}_e &= \frac{1}{2}(q_{e4}\, \omega_e - \omega_e \times q_e) \\ &= \frac{1}{2} \begin{bmatrix} q_{e4} & -q_{e3} & q_{e2} \\ q_{e3} & q_{e4} & -q_{e1} \\ -q_{e2} & q_{e1} & q_{e4} \end{bmatrix} \omega_e \\ &= \frac{1}{2} Q_e \omega_e \end{aligned} \tag{5.6}$$

Therefore using eqns. (5.6) & (3.64), eqn. (5.4) can be simplified as,

$$\begin{aligned} & 2K_P.\frac{1}{2}Q_e\omega_e + K_D\, \dot{\omega}_e = 0 \\ \Longrightarrow \quad & K_P\, Q_e\omega_e + K_D J^{-1}[u_{eq} - \omega_e \times (J\omega_e + h_w)] = 0 \\ \Longrightarrow \quad & K_D J^{-1}[u_{eq} - \omega_e \times (J\omega_e + h_w)] = -K_P\, Q_e\omega_e \\ \Longrightarrow \quad & u_{eq} = \omega_e \times (J\omega_e + h_w) - \frac{K_P}{K_D} J Q_e \omega_e \end{aligned} \tag{5.7}$$

5.4.2.2 Discontinuous Control Design ($u_{discont}$)

Followed by the existing literature on sliding mode, we consider the discontinuous part of control law to be,

$$u_{discont} = -K sgn(S) \tag{5.8}$$

K represents gain of nonlinear control law. This structure of discontinuous law, helps to bring the states towards sliding surface within finite time.
Therefore, overall expression of control torque is given from eqns. (5.3),(5.7) & (5.8) as

below,

$$\begin{aligned} T_{control} &= u_{eq} - Ksgn(S) \\ \implies T_{control} &= \omega_e \times (J\omega_e + h_w) - \frac{K_P}{K_D} JQ_e\omega_e - Ksgn(S) \end{aligned} \tag{5.9}$$

where $sgn(S) = [sgn(S_x), sgn(S_y), sgn(S_z)]^T$, sgn denotes signum function.
K_p, K_D, K are the parameters to be tuned in this problem. Tuning method of these parameters is discussed in section (5.8).

5.4.3 Proof of Finite Time Convergence & Stability

To support the simulation results, it is sufficient to prove the finite time convergence (*Reachability Analysis*) and stability condition for the proposed $PD - SMC$ control law.

5.4.3.1 Proof of Finite Time Convergence

One of the requirement from the sliding mode based control law is that system should converge to sliding surface in finite time. Therefore it is necessary to prove that finite time convergence is ensured by the PD-SMC law proposed in 5.9.

A lemma has been stated [43] first, which will be useful in the proof of finite time convergence for all the sliding mode based non linear control laws proposed in this work.

Lemma 1. *Consider a continuous system: $\dot{x} = f(x), f(0) = 0, x \in \mathbb{R}^n$. Assume there exists a continuous positive definite function $V : \mathbb{R}^n \mapsto \mathbb{R}, a \in \mathbb{R}_+, \kappa \in (0,1)$ and there is a neighbourhood of origin $U_0 \subseteq \mathbb{R}^n$ such that,*

$$\dot{V}(x) + aV^{\kappa}(x) \leq 0, x \in U_0/\{0\} \tag{5.10}$$

i.e. $\dot{V}(x) + aV^{\kappa}(x)$ is negative semi-definite function. Then origin is a balance point which can be reached in finite time. If $U_0 = \mathbb{R}^n$, then origin is a global balance point, reachable in finite time duration.

Proof. Finite time convergence to the sliding surface is proved using *Lyapunov function method*. Therefore consider a Lyapunov function ,

$$V_{PD-SMC} = \frac{1}{2K_D} S^T JS, \tag{5.11}$$

Where $K_D > 0$ and J is moment of inertia matrix(hence positive defintie). Therefore $\frac{1}{K_D}J$ is positive definite matrix. S is the sliding surface defined incase of $PD - SMC$(5.2) law. Taking time derivative of both sides of (5.11),

$$
\begin{aligned}
\dot{V}_{PD-SMC} &= \frac{1}{K_D} S^T J \dot{S} \\
&= \frac{1}{K_D} S^T J (K_P Q_e \omega_e + K_D J^{-1}[T_{control} + T_d - \omega_e \times (J\omega_e + h_w)]) \\
&\qquad \text{(using (5.7))} \\
&= \frac{1}{K_D} S^T J (K_P Q_e \omega_e + K_D J^{-1}[\omega_e \times (J\omega_e + h_w) - \frac{K_P}{K_D} J Q_e \omega_e \\
&\quad - K sgn(S) + T_d - \omega_e \times (J\omega_e + h_w)]) \qquad \text{(using (5.9))} \\
&= \frac{1}{K_D} S^T J (K_P Q_e \omega_e + K_D J^{-1}[-\frac{K_P}{K_D} J Q_e \omega_e - K sgn(S) + T_d]) \\
&= \frac{1}{K_D} K_D S^T J J^{-1} (T_d - K sgn(S)) \\
&= -S^T (K sgn(S) - T_d) \qquad (5.12)
\end{aligned}
$$

If K is positive scalar such that $K \geq \|T_d\|_\infty$, then from (5.12),

$$
\begin{aligned}
\dot{V}_{PD-SMC} &\leq -\|S\|_1 \qquad (\eta \text{ reachability condition}) \\
\implies \dot{V}_{PD-SMC} &\leq -\|S\|_2 \\
\implies \dot{V}_{PD-SMC} &\leq -\sqrt{\frac{2K_D}{\lambda_{max}(J)}} V_{PD-SMC}^{\frac{1}{2}} \qquad \text{(from (5.11))} \qquad (5.13)
\end{aligned}
$$

Where λ_{max} is the maximum eigen value of J.Also, let $\eta = \sqrt{\frac{2K_D}{\lambda_{max}(J)}}$.
Then (5.13) gives,

$$\dot{V}_{PD-SMC} + \eta V_{PD-SMC}^{\frac{1}{2}} \leq 0 \qquad (5.14)$$

Since the function $\dot{V}_{PD-SMC} + \eta V_{PD-SMC}^{\frac{1}{2}}$ is negative semi-definite. Therefore from the lemma 1. stated above, we can conclude that system reaches sliding surface in finite time i.e. finite time convergence of the system is proved. □

5.4.3.2 Proof of Stability

After reaching the sliding surface, system states must slide towards origin. This is guaranteed by proving that system is stable during sliding motion.

Here first we state *Lyapunov Stability* theorem[54], which will be useful in the proof.

Theorem 5.1. *Consider, a system $\dot{x} = f(x)$ with a fixed point at x^*. Suppose we define a continuously differentiable, real valued function $V(x)$ (also called Lyapunov function) with the following properties:*

1. *$V(x) > 0 \, \forall \, x \neq x^*$ and $V(x^*) = 0$ i.e. $V(x)$ is positive definite.*
2. *$\dot{V} < 0 \, \forall x \neq x^*$ i.e. all trajectories downhill towqrds x^*.*

Then x^* is globally asymptotically stable and for all initial conditions $x(t) \to x^*$ as $t \to \infty$.

Proof. To prove the stability, we consider the fact that after reaching phase is over S becomes 0. Then from eqn. (5.2) we can write,

$$\begin{gathered} 2K_P q_e + K_D \omega_e = 0 \\ \Longrightarrow \omega_e = -2\frac{K_P}{K_D} q_e \end{gathered} \tag{5.15}$$

Now for proving the stability, we choose the Lyapunov function candidate to be,

$$V_q = \frac{1}{2} q_e^T q_e \tag{5.16}$$

Now differentiating (5.16) w.r.t time we get,

$$\begin{aligned} \dot{V}_q &= q_e^T \dot{q}_e \\ &= \frac{1}{2} q_e^T Q_e \omega_e && \text{(using (5.6))} \\ &= \frac{1}{2} q_e^T Q_e . (-2\frac{K_P}{K_D}) q_e && \text{(using (5.15))} \\ &= -\frac{K_P}{K_D} q_e^T Q_e q_e \\ &= -\frac{K_P}{K_D} q_{e4} \|q_e\|^2 \end{aligned} \tag{5.17}$$

Under the condition $K_P > 0, K_D > 0$, and also keeping $q_{e4} > 0$ always, we have $\dot{V}_q <= 0$. Hence V_q satisfies the following criterions:

1. $V_q > 0$ if $q_e \neq 0$

2. $V_q = 0$ if $q_e = 0$

3. $\dot{V}_q <= 0$, $\dot{V}_q$=0 if and only if $q_e = [0, 0, 0]^T$

By using Lyapunov's Theorem we can conlcude that, $q_e = [0, 0, 0]^T$ is asymptotically stable and $q_e \rightarrow$[0,0,0]^T is guaranteed.

□

5.4.4 Calculation of Reaching Time:

Let the time for reaching the sliding surface be t_{reach}. This t_{reach} is a performance index for sliding mode type controller. The expression for reaching time is analytically calculated as following. It is known that after reaching the sliding surface, $S = 0$. Hence Lyapunov function V_{PD-SMC} is also 0 after reaching sliding surface.

For simplicity in notation, let us denote V_{PD-SMC} by V_1. Now say V at t=0 be $V_1(S_0)$.Then from (5.14),

$$\begin{aligned}
& \dot{V}_1 \leq -\eta V_1^{\frac{1}{2}} \\
\implies \quad & \int_0^{t_{reach}} V_1^{-\frac{1}{2}} dV_1 \leq -\eta \int_0^{t_{reach}} dt \\
\implies \quad & -2\sqrt{V_1(S_0)} \leq -\eta t_{reach} \\
\implies \quad & t_{reach} \leq \frac{2}{\eta}\sqrt{V_1(S_0)} \qquad (5.18)
\end{aligned}$$

Hence expression for maximum reaching time is given by,

$$t_{reach}\Big|_{max} = \frac{2}{\eta}\sqrt{V_1(S_0)} \qquad (5.19)$$

Putting value of η in (5.19),

$$t_{reach}\Big|_{max} = \sqrt{\frac{2}{K_D}\ \lambda_{max}(J)\ V_1(S_0)} \qquad (5.20)$$

5.5 PD-SMC with Modified Reaching Law

The main disadvantage of sliding mode based control laws is Chattering effect. As discussed earlier *boundary layer control* technique is a method to reduce chattering. But disadvantage with boundary layer control is that sliding variable does not becomes zero. Now robustness property is ensured if and only if sliding surface is achieved (i.e. sliding variable becomes zero). Therefore we can conclude that boundary layer control reduces chattering in exchange of robustness property.

Another attractive solution present in literature, to address the chattering is power rate type reaching law.This law ensures increment in reaching speed when states are away from sliding surface, and decreases the speed when states are closer to sliding surface, causing reduction of chattering [6].

Therefore we incorporate power rate type reaching law with $PD - SMC$ law in this section with aim to check whether this modified law provides any further improvement in system performance.
Here sliding surface is kept same as in (5.2) i.e., $S = 2K_P\, q_e + K_D\, \omega_e$.
Modified reaching law selected in this work is as following,

$$\dot{S} = -K_m|S|^{\alpha} sgn(S) \tag{5.21}$$

where K_m is gain of modified reaching law and $0 < \alpha < 1$, $|S|^{\alpha} = diag\{|S_x|^{\alpha}, |S_y|^{\alpha}, |S_z|^{\alpha}\}$, α is the parameter that controls the convergence rate of the system states towards sliding surface.

5.5.1 Control Law Design

Modified reaching law in (5.21) is used to design control law ($T_{control}$).
From eqn (5.2) we have,

$$\dot{S} = 2K_P\, \dot{q}_e + K_D\, \dot{\omega}_e \tag{5.22}$$

Now comparing (5.22) with (5.21) we get,

$$\begin{aligned}
& 2K_P\, \dot{q}_e + K_D\, \dot{\omega}_e = -K_m|S|^{\alpha} sgn(S) \\
\implies \quad & 2K_P.\frac{1}{2}Q_e\omega_e + K_D\, \dot{\omega}_e = -K_m|S|^{\alpha} sgn(S) \qquad \text{(using (5.6))} \\
\implies \quad & K_P Q_e\omega_e + K_D J^{-1}[T_{control} - \omega_e \times (J\omega_e + h_w)] = -K_m|S|^{\alpha} sgn(S) \qquad (5.23)
\end{aligned}$$

Hence the expression of control torque for $PD-SMC$ with modified reaching law is given by,

$$T_{control} = \omega_e \times (J\omega_e + h_w) - \frac{K_P}{K_D} J Q_e \omega_e - \frac{K_m}{K_D} J |S|^{\alpha} sgn(S) \tag{5.24}$$

In this case 4 parameters are to be tuned namely, K_P, K_D, α, K_m. Tuning of K_P, K_D, K_m, α is discussed in section (5.8).

5.5.2 Proof of Finite Time Convergence & Stability

Finite Time Convergence & stability has been proved here for $PD - SMC$ law with modified reaching law.

5.5.2.1 Proof of Finite Time Convergence

Proof. For this proof, Lyapunov function is chosen as,

$$V_{mod} = \frac{1}{2} S^T S \tag{5.25}$$

Where S being the sliding surface used for $PD - SMC$ law with modified reaching law (5.2). From eqn. (5.25),

$$\begin{aligned} \dot{V}_{mod} &= S^T \dot{S} \\ \implies \dot{V}_{mod} &= S^T(-K_m |S|^{\alpha} sgn(S)) \qquad \text{(using (5.21))} \end{aligned} \tag{5.26}$$

IF $K_m > 0$, then the diagonal matrix $K_m |S|^{\alpha}$ is a positive definite. Hence from (5.26), using properties of quadratic function we get,

$$\begin{aligned} \dot{V}_{mod} &\leq -\|S\|_1 \\ \implies \dot{V}_{mod} &\leq -\|S\|_2 \\ \implies \dot{V}_{mod} &\leq -\sqrt{2} V_{mod}^{\frac{1}{2}} \qquad \text{(using (5.25))} \end{aligned} \tag{5.27}$$

Therefore,

$$\dot{V}_{mod} + \sqrt{2} V_{mod}^{\frac{1}{2}} \leq 0 \tag{5.28}$$

Again from finite time convergence lemma 1 , it can be inferred that sliding surface is achieved in finite time. □

5.5.2.2 Proof of Stability

Proof. For the stability proof, same steps need to be followed as discussed in previous case ($PD - SMC$) and finally it can be shown that the system is asymptotically stable. Therefore, the steps for the proof is not discussed here again. □

5.5.3 Calculation of Reaching Time

Denote V_{mod} (as defined in (5.25)) by V_2 for simplicity and also say V_2 at t=0 be $V_2(S_0)$ and t_{reach} be the reaching time. Then from (5.28) it follows,

$$\begin{aligned} & \dot{V}_2 \leq -\sqrt{2} V_2^{\frac{1}{2}} \\ \implies \quad & \int_0^{t_{reach}} V_2^{-\frac{1}{2}} dV_2 \leq -\sqrt{2} \int_0^{t_{reach}} dt \\ \implies \quad & -2\sqrt{V_2(S_0)} \leq -\sqrt{2} t_{reach} \\ \implies \quad & t_{reach} \leq \sqrt{2V_2(S_0)} \end{aligned} \tag{5.29}$$

Hence expression for maximum reaching time is given by,

$$t_{reach}\Big|_{max} = \sqrt{2V_2(S_0)} \tag{5.30}$$

5.6 Fractional Order PD Sliding Mode Controller($PD^\beta - SMC$)

Fractional order non linear controller laws are proposed here in this work. The main aim of such design is to testify the effect of fractional operator over the sliding mode control law. Design of $PD^\beta - SMC$ is similar to conventional SMC design. Therefore design of $PD^\beta - SMC$ consists of two stages namely,

(i) Design of Sliding Surface

(ii) Design of control law which makes system states attracted to the surface.

5.6.1 Sliding Surface Design

Design of sliding variable is followed from PD^β control law for satellite attitude control. Therefore,

$$S = 2K_P\, q_e + K_D D^\beta \omega_e \tag{5.31}$$

In the above eqn., K_P, K_D are the gain values of PD^β controller and D^β indicates *Caputo fractional derivative operator* of order β.

5.6.2 Control Law Design

Similar to $PD - SMC$ law design,here also control law design is followed from design of equivalent control law u_{eq} and then discontinuous law($u_{discont}$).

5.6.2.1 Equivalent Control Law Design (u_{eq})

Similar to PD-SMC, here also u_{eq} is derived by differentiating eqn. 5.31 w.r.t time and equating the derivative to 0.

$$\begin{aligned}
\dot{S} &= 2K_P\dot{q}_e + K_D D^\beta \dot{\omega}_e = 0 \\
\implies & \quad 2K_P.\frac{1}{2}Q_e\omega_e + K_D D^\beta \dot{\omega}_e = 0 \qquad \text{(using (5.6))} \\
\implies & \quad K_P Q_e \omega_e + K_D D^\beta J^{-1}[u_{eq} - \omega_e \times (J\omega_e + h_w)] = 0 \\
\implies & \quad K_D D^\beta J^{-1}[u_{eq} - \omega_e \times (J\omega_e + h_w)] = -K_P Q_e \omega_e \\
\implies & \quad u_{eq} = \omega_e \times (J\omega_e + h_w) - \frac{K_P}{K_D} J D^{-\beta} Q_e \omega_e
\end{aligned} \tag{5.32}$$

5.6.2.2 Discontinuous Control Law Design ($u_{discont}$)

Discontinuous part of control law is selected as following,

$$u_{discont} = -K_f D^{-\beta} sgn(S) \tag{5.33}$$

Where k_f is the gain of discontinuous control law.
Hence From eqns. (5.3),(5.32) & (5.33), we get the expression of net control torque as below,

$$T_{control} = \omega_e \times (J\omega_e + h_w) - \frac{K_P}{K_D} J D^{-\beta} Q_e \omega_e - K_f D^{-\beta} sgn(S) \tag{5.34}$$

Where K_P, K_D, K_f, β are the parameters to be designed. Method of design of this parameters is similar to K_P, K_D, K for $PD - SMC$. Design procedure of these parameters is discussed in section (5.8).

5.6.3 Proof of Finite Time Convergence & Stability

Finite time convergence towards sliding surface & stability in case of $PD^{\beta} - SMC$ law, are proved here.

5.6.3.1 Proof of Finite time Convergence

Proof. In this case, Lyapunov function used is chosen same as (5.11),

$$V_{PD^{\beta}-SMC} = \frac{1}{2K_D} S^T J S \tag{5.35}$$

Where S is the sliding surface for $PD^{\beta} - SMC$ law,as described by eqn. (5.31).

Now differentiating $V_{PD^{\beta}-SMC}$ w.r.t time we get,

$$\begin{aligned}
\dot{V}_{PD^{\beta}-SMC} &= \frac{1}{K_D} S^T J \dot{S} \\
&= \frac{1}{K_D} S^T J (K_P Q_e \omega_e + K_D D^{\beta} J^{-1} [T_{control} + T_d - \omega_e \times (J\omega_e + h_w)]) \\
& \qquad \text{(using (5.31))} \\
&= \frac{1}{K_D} S^T J (K_P Q_e \omega_e + K_D D^{\beta} J^{-1} [\omega_e \times (J\omega_e + h_w)] - \frac{K_P}{K_D} J D^{-\beta} Q_e \omega_e \\
& \quad - K_f D^{-\beta} sgn(S) + T_d - \omega_e \times (J\omega_e + h_w)]) \qquad \text{(using (5.34))} \\
&= \frac{1}{K_D} S^T J (K_P Q_e \omega_e + K_D D^{\beta} J^{-1} [-\frac{K_P}{K_D} J D^{-\beta} Q_e \omega_e - K_f D^{-\beta} sgn(S) + T_d]) \\
&= \frac{1}{K_D} K_D S^T J J^{-1} D^{\beta} (T_d - K_f D^{-\beta} sgn(S)) \\
&= -S^T (K_f sgn(S) - D^{\beta} T_d)
\end{aligned} \tag{5.36}$$

If K_f is positive scalar such that $K_f \geq \|D^{\beta} T_d\|_{\infty}$. Then from eqn. (5.36),

$$\begin{aligned}
\dot{V}_{PD^{\beta}-SMC} &\leq -\|S\|_1 \\
\implies \dot{V}_{PD^{\beta}-SMC} &\leq -\|S\|_2 \\
\implies \dot{V}_{PD^{\beta}-SMC} &\leq -\sqrt{\frac{2K_D}{\lambda_{max}(J)}} V^{\frac{1}{2}}_{PD^{\beta}-SMC} \qquad \text{(from (5.35))}
\end{aligned} \tag{5.37}$$

Let, $\eta_f = \sqrt{\dfrac{2K_D}{\lambda_{max}(J)}}$, then (5.37) simplifies to,

$$\dot{V}_{PD^{\beta}-SMC} + \eta_f V^{\frac{1}{2}}_{PD^{\beta}-SMC} \leq 0 \tag{5.38}$$

Using eqn. (5.38), finite time convergence to sliding surface is confirmed when $PD^{\beta} - SMC$ control law is used [43]. □

5.6.4 Proof of Stability

Before we prove stability, a theorem has been, which is basically modification of Lyapunov stability theorem for fractional order systems [49].

Theorem 5.2. *Let x=0 be an equilibrium point for a fractional order system and $U \subset \mathbb{R}^n$ be a domain containing the origin. Let $V(t, x(t))) : [0, \infty) \times U \to \mathbb{R}$ be a continuously differentiable function and locally Lipschitz with respect to x such that*

1. $\alpha_1 \|x\| \leq V(t, x(t)) \leq \alpha_2 \|x\|$
2. $D^q \, V(t, x(t)) \leq 0$

Where α_1, α_2 are positive constants . Then $x = 0$ is asymptotically stable for any $\|x_0\| \leq \gamma$ (x_0 being the initial value of x)

Proof. Stability is proved by making S equals to 0.

Hence from eqn. (5.31) we get,

$$\begin{aligned} & 2K_P q_e + K_D D^{\beta} \omega_e = 0 \\ \implies \quad & \omega_e = -\frac{2K_P}{K_D} D^{-\beta} q_e \\ \implies \quad & \omega_e = -\frac{2K_P}{K_D} \frac{1}{\Gamma(\beta)} \int_0^t (t-\tau)^{\beta-1} q_e(\tau) d\tau \end{aligned} \tag{5.39}$$

Taking the following inequality, $q_e(t) \leq q_e(0)$ into account, eqn. (5.39) can be further simplified as,

$$\begin{aligned} & \omega_e \leq -\frac{2K_P \, q_e(0)}{K_D \Gamma(\beta)} \int_0^t (t-\tau)^{\beta-1} d\tau \\ \implies \quad & \omega_e \leq -\frac{2K_P \, q_e(0)}{K_D \Gamma(\beta)} \frac{t^{\beta}}{\beta} \end{aligned} \tag{5.40}$$

Now consider Lyapunov function be,

$$V_{qfrac} = \frac{1}{2} q_e^T q_e \tag{5.41}$$

Applying fractional derivative operator D^{β} on both sides of eqn. (5.41) ,

$$\begin{aligned} D^{\beta} V_{qfrac} &= D^{\beta-1}(q_e^T \dot{q}_e) \\ &= \frac{1}{2} D^{\beta-1}(q_e^T Q_e \omega_e) && \text{(using 5.6)} \\ &\leq -\frac{K_P}{K_D\, \beta\, \Gamma(\beta)} D^{\beta-1}(q_e^T Q_e q_e(0) t^{\beta}) && \text{(using (5.40))} \end{aligned} \tag{5.42}$$

Now consider the following inequality

$$q_e^T Q_e q_e(0) \leq q_{e4}(0) \| q_e(0) \|^2 \tag{5.43}$$

Also consider the following property of fractional derivative,

$$D^{\alpha}(x-a)^{\gamma} = \frac{\Gamma(1+\gamma)}{\Gamma(1+\gamma-1)}(x-a)^{\gamma-\alpha} \tag{5.44}$$

where x is the variable and a is constant.
If we substitute $\alpha = \beta - 1$, $\gamma = \beta$, $a = 0$ and also replace x by t in eqn. (5.44), we get

$$\begin{aligned} & D^{\beta-1}(t)^{\beta} = \frac{\Gamma(1+\beta)}{\Gamma(\beta)} t \\ \Longrightarrow \quad & D^{\beta-1}(t)^{\beta} = (\beta+1)t \end{aligned} \tag{5.45}$$

Finally using (5.43), (5.45) in eqn. (5.42) we get,

$$\begin{aligned} D^{\beta} V_{qfrac} &\leq -\frac{K_P}{K_D\, \beta\, \Gamma(\beta)} D^{\beta-1}(q_{e4}(0) \| q_e(0) \|^2 t^{\beta})) \\ &\leq -\frac{K_P\, q_{e4}(0) \| q_e(0) \|^2}{K_D\, \beta\, \Gamma(\beta)} D^{\beta-1}(t^{\beta})) \\ &\leq -\frac{K_P\, q_{e4}(0) \| q_e(0) \|^2}{K_D\, \beta\, \Gamma(\beta)} (\beta+1)t \end{aligned} \tag{5.46}$$

Therefore,

$$D^{\beta} V_{qfrac} \leq 0 \qquad \text{(considering } q_{e4} > 0) \tag{5.47}$$

So, V_{qfrac} satisfies the following:

1. V_{qfrac} (function of q_e) is continuously differentiable and satisfies Liptschitz's condition locally such that, $V_{qfrac} \leq \| q_e \|$
2. $D^{\beta} V_{qfrac} \leq 0$ with $0 < \beta < 1$

By using theorem 5.2, $q_e = [0,0,0]^T$ is proven to be asymptotically stable for any $\|q_e(0)\| < 1$. Hence q_e asymptotically converges to $[0,0,0]^T$. $\square$

5.6.5 Calculation of Reaching Time:

Consider the reaching time to be t_{reach}. Denote the Lyapuonv function $V_{PD^\beta-SMC}$ by V_3 for simplicity in notation. Also consider, V_3 at t=0 be $V_3(S_0)$. Now from eqn. (5.38),

$$\begin{aligned} & \dot{V}_3 \leq -\eta_f V_3^{\frac{1}{2}} \\ \implies \quad & \int_0^{t_{reach}} V_3^{-\frac{1}{2}} dV_3 \leq -\eta_f \int_0^{t_{reach}} dt \\ \implies \quad & -2\sqrt{V_3(S_0)} \leq -\eta_f t_{reach} \\ \implies \quad & t_{reach} \leq \frac{2}{\eta_f}\sqrt{V_3(S_0)} \end{aligned} \tag{5.48}$$

.where $\eta_f = \sqrt{\frac{2K_D}{\lambda_{max}(J)}}$ as defined in (5.38). Hence expression for maximum reaching time is given by,

$$t_{reach}\Big|_{max} = \frac{2}{\eta_f}\sqrt{V_3(S_0)} \tag{5.49}$$

Putting value of η_f in (5.49),

$$t_{reach}\Big|_{max} = \sqrt{\frac{2}{K_D}(\lambda_{max}(J))V_3(S_0)} \tag{5.50}$$

5.7 PD^β-SMC with Modified Reaching Law

PD^β-SMC law designed in the previous section, is affected by chattering effect. Therefore in this section $PD^\beta - SMC$ law is modified using power rate type reaching law, similar to $PD - SMC$ case. Apart from checking the alleviation from chattering, the aim of this design is also to test whether this control law provides any other improvement in closed loop performance.

5.7.1 Sliding Surface Design

Here sliding surface is chosen same as in (5.31) i.e. $S = 2K_P\, q_e + K_D D^\beta \omega_e$.
Also the modified reaching law is similar to the reaching law proposed in (5.21),

$$\dot{S} = -K_{mf}|S|^\alpha sgn(S) \tag{5.51}$$

Where K_{mf} is gain of modified reaching law.

5.7.2 Control Law Design

For design of control law, derivative of S (from (5.31)) is compared to (5.51) and we get,

$$\begin{aligned}
& 2K_P.\frac{1}{2}Q_e\omega_e + K_D D^\beta \dot{\omega}_e = -K_{mf}|S|^\alpha sgn(S) \qquad \text{(using (5.6))} \\
\implies \quad & K_P Q_e \omega_e + K_D D^\beta J^{-1}[T_{control} - \omega_e \times (J\omega_e + h_w)] = -K_{mf}|S|^\alpha sgn(S) \\
\implies \quad & K_D J^{-1} D^\beta [T_{control} - \omega_e \times (J\omega_e + h_w)] = -K_P Q_e \omega_e - K_{mf}|S|^\alpha sgn(S) \\
\implies \quad & T_{control} = \omega_e \times (J\omega_e + h_w) - \frac{K_P}{K_D} J D^{-\beta} Q_e \omega_e - \frac{K_{mf}}{K_D} J D^{-\beta}(|S|^\alpha sgn(S))
\end{aligned} \tag{5.52}$$

Above expression of control law has 5 parameters to be designed namely, K_P, K_D,K_{mf}, α, β, which has been discussed in section (5.8).

5.7.3 Proof of Finite Time Convergence & Stability

Finite time convergence $\&$ stability for $PD^\beta - SMC$ with modified reaching law, are provided in this subsection.

Proof. To prove Finite Time Convergence, Lyapunov function chosen here(same as (5.25)) is,

$$V_{frac-mod} = \frac{1}{2} S^T S \tag{5.53}$$

where S is same as sliding surface designed for $PD^\beta - SMC$ law (5.31). Following the same steps for proving finite time convergence(as done in previous cases), we differentiate $V_{frac-mod}$ w.r.t time and it follows as,

$$\begin{aligned}
\dot{V}_{frac-mod} &= S^T \dot{S} \\
\implies \dot{V}_{frac-mod} &= S^T(-K_{mf}|S|^\alpha sgn(S)) \qquad \text{(from (5.51))}
\end{aligned} \tag{5.54}$$

Now $K_{mf}|S|^{\alpha}$ is a positive definite diagonal matrix if $K_{mf} > 0$. Hence from (5.54) using quadratic function properties,

$$\begin{aligned} \dot{V}_{frac-mod} &\leq -\|S\|_1 \\ \implies \dot{V}_{frac-mod} &\leq -\|S\|_2 \\ \implies \dot{V}_{frac-mod} &\leq -\sqrt{2}V_{frac-mod}^{\frac{1}{2}} \qquad \text{(using (5.53))} \end{aligned} \tag{5.55}$$

Therefore,

$$\dot{V}_{frac-mod} + \sqrt{2}V_{frac-mod}^{\frac{1}{2}} \leq 0 \tag{5.56}$$

Hence, by using lemma of [43], finite time convergence towards sliding surface (S) is confirmed. □

5.7.4 Proof of Stability

Proof. The sliding surface for this control law being same to eqn. (5.31), the stability proof is same as stability proof for $PD^{\beta} - SMC$ control law . So, the stability proof is not repeated for this control structure. □

5.7.5 Calculation of Reaching Time

Reaching time calculation method is similar to previous control designs.
Suppose, the reaching time for the reaching the sliding surface be denoted by t_{reach}. Let the Lyapunov function $V_{frac-mod}$ be denoted by V_4. Also let, value of Lyapunov function at t=0 be denoted by $V_4(S_0)$. Therefore eqn. (5.56) can be simplified as,

$$\begin{aligned} & \dot{V}_4 \leq -\sqrt{2}V_4^{\frac{1}{2}} \\ \implies \quad & \int_0^{t_{reach}} V_4^{-\frac{1}{2}} dV_4 \leq -\sqrt{2}\int_0^{t_{reach}} dt \\ \implies \quad & -2\sqrt{V_4(S_0)} \leq -\sqrt{2}t_{reach} \\ \implies \quad & t_{reach} \leq \sqrt{2V_4(S_0)} \end{aligned} \tag{5.57}$$

Hence expression for maximum reaching time is given by,

$$t_{reach}\Big|_{max} = \sqrt{2V_4(S_0)} \tag{5.58}$$

5.8 Tuning of Parameters

Each of the above control laws has certain parameters to be tuned. A general optimization procedure has been proposed in this work for tuning the parameters of each type of control law. The optimization problem is formulated below:

$$\begin{aligned}\underset{x}{\text{minimize}} \quad & C_0 \sum_{i=1}^{3} \int_t t|\omega_{ei}(x,t)|dt + C_1 \sum_{i=1}^{3} \int_t T^2_{control,i}(x,t)dt + C_2 \sum_{i=1}^{3} \int_t \omega^2_{ei}(x,t)dt \\ & + C_3 \sum_{i=1}^{3} \int_t t|q_{ei}(x,t)|dt \end{aligned} \tag{5.59}$$

$i = 1(.)3$ denoting 3 axes considered in this work.

It can be noticed that above optimization problem is unconstrained in nature with objective function being linear combination of 3 types of performance indices namely, Control Effort, Integral Time Absolute Error (ITAE), Integral Square Error (ISE).
As ω_s is the main variable to be controlled in our problem, hence both ISE and ITAE performance indices are considered w.r.t ω_e, to control both transient and steady state portion of the response. For q_e, only steady state performance index (ITAE) is chosen considering that there is no large variation during transient state of q_e. Again power consumption by various subsystems of satellite, is another crucial factor to be optimized. Here control effort performance index is chosen to minimize the power consumption of Satellite ADCS.
However only control effort index minimization will not ensure transient or steady state improvement. Similarly ISE or ITAE will not directly help in minimization of consumed power. Hence it is obvious to consider combination of all performance indices to take advantage of each of them.

The coefficients C_0, C_1, C_2, C_3 are the weights of respective performance indices. Weights need to be designed depending on importance given to the respective performance indices, such that $\sum_{j=0}^{3} C_j = 1$.

Depending on control law, structure of x will vary. For example, $PD - SMC$ control law 3 parameters need to be tuned namely, $x = [K_P, K_D, K]$. $PD^\beta - SMC$ has 4 parameters to be tuned namely, $x = [K_P, K_D, K_f, \beta]$.

Now,control algorithms with modified reaching law namely $PD-SMC$ *with modified Reaching Law* and $PD^\beta-SMC$ *with modified Reaching Law* has 4 (K_P, K_D, K_m, α) and 5 ($K_P, K_D, K_{mf}, \beta, \alpha$) parameters to be tuned respectively. Except α remaining parameters of $PD - SMC$ ***with modified Reaching Law*** and $PD^{\beta} - SMC$ ***with modified Reaching Law*** control laws namely, $x = [K_P, K_D, K_m]$, and $x = [K_P, K_D, K_{mf}, \beta]$ respectively, are to be tuned via optimization procedure discussed above. But α cannot be any number, it has crucial role in power rate type reaching law. Choice of α is discussed in next chapter. (6.3.2.1).

5.9 Summary

In this chapter, various sliding mode based non linear control laws are proposed to ensure better disturbance rejection and enhanced robustness. The control laws include both integer and fractional order control (FOC) namely, $PD - SMC$ and $PD^{\beta} - SMC$. To alleviate chattering problem, sliding mode control laws with power rate based reaching law are also proposed in this chapter. Finite time convergence and stability in proved for each of the non linear controllers. Finally a general optimization procedure has been proposed for tuning all of these controllers.

Chapter 6

Simulation Results and Performance Analysis

6.1 Introduction

In this chapter, open loop response of satellite is obtained first. Satellite model is developed for a given data set, on the basis of theories discussed in chapter 2 & 3. Thereafter gain values of controllers (both linear and non linear) are obtained for a given data set of satellite, following the optimization method described in chapter 4 & 5. Finally different control algorithms are tested on the satellite model and corresponding performance indices evaluated and compared.

6.2 Open Loop Response

Parameters	**Value**
Initial quaternion	$[0.5 \;\; 0.5 \;\; 0.5 \;\; 0.5]$
Initial angular velocity	$[0.02 \;\; -0.07 \;\; 0.05]$
Desired quaternion	$[0 \;\; 0 \;\; 0 \;\; 1]$
Desired angular velocity	$[0 \;\; 0 \;\; 0]$
Inertia matrix of the satellite	$diag\{50, 75, 100\}$
Inertia matrix of reaction wheel	$0.7259 \times 10^{-4} I_{3\times3}$
Time constant of the reaction wheel	$100ms$

Table 6.1: Parameters for Open Loop Simulation

The simulation parameters for the open loop simulation is tabulated in Table 6.1

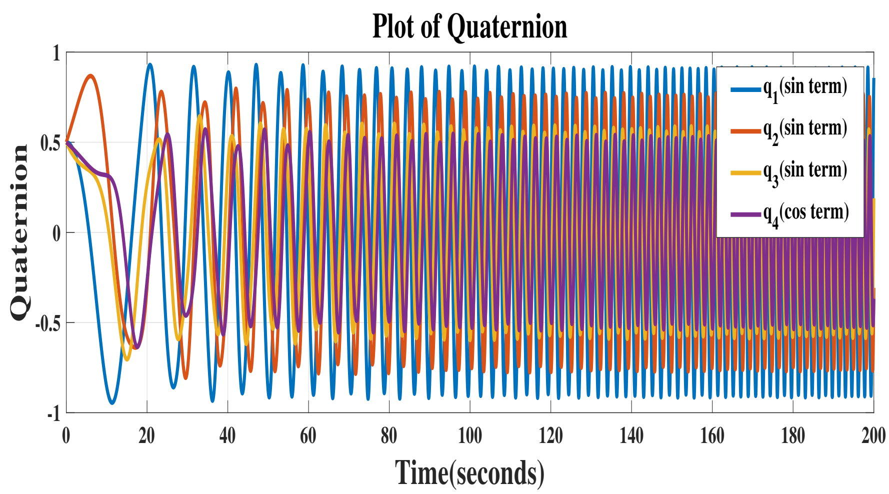

Figure 6.1: Quaternion Response for Open Loop Simulation

The attitude of satellite and its angular velocity for the open loop system is shown in Figures 6.1 and 6.2 respectively. It is observed that the angular velocity has increasing trend with time and the quaternion response is continuously oscillating. It indicates the system to be unstable.
Hence it justified that controller is required for stabilizing the system and to provide the desired responses.

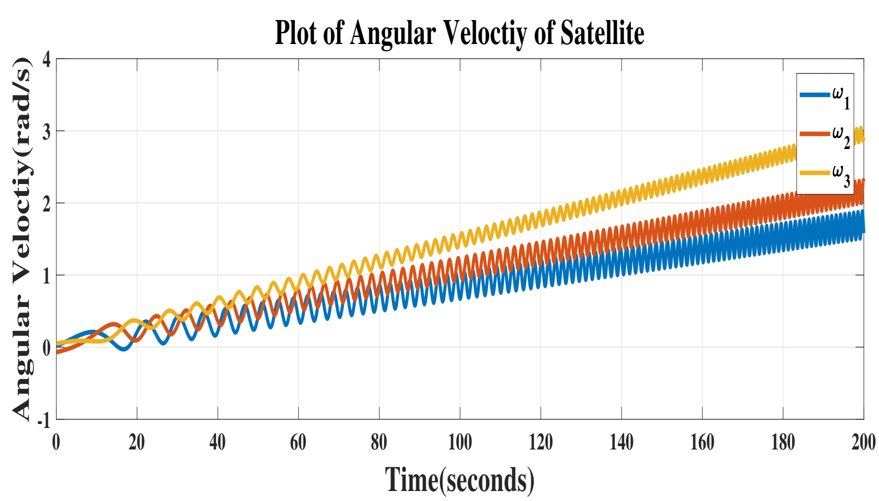

Figure 6.2: Angular Velocity Response for Open Loop Simulation

6.3 Optimization of Controller Gain

Open loop response showed above clearly indicates the requirement of controller. Now for designing controller, optimization methods proposed in chapter 4 & 5, are followed, and gain values of controllers are obtained, for the satellite parameters shown in 6.1.

6.3.1 Optimization of Linear Controllers

Linear controllers namely PD & PD^{β}, are designed solving the optimization problems formulated in chapter 4. As specified earlier gain cross over frequency (ω_{gc}), and phase margin upper limit (ϕ_m) are chosen as 1 rad/s and 80° respectively.
MATLAB optimization tool **fmincon** is used for solving the optimization problem for both PD and PD^{β} control algorithms. optimization results are listed below:

6.3.1.1 PD controller

In case of PD controller, optimization result is as following:

- $K_P = diag\{16.6086; 20.9914; 43.3096\}$
- $K_D = diag\{99.0545; 149.493; 196.867\}$
- Objective function, $\|\vec{u}(t)\|_2^2$=382.8 (for simulation duration 200 sec)

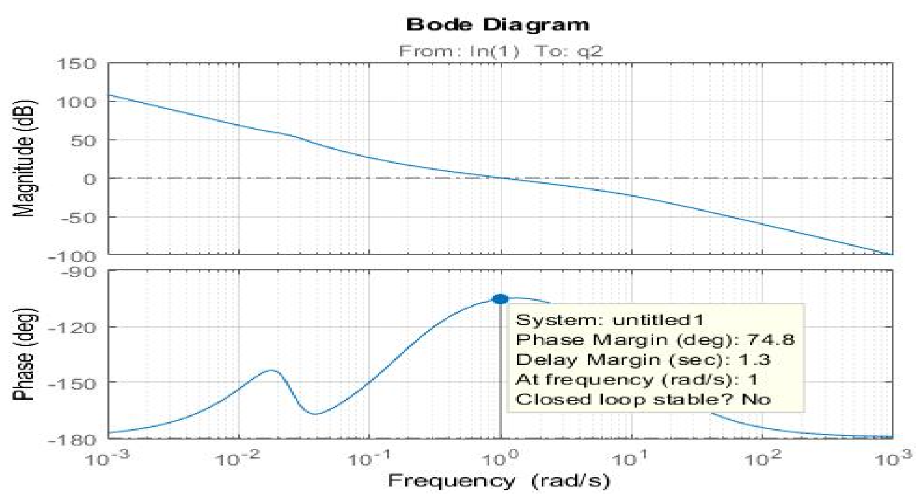

Figure 6.3: Bode plot for X axis transfer function

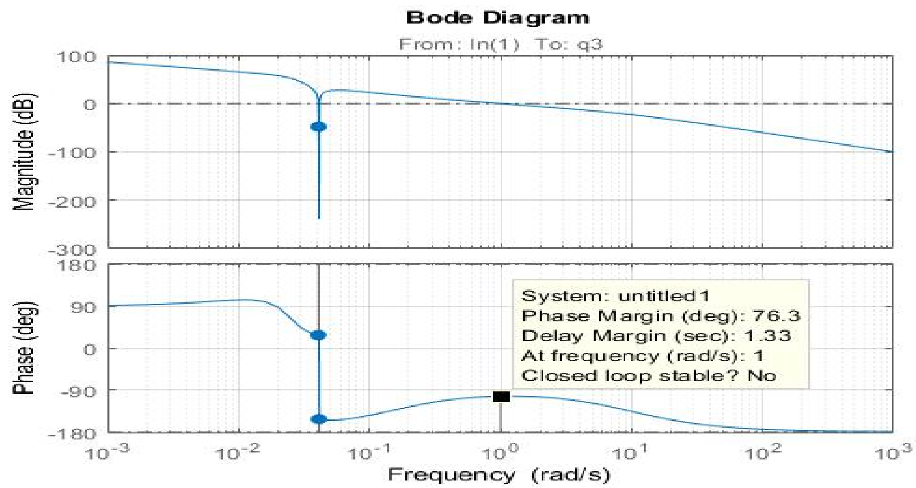

Figure 6.4: Bode plot for Y axis transfer function

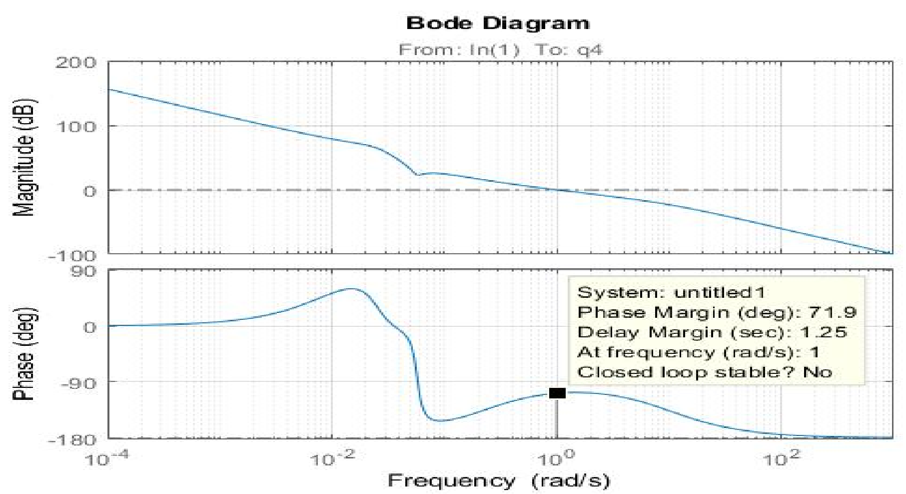

Figure 6.5: Bode plot for Z axis transfer function

Figures 6.3,6.4,6.5 shows the bode plot of linearized plant along with the designed PD controller (as discussed earlier linearized satellite model contains 3 transfer function along 3 axes). It can be seen that all the constraints posed in the optimization of PD controller namely, $\omega_{gc} = 1$ rad/s and phase margin $< \phi_m$, are satisfied (along each axis) by using the optimized controller.

6.3.1.2 PD^{β} Controller

In case of PD^{β} controller, Isodamping condition is considered as 3^{rd} condition apart from gain cross over frequency and phase margin constraints. Optimization result is listed below:

- $K_P = diag\{16.608; 20.99; 43.309\}$
- $K_D = diag\{99.05; 149.5; 196.8\}$
- $\beta = [0.7439; 0.8120; 0.6632]^T$
- Objective function, $\|\vec{u}(t)\|_2^2$=428.5 (for simulation duration 200 sec)

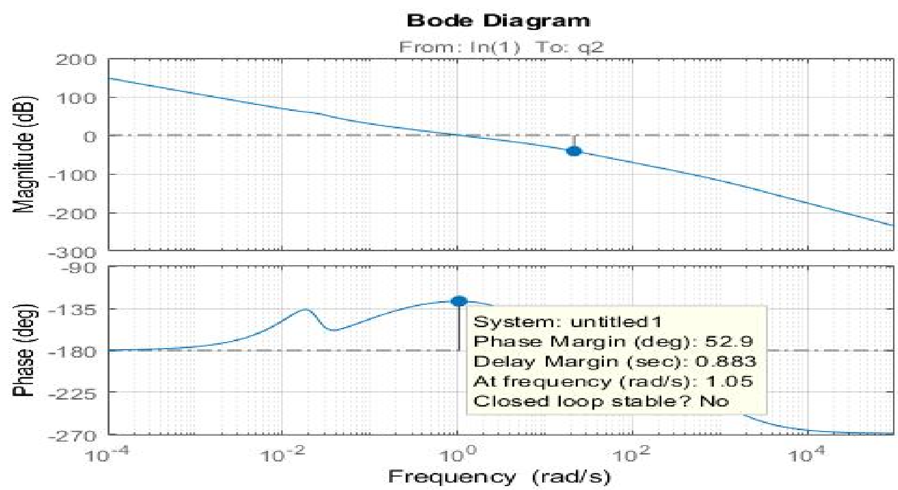

Figure 6.6: Bode plot for X axis transfer function

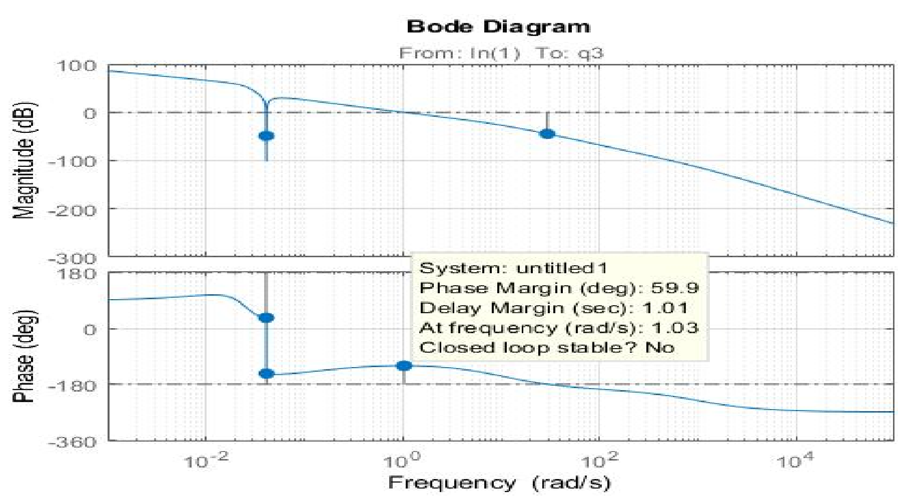

Figure 6.7: Bode plot for Y axis transfer function

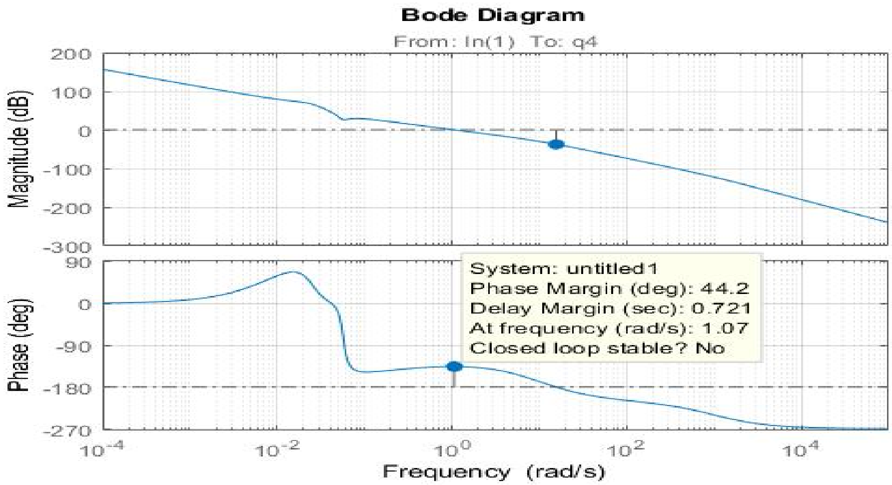

Figure 6.8: Bode plot for Z axis transfer function

Figures 6.6,6.7,6.8 shows the bode plot of linearized plant along with the designed PD^{β} controller. Like PD controller case, here also optimized controller satisfies all the constraints posed namely, ω_{gc}=1 rad/s, phase margin $< \phi_m$ and isodamping condition.

6.3.2 Optimization of Non Linear Controller

As discussed in chapter 5, each non linear controllers has few parameters to be optimized. For that an general structure of optimization problem is formulated(5.59). Objective function of (5.59), has 4 coefficients to be chosen namely, $C_x = [C_0; C_1; C_2; C_3]^T$. They are the coefficient of performance indices: ITAE of ω_e, control effort, ISE of ω_e, ITAE of q_e. In this work the coefficients are chose as,$C_x = [0.31; 0.15; 0.18; 0.36]^T$.

It can be seen that ITAE of q_e and ITAE of ω_e are given the most and second most preference respectively. Reason behind this is: q_e, ω_e should converge to zero after certain amount of time. This is the basic requirement of attitude control problem. ITAE index ensures that. Considering one of the aim of this work is to reduce the transient oscillation of angular velocity, ISE of ω_e is also given significant weightage. Although remaining weightage is given to control effort but it is ensured that weightage of control effort is maintained significant compared to other coefficients. As discussed earlier, ISE of q_e is not included in objective function considering small amount transient oscillation of q_e.
MATLAB optimization tool **fminsearch** has been used to design the parameters of each controller. Optimized parameter values of each controllers are listed in Table 6.2 with corresponding components of objective function(for simulation duration 200 sec).

Controller Name	Parameters of Controller				Components of Objective Function			
	K_P	K_D	β	Gain (K or K_m or K_f or K_{mf})	$ITAE_\omega$	Control Effort	ISE_ω	$ITAE_q$
PD -SMC	2.3997	12.452	None	0.72167	21.24	314.4	0.1082	137.27
PD-SMC modified	2.53382	10.3046	None	0.21542	11.64	39.18	0.1159	43.639
PD^β SMC	2.3811	22.6834	0.001	0.6837	20.96	284.8	0.1216	120.09
PD^β SMC modified	2.2807	25.0744	0.001	0.5374	12.23	42.53	0.1214	43.8920

Table 6.2: Optimization Results for Non linear Controllers

6.3.2.1 Choice of α

Here we discuss design method of power coefficient (α) of control laws ($PD - SMC$ with modified Reaching Law & $PD^\beta - SMC$ with modified Reaching Law), having power rate type reaching law.

As described earlier, for higher values of α, power rate type reaching law ensures increment in reaching speed when states are away from sliding surface, and decrement in speed when states are closer to sliding surface, causing reduction of chattering.This property naturally supports for choice of larger values of α. Again it has been observed that, if value of α is chosen near 1,then sliding motion phase may even be skipped by system states and it directly effects on robustness property[6] of the system.

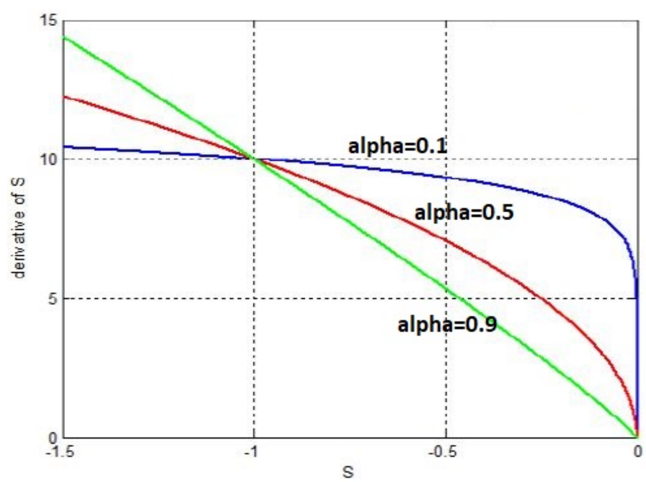

Figure 6.9: Variation of derivative of S with S for power rate type reaching law [6]

Figure 6.9. of $\dot{S}$ vs. S for different α [6], is helpful to choose proper value of alpha such that chattering effect is removed, at the same time sliding motion is also not avoided, hence ensuring the robustness property.

- α is chosen 0.5 for both modified reaching law problems in this work.

6.4 Close Loop Response

Under this section, first linear controllers response are given, followed by response of non linear controllers.

6.4.1 Simulation Results for Linear Controller

Response of PD and PD^{β} controllers are discussed here.

6.4.1.1 PD Controller Response

Parameters	**Value**
Initial quaternion	$[0.5 \quad 0.5 \quad 0.5 \quad 0.5]$
Initial angular velocity	$[0.02 \quad -0.07 \;\; 0.05]$
Desired quaternion	$[0 \;\; 0 \;\; 0 \;\; 1]$
Desired angular velocity	$[0 \;\; 0 \;\; 0]$
Inertia matrix of the satellite	$diag[50, 75, 100]$
Inertia matrix of reaction wheel	$0.7259 \times 10^{-4} I_{3\times3}$
Time constant of the reaction wheel	$100ms$
Proportional Gain matrix, K_p	$diag\{16.6086; 20.9914; 43.3096\}$
Derivative Gain matrix, K_d	$diag\{99.0545; 149.493; 196.867\}$

Table 6.3: Parameters for PD Controller

Case 1 : Simulations without Disturbances

The simulation results of the attitude control problem with PD controller is shown from Figure 6.10 to Figure 6.12.

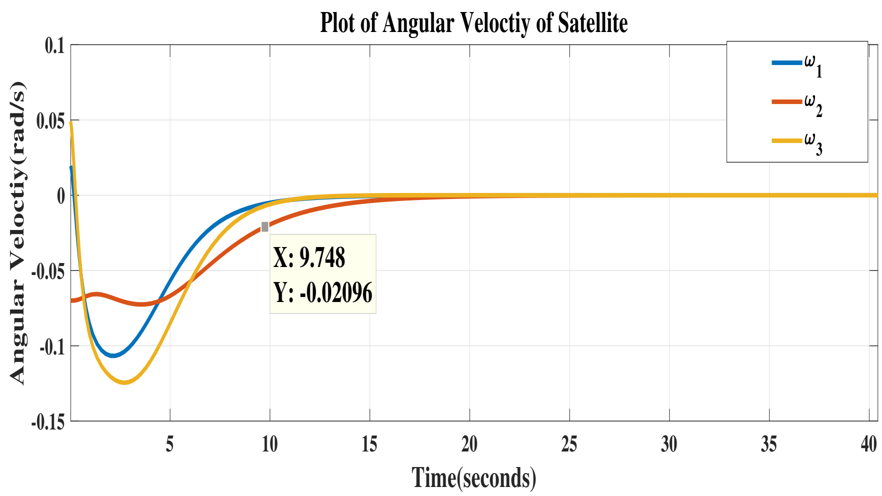

Figure 6.10: Angular Velocity Response with PD Controller

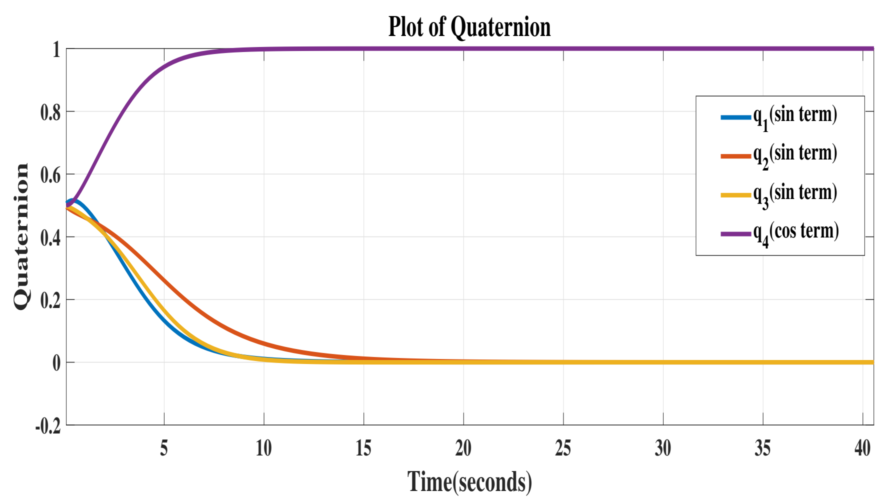

Figure 6.11: Quaternion Response with PD Controller

From the simulation results, it is observed that the angular velocity and attitude quaternion converges to the desired value with the PD controller designed. However the response of control torque signal provided by the PD controller is large enough to exceed the limits of practical reaction wheels and hence saturation is essential in the output of the controller.

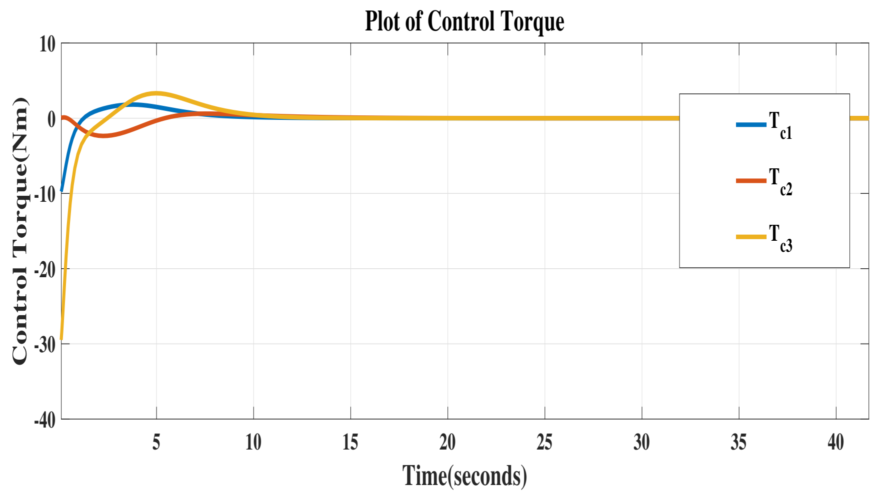

Figure 6.12: Control Torque Response with PD Controller

Case 2 : Simulations with Disturbances

For checking the disturbance rejection capability of the PD controller, a random disturbance is added to satellite dynamics, in between 60 sec to 120 sec. Figure 6.13 to Figure 6.15 shows the angular velocity response, quaternion response and control torque for the designed PD controller. It is noted that the designed PD controller has got poor disturbance rejection capability.

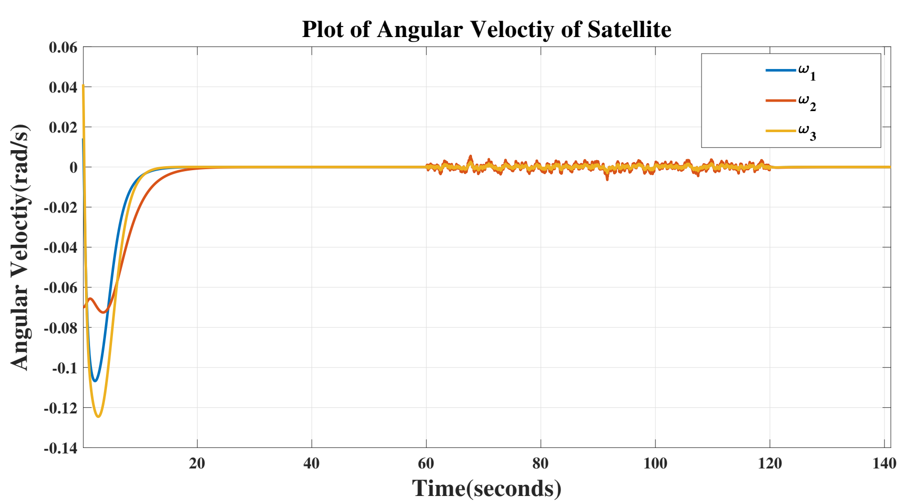

Figure 6.13: Angular Velocity Response with PD Controller in presence of Disturbance

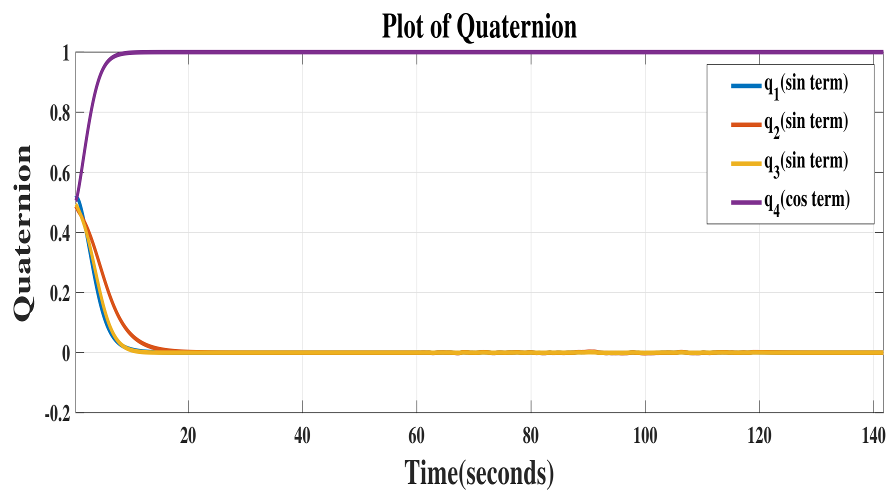

Figure 6.14: Quaternion Response with PD Controller in presence of Disturbance

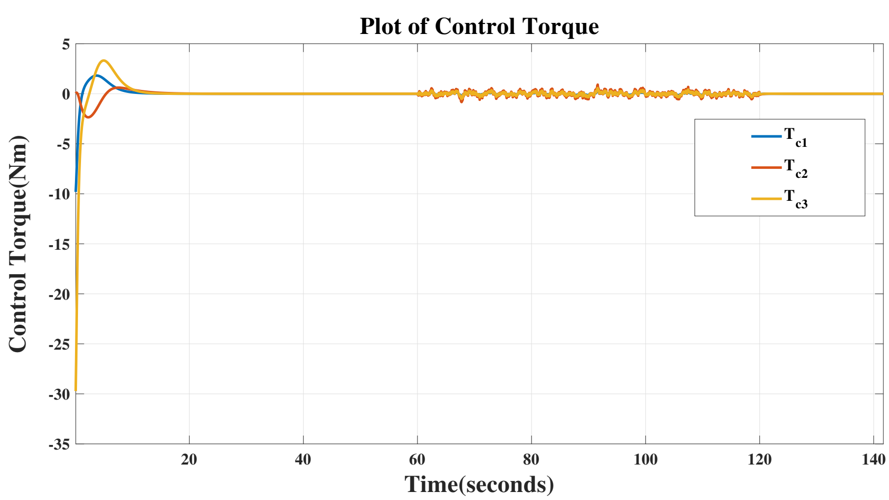

Figure 6.15: Control Torque Response with PD Controller in presence of Disturbance

Case 3: Simulation with Inertia Matrix Perturbation

To check the robustness of the controller,inertia matrix of satellite is perturbed at t=120 sec and it is checked whether satellite is able to withstand that perturbation. The simulation is performed with 40% and 60% perturbation in inertia matrix at 50 sec and the corresponding responses are shown in Figure 6.25(a), 6.25(b). It is seen that the designed PD controller provides robustness against inertia uncertainty.

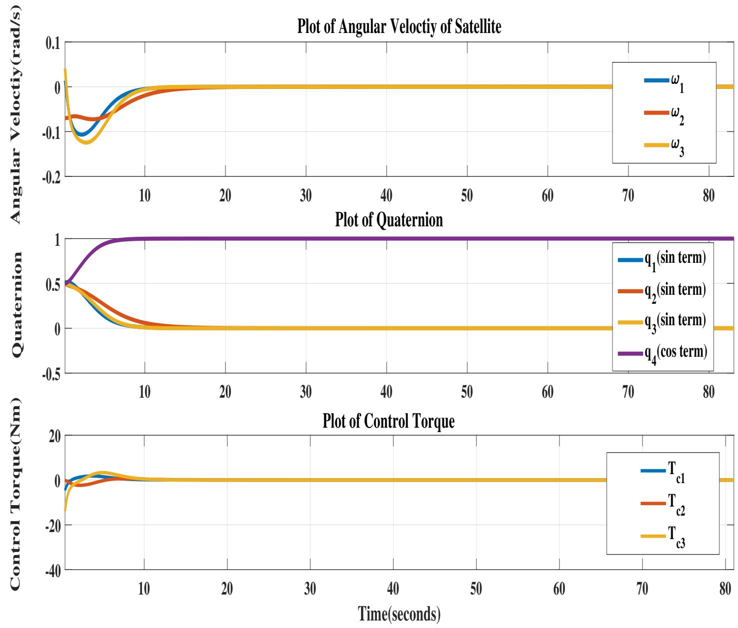

(**(a)**) with 40% Perturbation

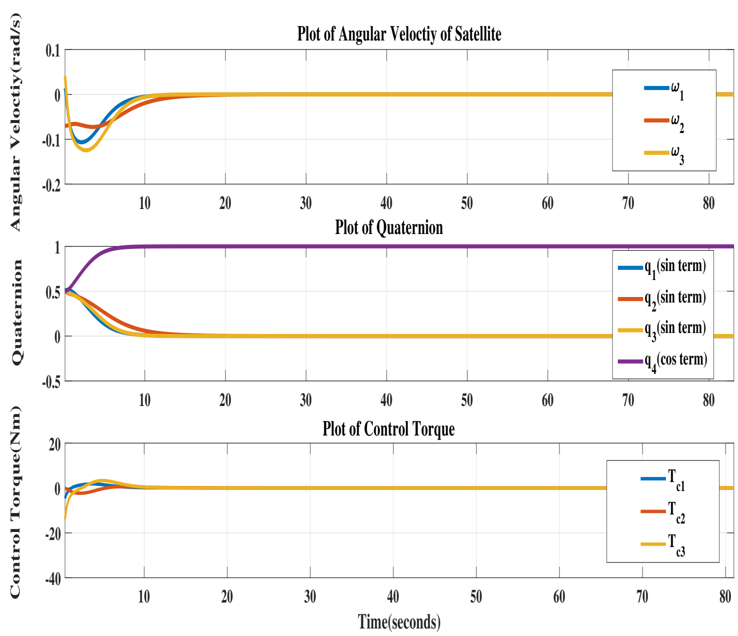

(**(b)**) with 60% Perturbation

Case 4 : Simulations with Control Input saturation

In this work, it is considered that maximum control signal that can be provided to reaction wheel is of the limit $\pm$ 1 Nm. Therefore control torque provided by the PD controller shown in Figure 6.12 exceeds the limits of the reaction wheel and hence saturation is introduced at the output of the controller.

The simulation carried out with control input(of reaction wheel) saturation, is shown from Figure 6.16 to Figure 6.18. From the figures it is observed that the settling time for the quaternion, angular velocity and control torque increased from 9.748 sec to 27.36 sec. As saturation block limits the error correction therefore it takes more time to settle to the given reference.

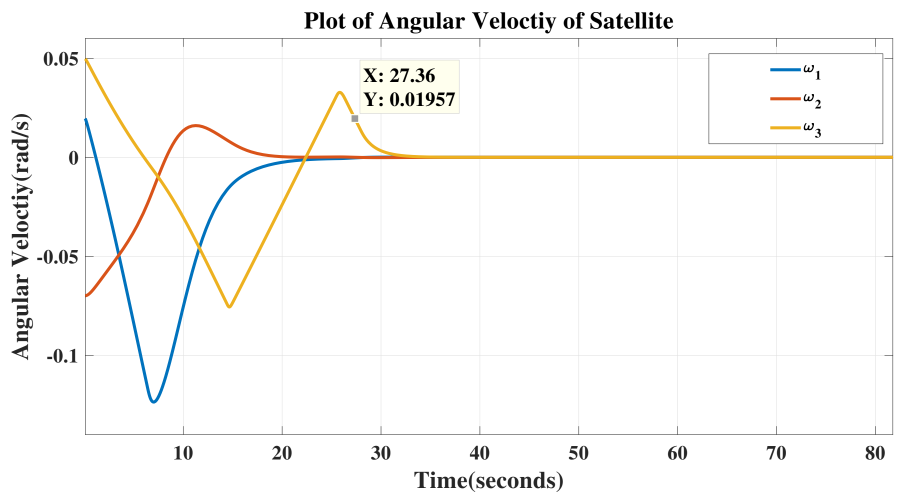

Figure 6.16: Angular Velocity with Control Input Saturation for PD Controller

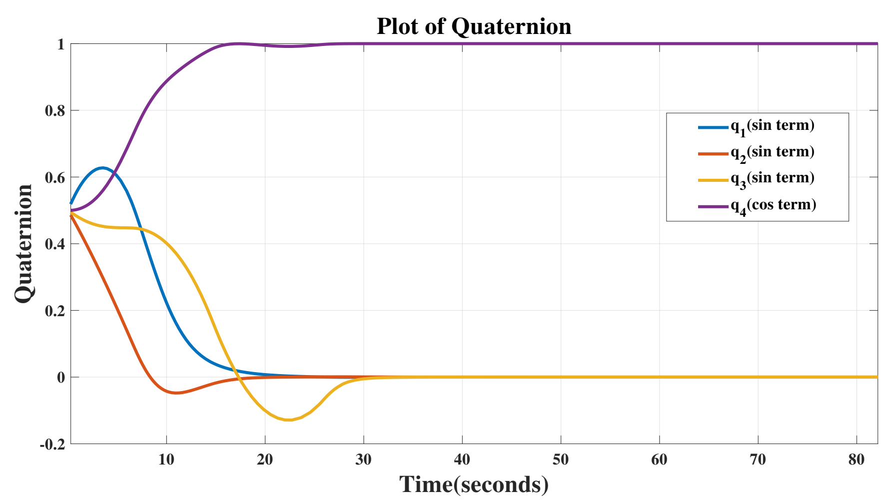

Figure 6.17: Quaternion Response with Control Input Saturation for PD Controller

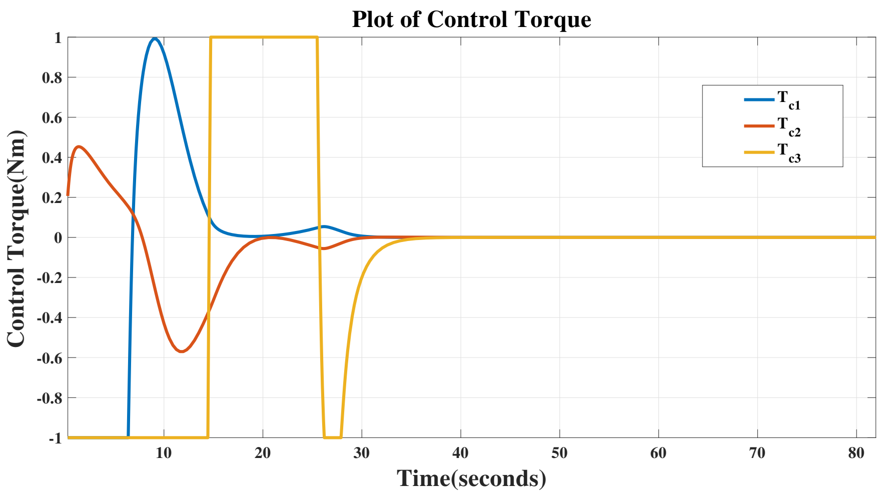

Figure 6.18: Control Torque with Control Input Saturation for PD Controller

6.4.1.2 PD^{β} Controller

Now simulation results for PD^{β} control law is discussed.

Parameters	**Value**
Initial quaternion	$[0.5 \quad 0.5 \quad 0.5 \quad 0.5]$
Initial angular velocity	$[0.02 \quad -0.07 \;\; 0.05]$
Desired quaternion	$[0 \;\; 0 \;\; 0 \;\; 1]$
Desired angular velocity	$[0 \;\; 0 \;\; 0]$
Inertia matrix of the satellite	$diag[50, 75, 100]$
Inertia matrix of reaction wheel	$0.7259 \times 10^{-4} I_{3\times3}$
Time constant of the reaction wheel	$100ms$
Proportional Gain matrix, K_p	$diag\{16.608; 20.99; 43.309\}$
Derivative Gain matrix, K_d	$diag\{99.05; 149.5; 196.8\}$
Fractional Order, β	$[0.7439; 0.8120; 0.6632]$

Table 6.4: Parameters for PD^{β} Controller

Case 1 : Simulations without Disturbances

Simulation results with PD^{β} controller are shown from Figure 6.19 to Figure 6.21. From the simulation results, it can be observed that the angular velocity and attitude quaternion converges to the desired value with the designed PD^{β} controller. Like PD controller, here also the control torque provided by the PD^{β} controller exceeds the limits of the reaction wheel and hence saturation is necessary in the output of the controller.

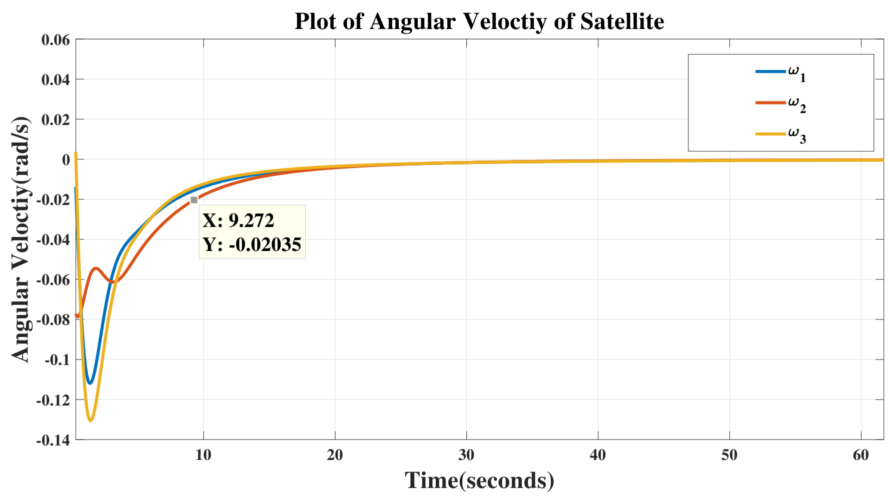

Figure 6.19: Angular Velocity Response with PD^{β} Controller

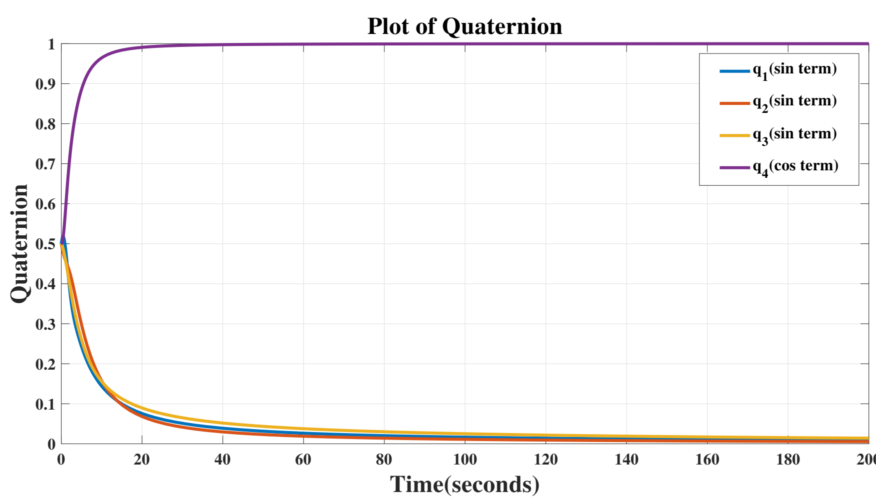

Figure 6.20: Quaternion Response with PD^{β} Controller

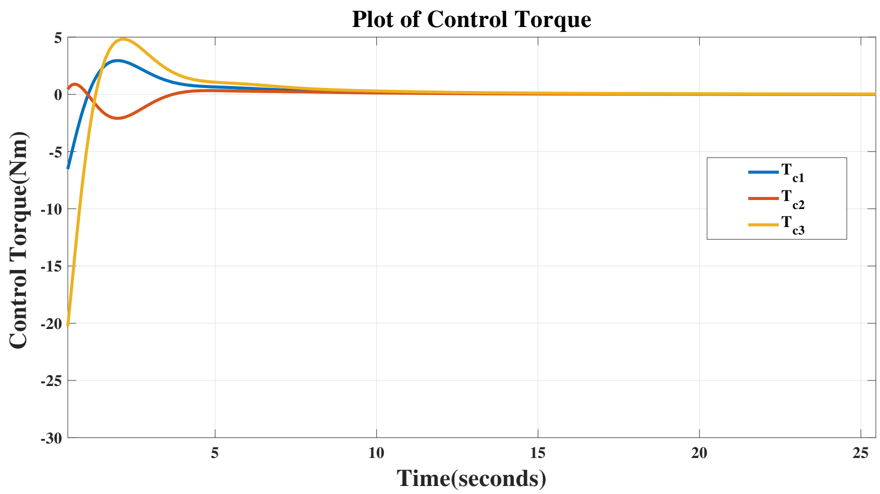

Figure 6.21: Control Torque Response with PD^β Controller

Case 2 Simulations with Disturbances

PD^β controller is tested against a random disturbance, introduced between 60 sec to 120 sec. Figure 6.22 to Figure 6.24 shows the angular velocity response, quaternion response and control torque response for the PD^β controller designed . Like PD controller, PD^β controller, PD^β controller also has poor disturbance rejection capability.

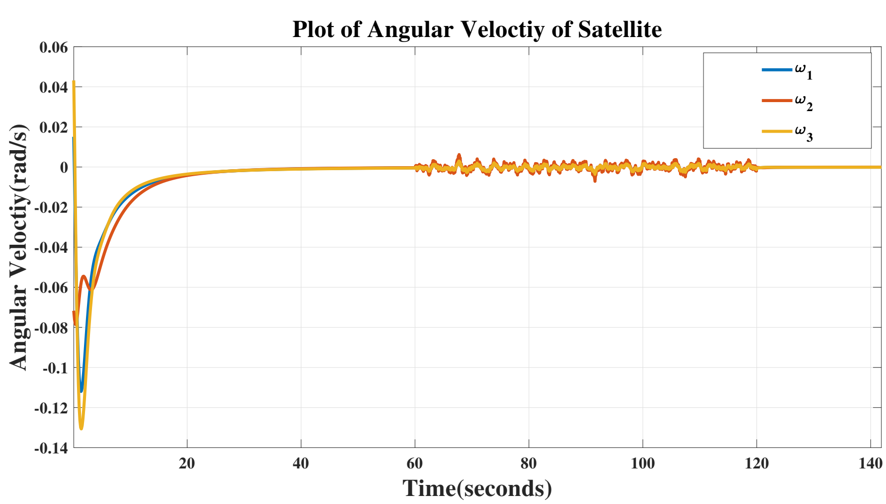

Figure 6.22: Angular Velocity Response with PD^β Controller in presence of Disturbance

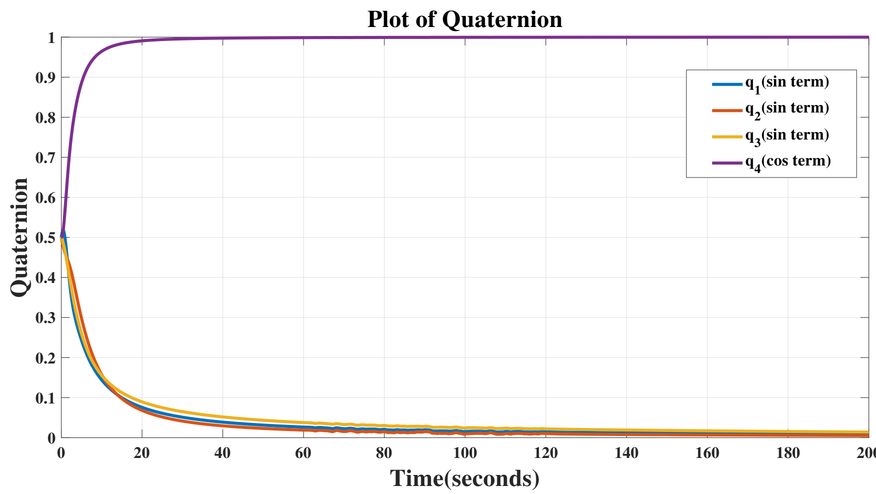

Figure 6.23: Quaternion Response with PD^{β} Controller in presence of Disturbance

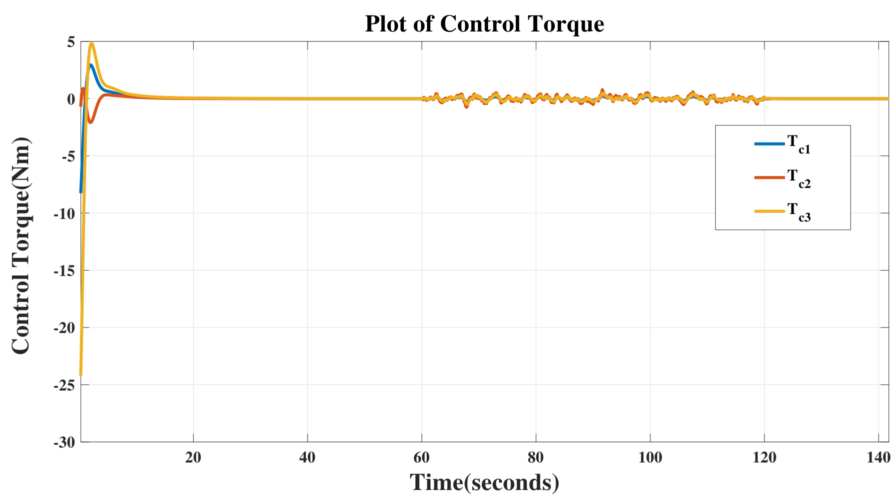

Figure 6.24: Control Torque with PD^{β} Controller in presence of Disturbance

Case 3: Simulation with Inertia Matrix Perturbation

To check the robustness of the controller, the simulation is performed with 40% and 60% perturbation in inertia matrix at 50 sec which is shown in Figure 6.25(a) and 6.25(b). It can be observed that the designed PD controller provides robustness against inertia matrix uncertainty.

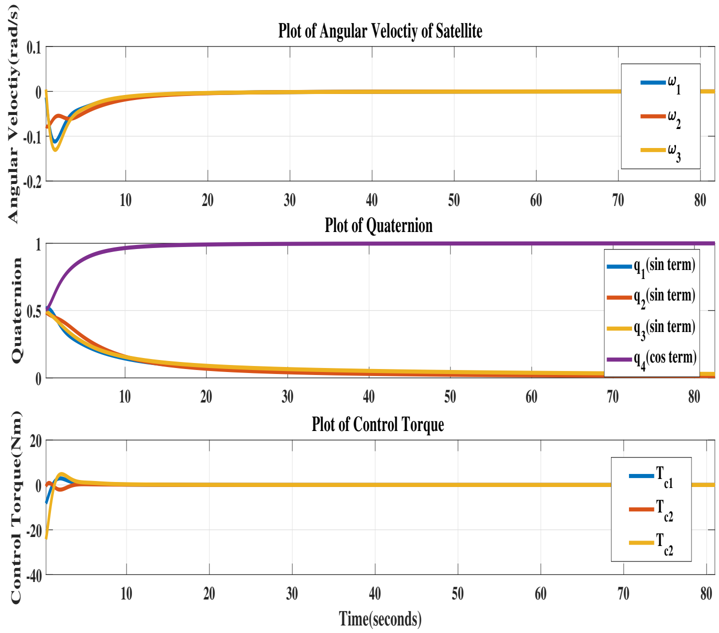

((**a**)) with 40% Perturbation

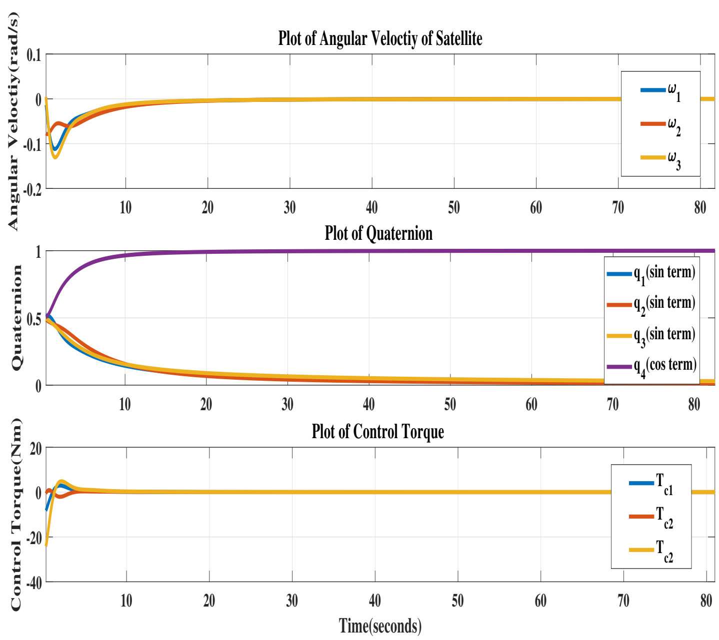

((**b**)) with 60% Perturbation

Figure 6.25: Responses with PD^{β} Controller in presence of Inertia Matrix Perturbation

Case 4 : Simulations with Control Input saturation

As seen in the case of simulation with no disturbance, upper limit of control torque exceeds the limit of the reaction wheel, which indicates the need of saturating the control torque signal applied to the reaction wheels.

Here simulation is performed with control input saturation of $\pm$ 1 Nm, as shown from Figure 6.26 to Figure 6.28. From those figures, it can be noticed that the settling time for the quaternion, angular velocity and control torque increased from 9.272 sec to 25.37 sec due to the introduction of saturation in the control torque.

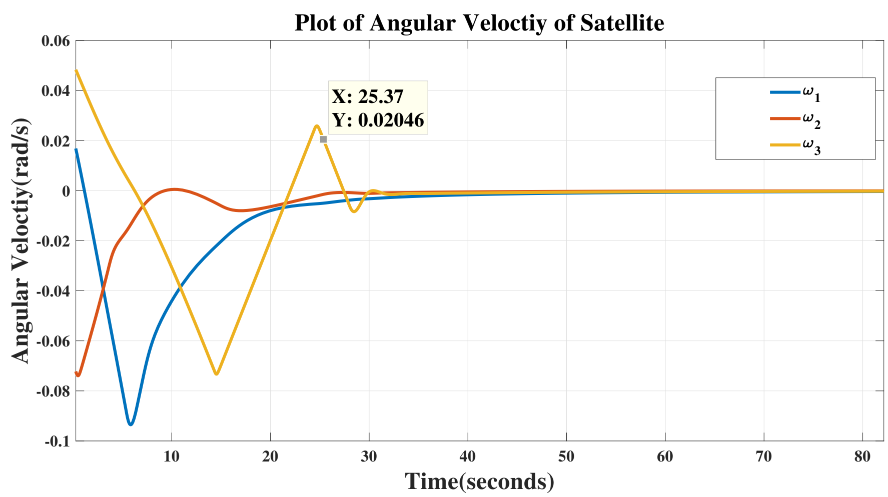

Figure 6.26: Angular Velocity with Control Input Saturation for PD^β Controller

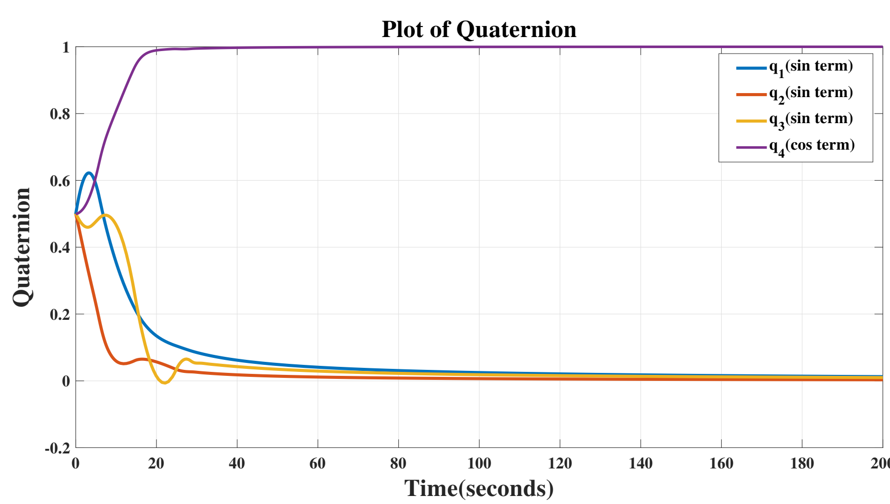

Figure 6.27: Quaternion Response with Control Input Saturation for PD^β Controller

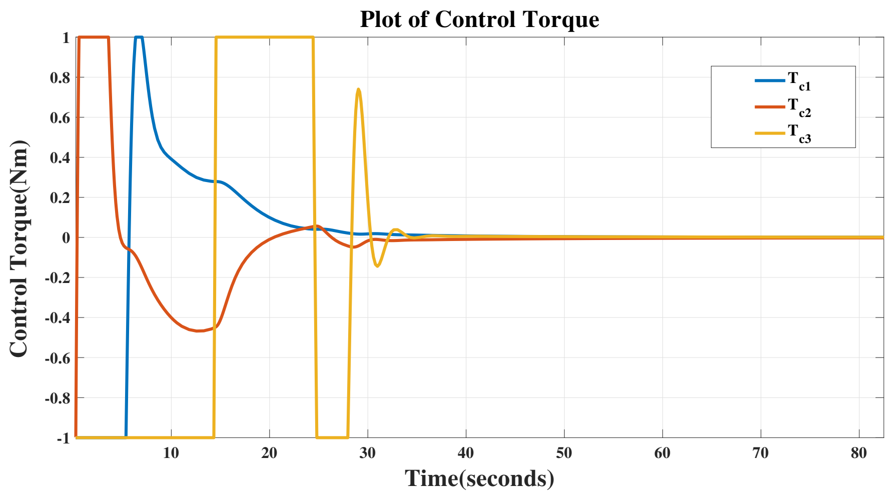

Figure 6.28: Control Torque Response with Control Input Saturation for PD^{β} Controller

Therefore it can be observed from simulations of linear controller that, controllers are able to achieve the desired attitude and angular velocity. They also show robustness in terms of inertia matrix perturbation. But none of the linear controller shows good disturbance rejection property.

6.4.2 Simulation Results for Nonlinear Controller

6.4.2.1 Response of PD-SMC Controller

Parameters	**Value**
Initial quaternion	$[0.5 \quad 0.5 \quad 0.5 \quad 0.5]$
Initial angular velocity	$[0.02 \quad -0.07 \quad 0.05]$
Desired quaternion	$[0 \ \ 0 \ \ 0 \ \ 1]$
Desired angular velocity	$[0 \ \ 0 \ \ 0]$
Inertia matrix of the satellite	$diag[50, 75, 100]$
Inertia matrix of reaction wheel	$0.7259 \times 10^{-4} I_{3\times3}$
Time constant of the reaction wheel	$100ms$
Value of K_P	2.3997
Value of K_D	12.452
Positive scalar, K	0.72167

Table 6.5: Parameters for PD-SMC Controller

Case 1: Simulations without Disturbance

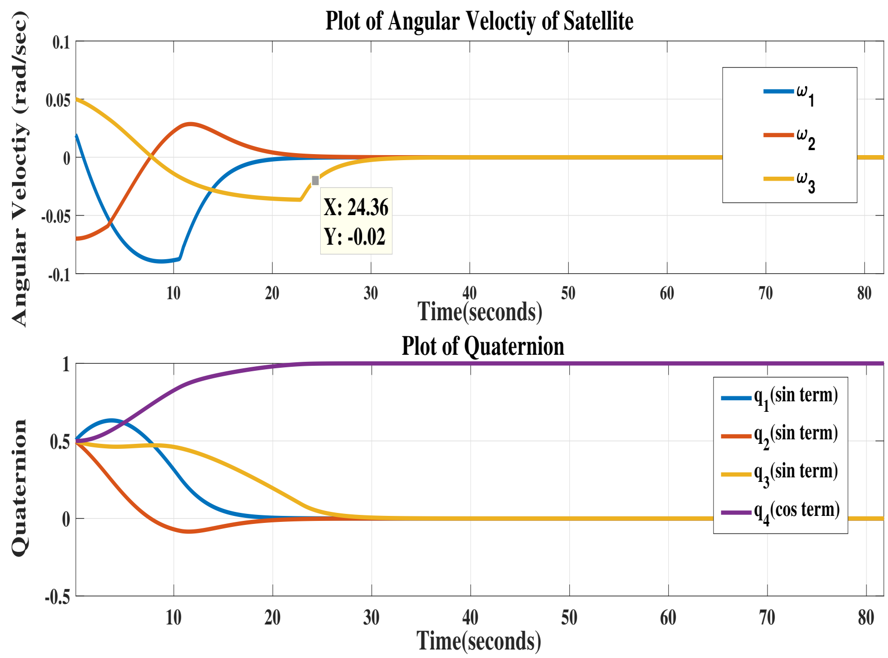

Figure 6.29: Angular Velocity and Quaternion Responses with PD-SMC

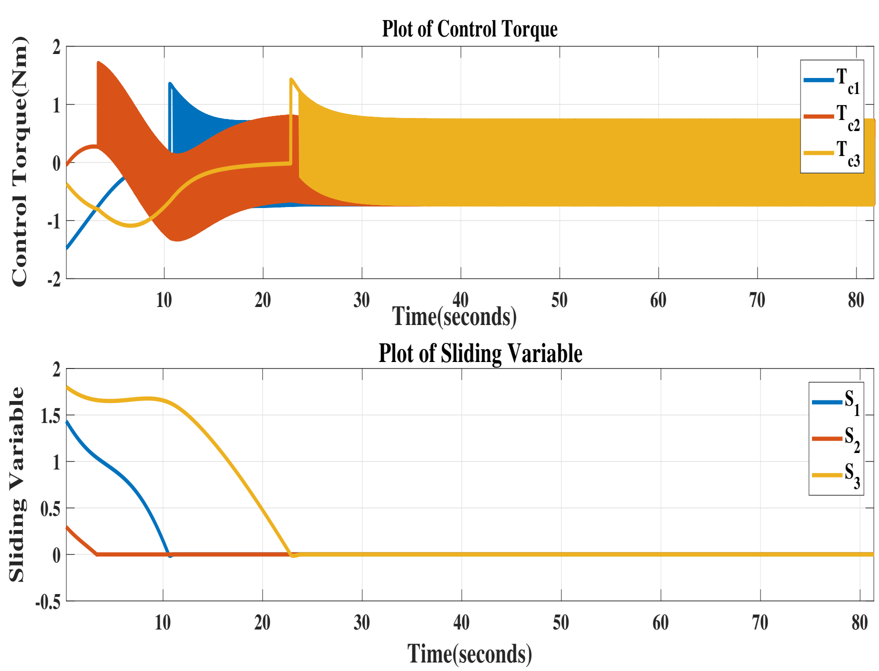

Figure 6.30: Control Torque and Sliding Variable Responses with PD-SMC

The simulation results of satellite attitude control problem with PD-sliding mode controller is shown in Figure 6.29 and Figure 6.30. The results shows that the desired attitude and angular velocity is attained within 30 seconds. The control torque required to control the satellite system switches between 2 Nm and -2 Nm. Chattering effect is visible in control torque response, which is the main disadvantage of sliding mode based control. Removal of chattering is discussed later.

Case 2: Simulations with Disturbance

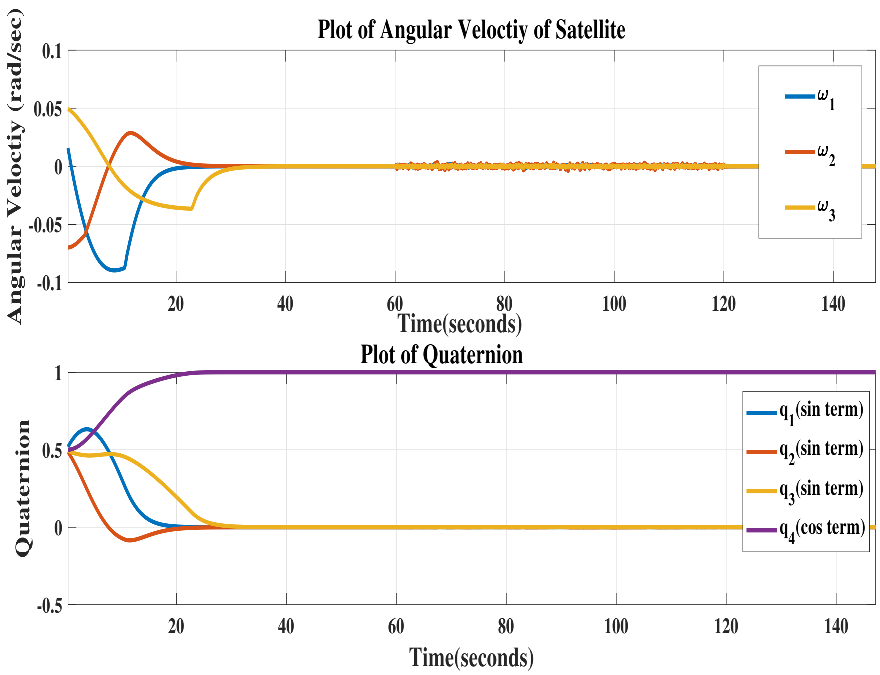

Figure 6.31: Angular Velocity and Quaternion with PD-SMC in presence of Disturbances

To check the disturbance rejection capability of PD-SMC, a random disturbance is introduced to the system during 60 sec to 120 sec. The simulation results are shown in Figure 6.31 and Figure 6.32. The effect of disturbance is negligible in the quaternion and angular velocity responses. i.e., PD-SMC has shown good disturbance rejection capability.

The zoomed view of disturbance in Figure 6.32 is shown in Figure 6.33 and it is observed that the control torque and sliding variable changes their values to balance the satellite in presence of the disturbance.

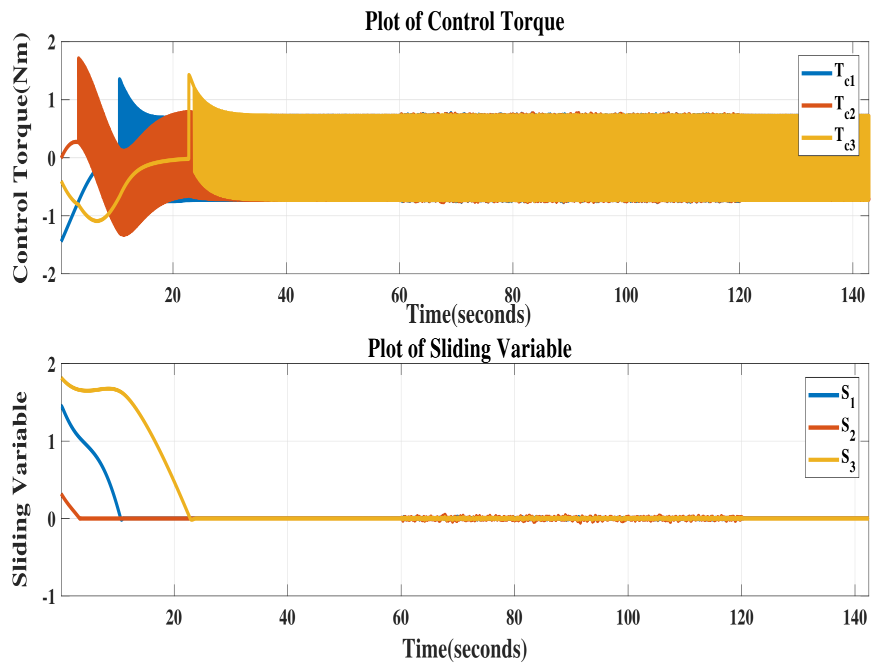

Figure 6.32: Control Torque and Sliding Variable with PD-SMC in presence of Disturbances

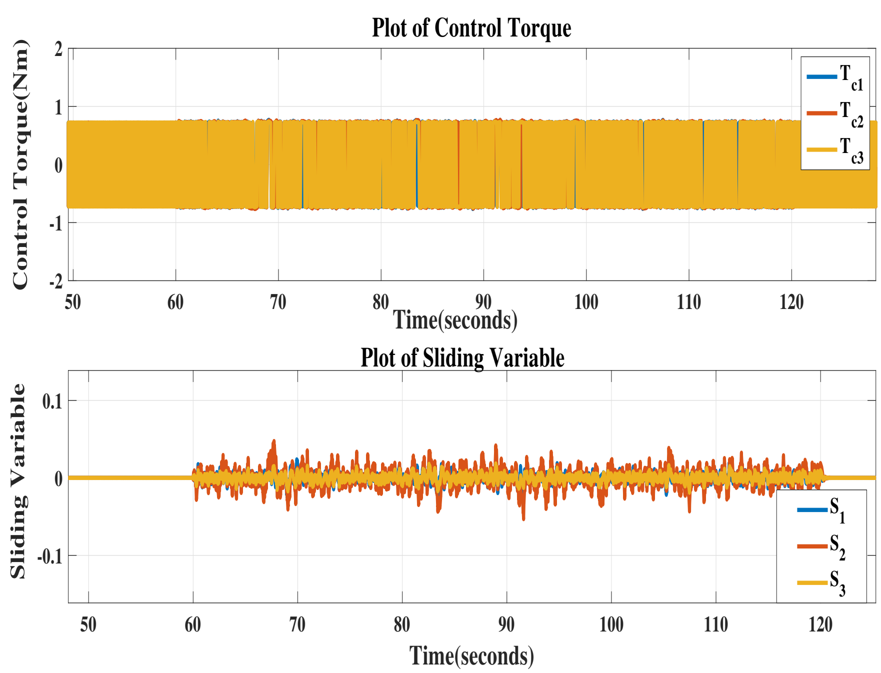

Figure 6.33: Zoomed View of Effect of Disturbance in PD-SMC

Case 3: Simulations with Inertia Matrix Perturbation

To check the robustness of the controller, inertia matrix of satellite is perturbed by 40% and 60% during $t = 50$ sec, as shown in Figure 6.34(a) and 6.34(b). From the simulation results it is observed that the designed PD-SMC is robust against inertia uncertainty.

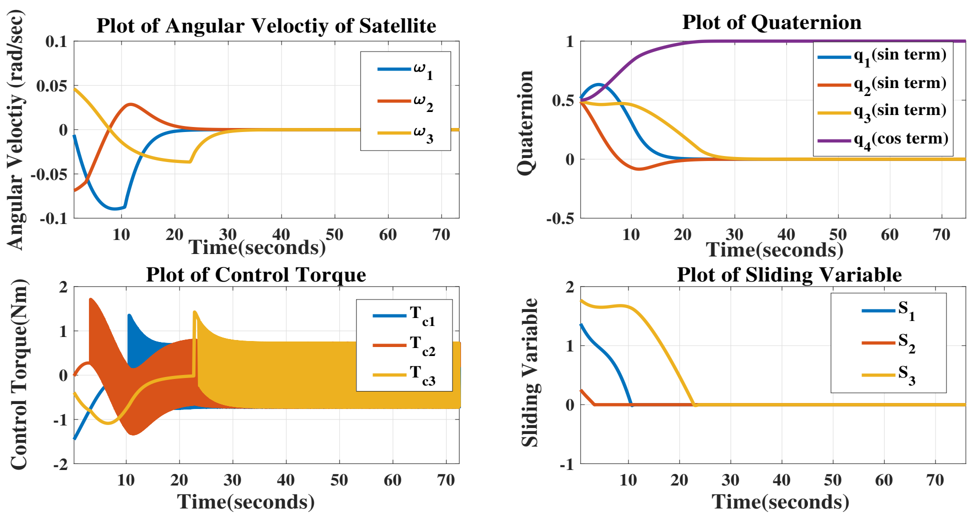

((a)) with 40% Perturbation

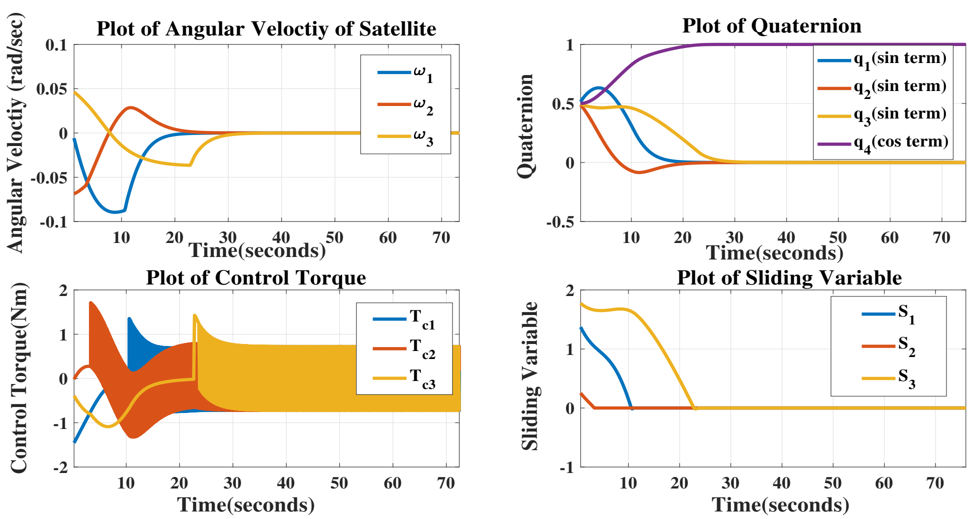

((b)) with 60% Perturbation

Figure 6.34: Responses of PD-SMC in presence of Inertia Matrix Perturbation

Case 4: Simulations with Saturation function

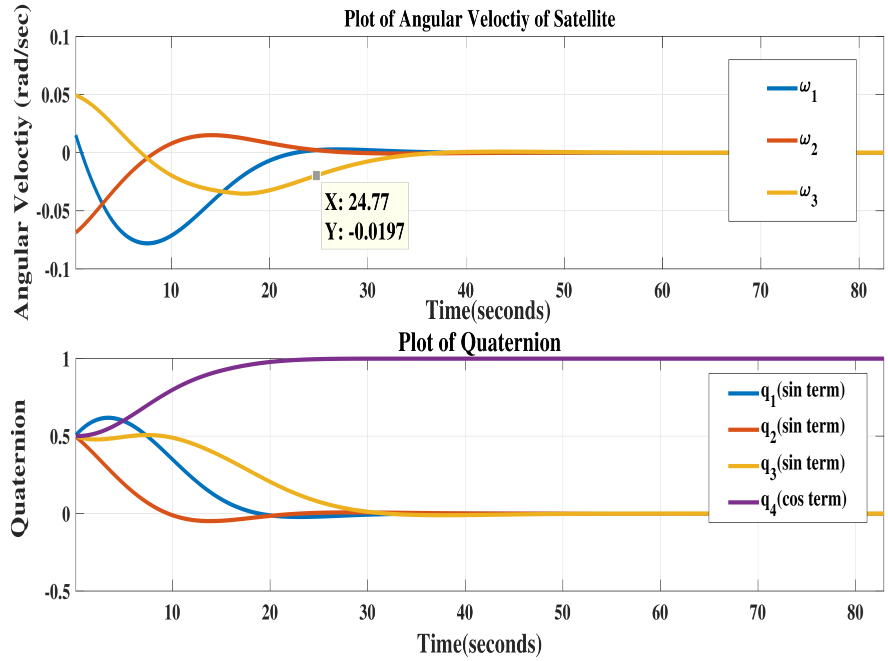

Figure 6.35: Angular Velocity and Quaternion with Saturation Function in PD-SMC

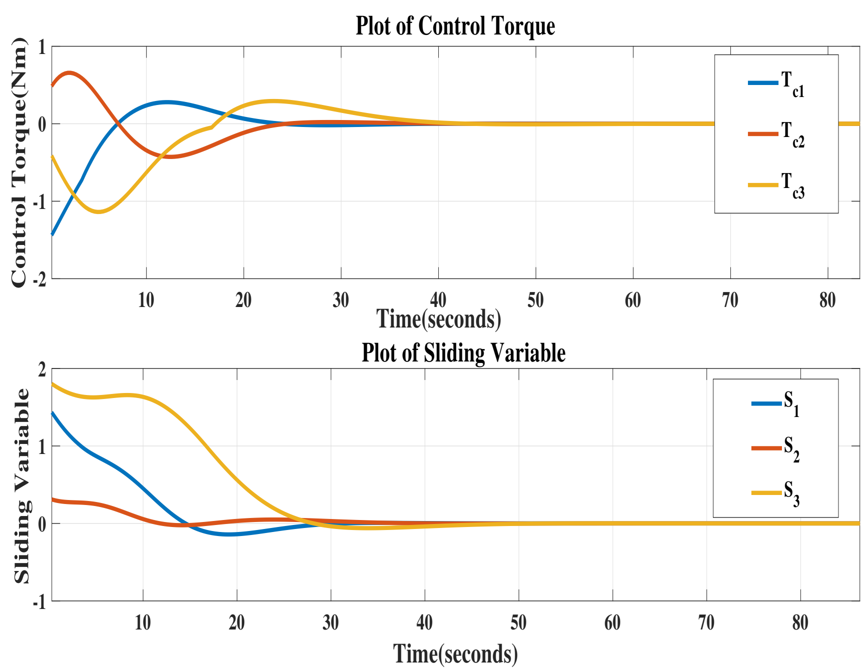

Figure 6.36: Control Torque and Sliding Variable with Saturation Function in PD-SMC

As discussed in chapter 5, signum function(switching operation) causes the high frequency oscillation or chattering in case of SMC based control.

Therefore, to avoid the chattering, the signum function in the control signal is replaced with saturation function and the corresponding results are shown in Figure 6.35 and Figure 6.36. The results shows that the chattering effect is completely eliminated due to the introduction of saturation function.

Case 5 : Simulations with Control Input saturation

Even though chattering is removed by using saturation function, but range of control input to reaction wheel is still beyond the limits of reaction wheel.
To solve that problem, output of controller is saturated(saturation level $\pm$ 1 Nm) before the reaction wheel.

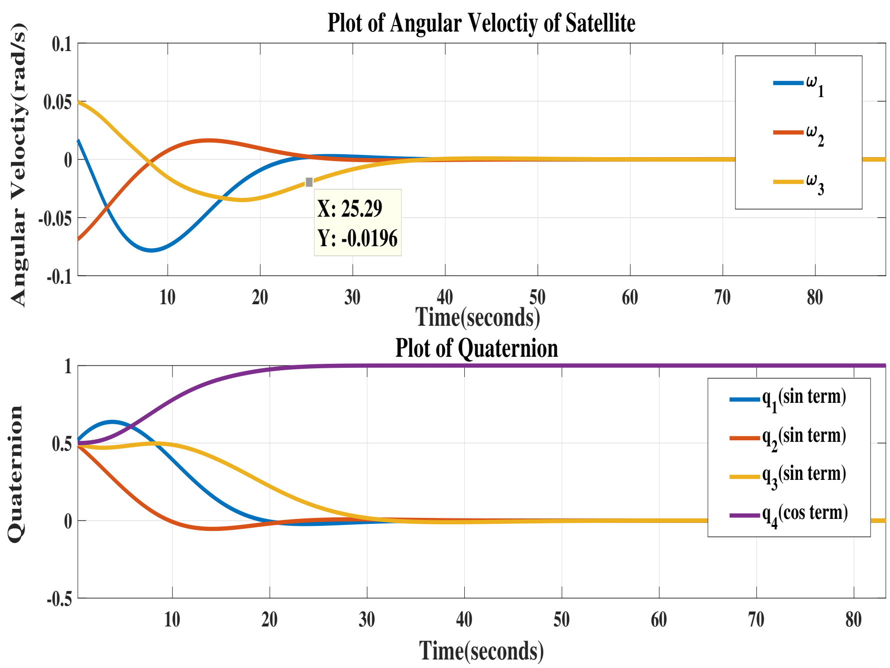

Figure 6.37: Angular Velocity and Quaternion with Control Input Saturation

From the simulation Figure 6.37 to Figure 6.38, it can be noticed that the settling time for the quaternion, angular velocity and control torque increased from 24.36 sec to 25.29 sec due to the introduction of saturation in the control torque.

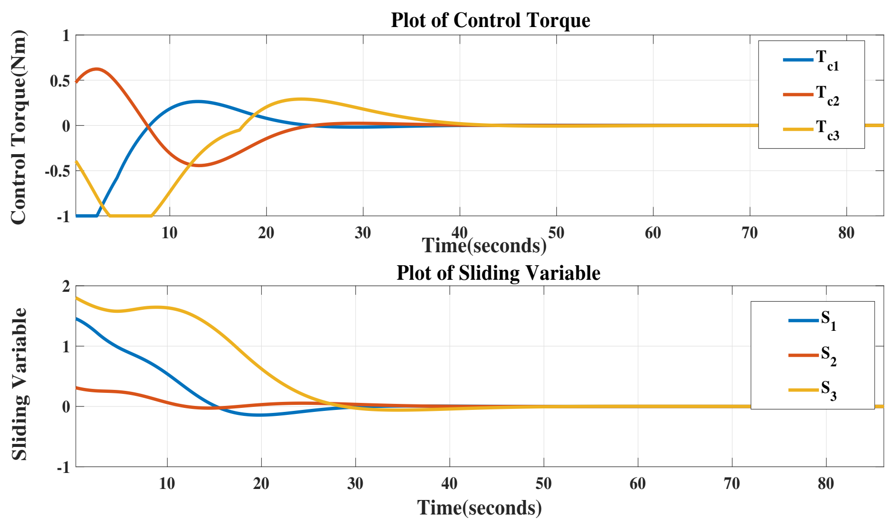

Figure 6.38: Control Torque and Sliding Variable with Control Input Saturation

6.4.2.2 Response of PD-SMC Controller with Modified Reaching Law

As discussed in chapter 5, Chattering effect is expected for SMC based control law. Boundary layer control (for example, saturation function used in this work) is one solution. But disadvantage of boundary layer control is that is reduces robustness property of the controller. Therefore power rate type reaching law is proposed in chapter 5, as an alternative to alleviate chattering.

Parameters	**Value**
Initial quaternion	$[0.5 \;\; 0.5 \;\; 0.5 \;\; 0.5]$
Initial angular velocity	$[0.02 \;\; -0.07 \;\; 0.05]$
Desired quaternion	$[0 \;\; 0 \;\; 0 \;\; 1]$
Desired angular velocity	$[0 \;\; 0 \;\; 0]$
Inertia matrix of the satellite	$diag[50, 75, 100]$
Inertia matrix of reaction wheel	$0.7259 \times 10^{-4} I_{3\times3}$
Time constant of the reaction wheel	$100ms$
Value of K_P	2.53382
Value of K_D	10.304605
Positive scalar, K_m	0.21542

Table 6.6: Parameters for PD-SMC Controller with modified Reaching Law

Case 1: Simulations without Disturbance

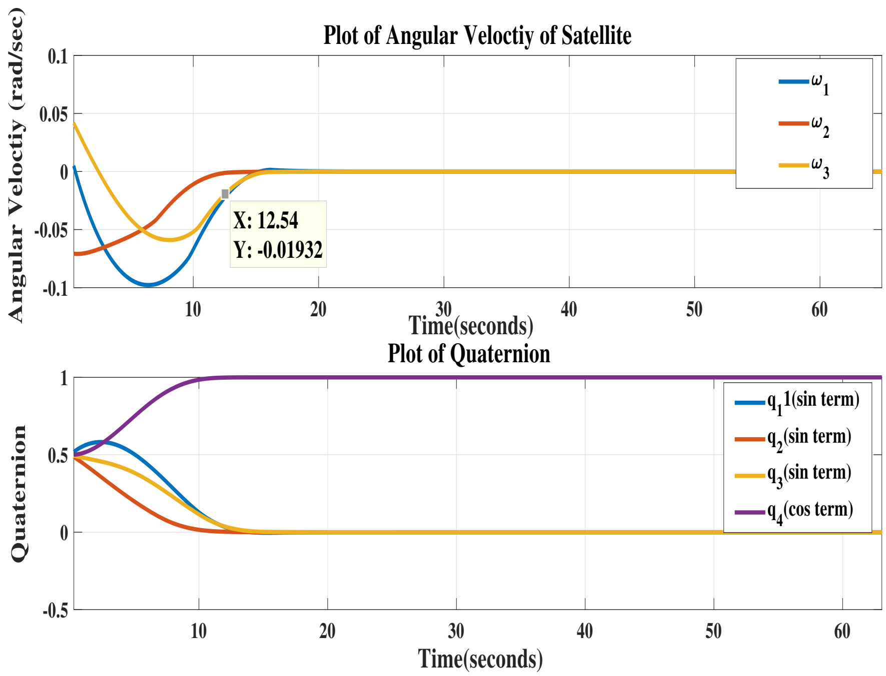

Figure 6.39: Angular Velocity and Quaternion Responses of Modified PD-SMC

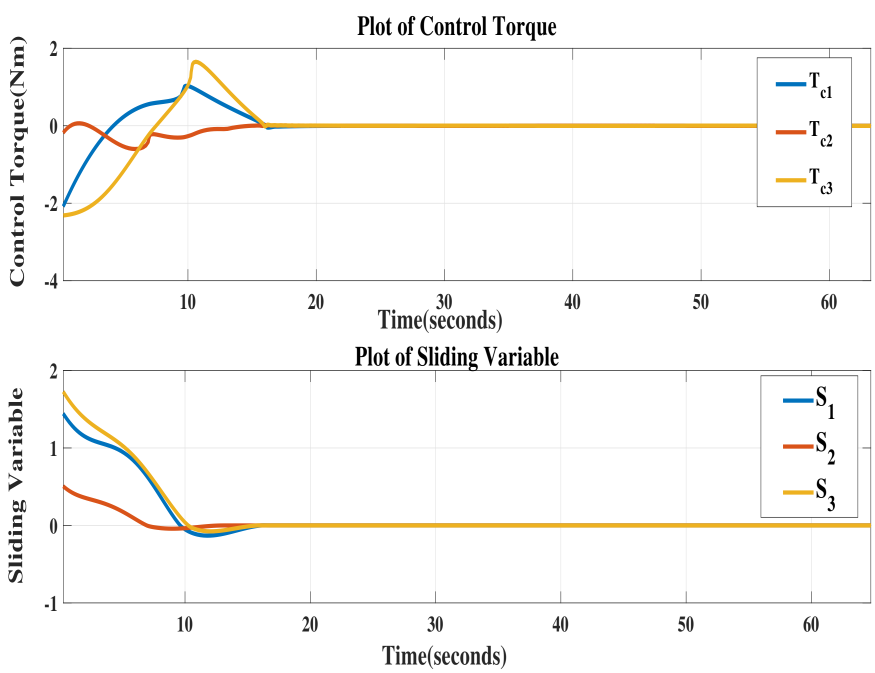

Figure 6.40: Control Torque and Sliding Variable Responses of Modified PD-SMC

The simulation results of PD-sliding mode controller with modified reaching law, is shown in Figure 6.39 and Figure 6.40. The results shows that the desired attitude and angular velocity is attained within 12.54 seconds. Control torque is limited between 2 Nm and -4 Nm. Most importantly, Chattering effect is alleviated, which is the main advantage of this modified control law.

Case 2: Simulations with Disturbance

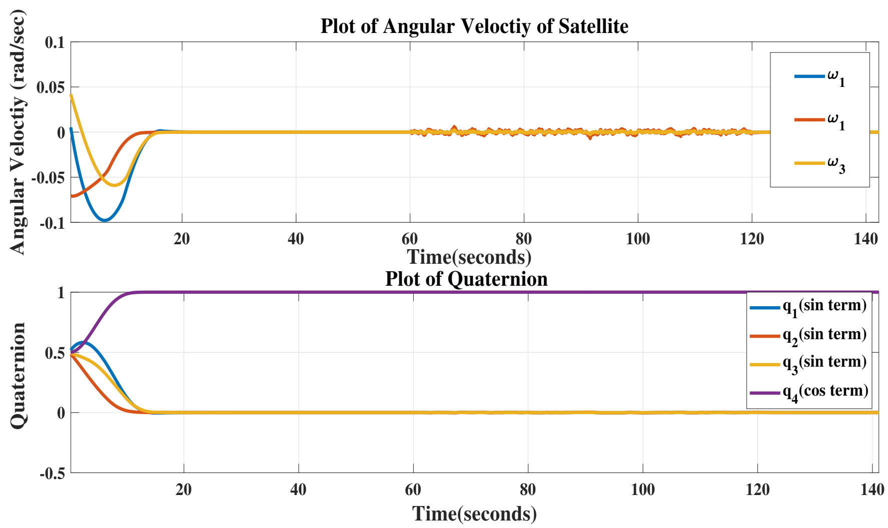

Figure 6.41: Angular Velocity and Quaternion Responses of Modified PD-SMC

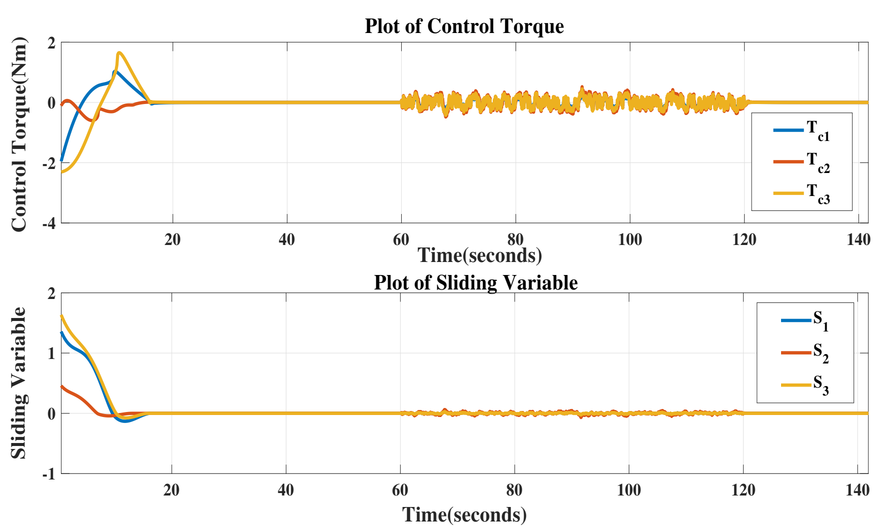

Figure 6.42: Control Torque and Sliding Variable Responses of Modified PD-SMC

A random disturbance is introduced to the system in between 60 sec to 120 sec to check disturbance rejection capability of the system. The simulation results are shown in Figure 6.41 and Figure 6.42. Like PD-SMC, here also the effect of disturbance is negligible in angular velocity and quaternion responses, which proves the disturbance rejection capability of 'PD-SMC with modified reaching law'.

Case 3: Simulations with Inertia Matrix Perturbation

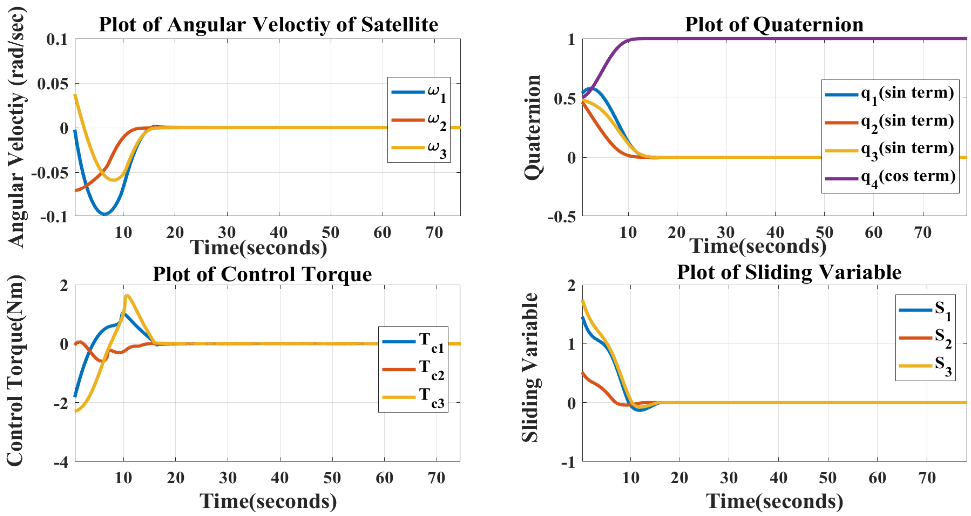

((**a**)) with 40% Perturbation

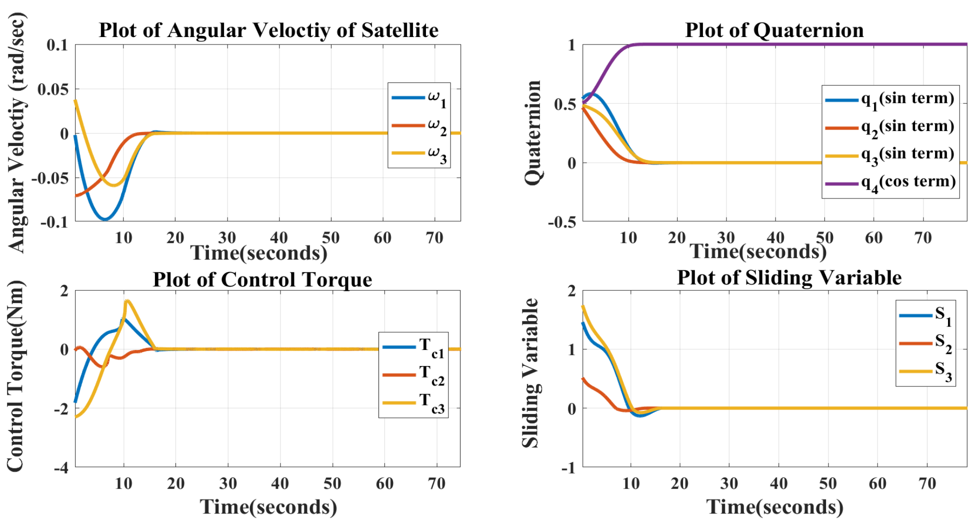

((**b**)) with 60% Perturbation

Figure 6.43: Responses of Modified PD-SMC in presence of Inertia Matrix Perturbation

For the verification the robustness of the controller, inertia matrix of satellite is perturbed by 40% and 60% during $t = 50$ sec, as shown in Figure 6.43(a) and 6.43(b). From the simulation results it is observed that our designed Controller shows robustness property against inertia perturbation.

Case 4 : Simulations with Control Input saturation

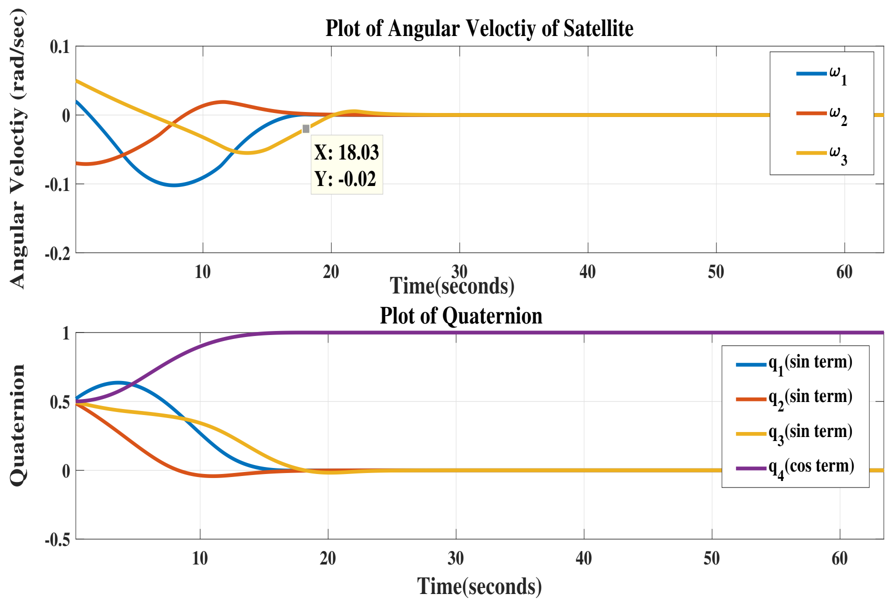

Figure 6.44: Angular Velocity and Quaternion Responses with Modified PD-SMC

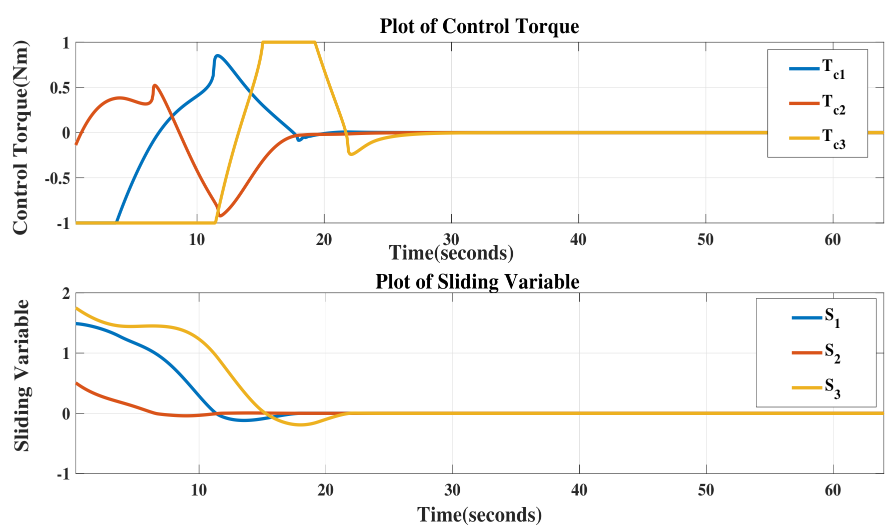

Figure 6.45: Control Torque and Sliding Variable Responses with Modified PD-SMC

In case of Modified PD-SMC, range of control torque signal as seen in Figure 6.40, is beyond the limits of reaction wheel. This problem is solved by saturating(saturation level $\pm$ 1 Nm) the controller output.

From Figure 6.44 to Figure 6.45, it can be observed that, control torque is saturated between $\pm$ 1 Nm but it happens in cost of increment of settling time for the quaternion, angular velocity and control torque from 12.54 sec to 18.03 sec .

- From the discussion of chapter 5 on fractional controller, it can be found that fractional controllers have certain advantages in terms of performance compared to integer order controller.

In the next two sections, fractional controllers (PD^{β}-SMC and PD^{β} -SMC with modified reaching law) responses are discussed, and the results will be finally compared to integer controllers to find out best control algorithm (in terms of performance specifications) for this problem of attitude control of satellite.

6.4.2.3 Response of PD^{β}-SMC

Parameters	**Value**
Initial quaternion	$[0.5 \ \ 0.5 \ \ 0.5 \ \ 0.5]$
Initial angular velocity	$[0.02 \ \ -0.07 \ \ 0.05]$
Desired quaternion	$[0 \ \ 0 \ \ 0 \ \ 1]$
Desired angular velocity	$[0 \ \ 0 \ \ 0]$
Inertia matrix of the satellite	$diag[50, 75, 100]$
Inertia matrix of reaction wheel	$0.7259 \times 10^{-4} I_{3\times3}$
Time constant of the reaction wheel	$100ms$
Value of K_P	2..3811
Value of K_D	22.6834
Value of β	0.001
Positive scalar, K_f	0.6837

Table 6.7: Parameters for $PD^{\beta} - SMC$ Controller

Case 1: Simulations without Disturbance

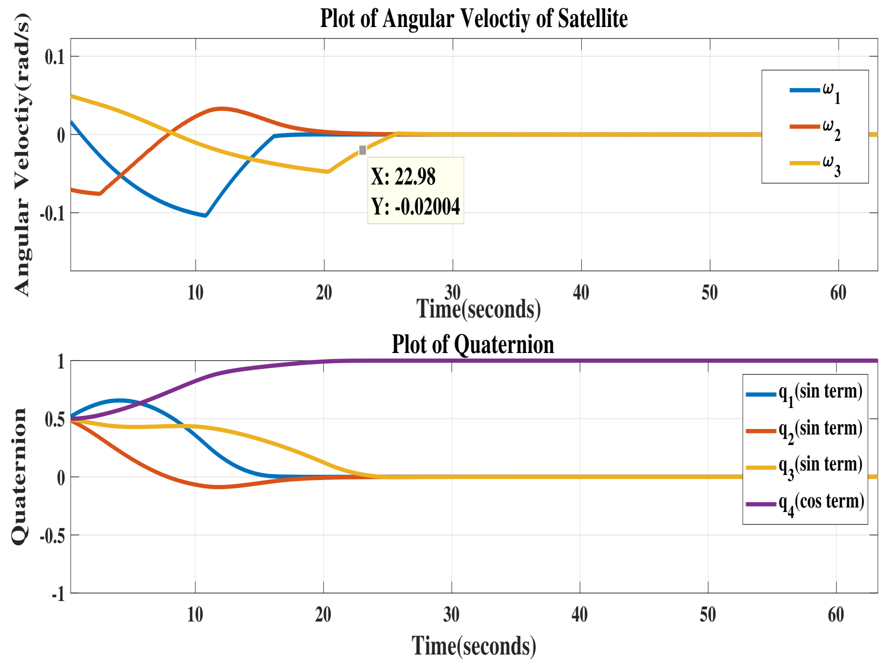

Figure 6.46: Angular Velocity and Quaternion Responses with PD^{β}-SMC

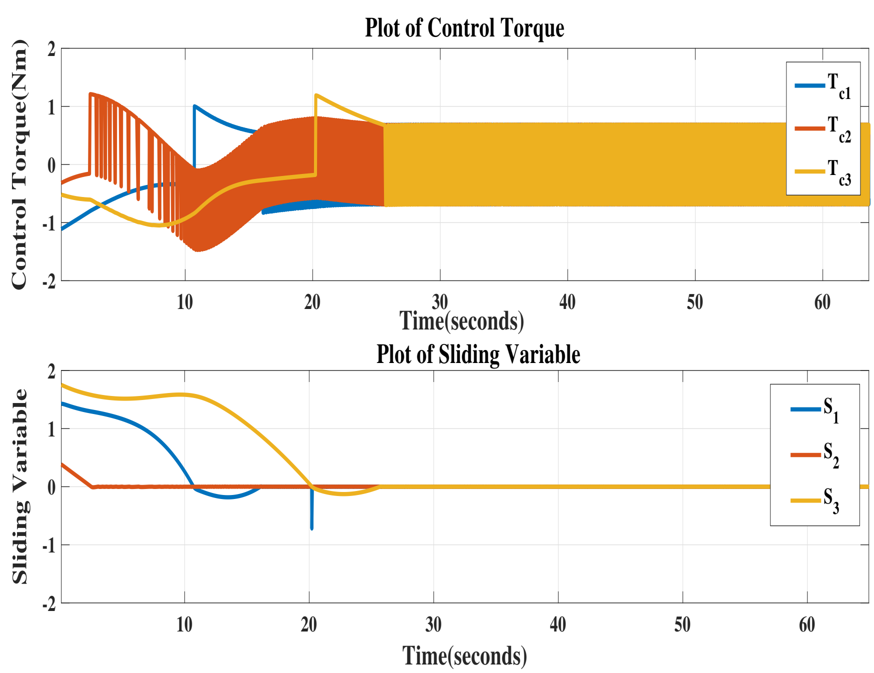

Figure 6.47: Control Torque and Sliding Variable Responses with PD^{β}-SMC

Simulation results of satellite attitude control problem with PD^{β}-sliding mode controller is shown in Figure 6.46 and Figure 6.47. The results shows that the desired attitude and angular velocity is attained within 25 seconds. The control torque required to control the satellite system switches between 1.5 Nm and -1.5 Nm. Like PD-SMC, here also Chattering effect is visible in control torque response. Removal of chattering is discussed later.

Case 2: Simulations with Disturbance

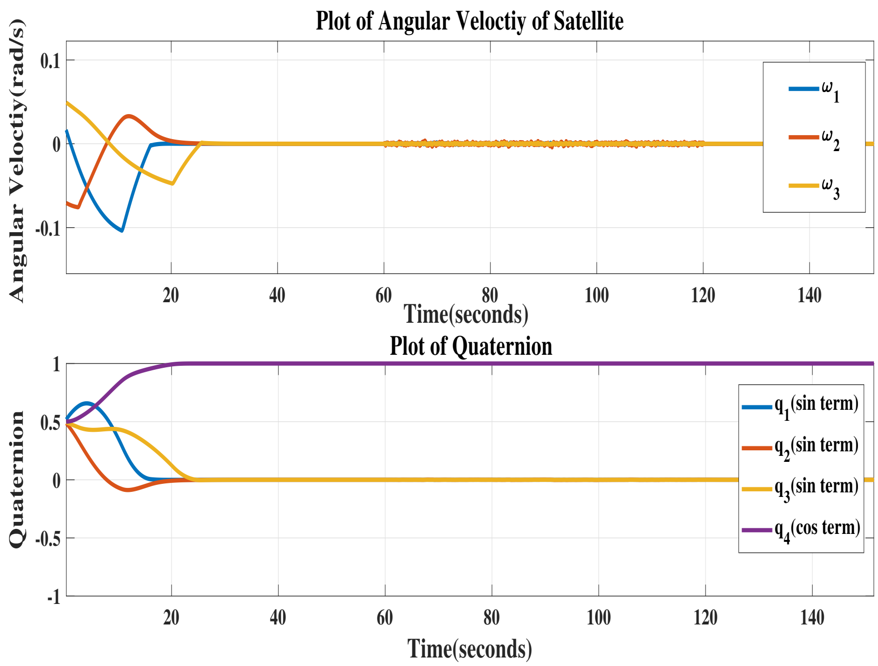

Figure 6.48: Angular Velocity and Quaternion with PD^{β}-SMC in presence of Disturbances

Disturbance rejection capability of PD^{β}-SMC is tested by introducing random disturbance in between 60 sec to 120 sec. The simulation results are shown in Figure 6.48 and Figure 6.49. Disturbance effect is negligible in the quaternion and angular velocity responses. i.e., PD^{β}-SMC has shown good disturbance rejection capability.

The zoomed view of response in presence of disturbance as given in Figure 6.49, is shown in Figure 6.50 and it is observed that the control torque and sliding variable changes their values for stabilization of satellite in presence of disturbance.

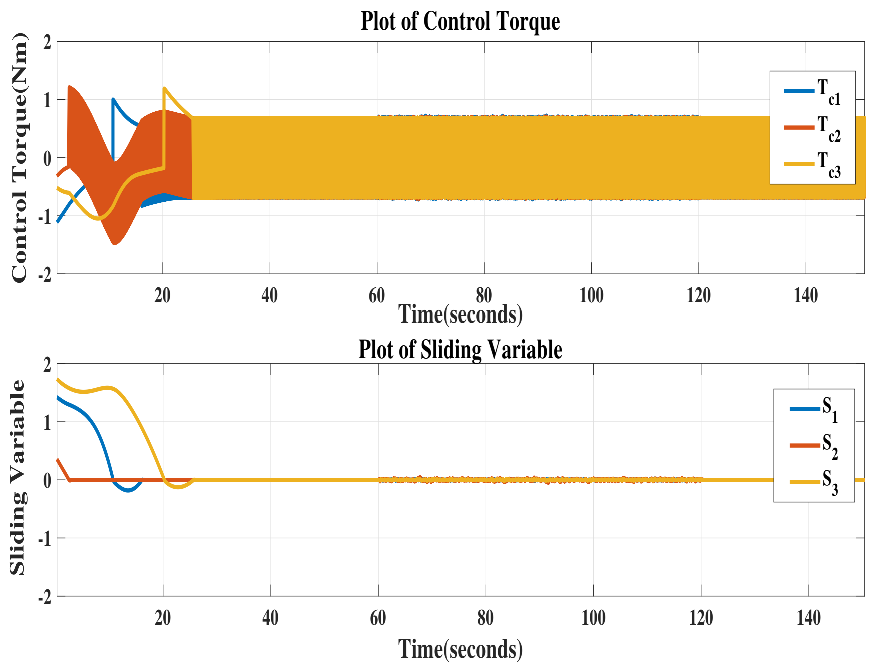

Figure 6.49: Control Torque and Sliding Variable with PD^β-SMC in presence of Disturbances

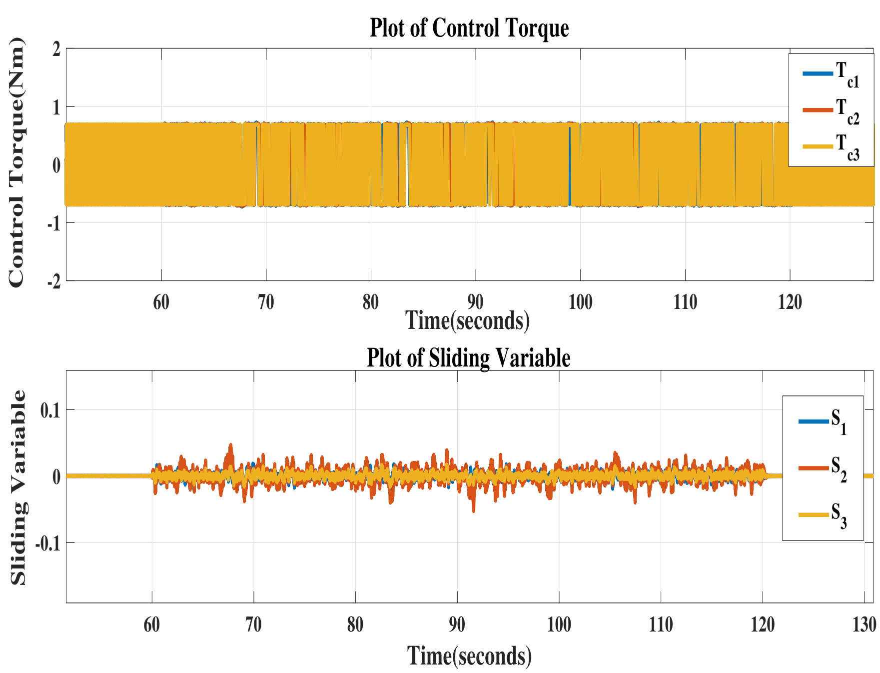

Figure 6.50: Zoomed View of Effect of Disturbance in PD^β-SMC

Case 3: Simulations with Inertia Matrix Perturbation

For checking the robustness property of the controller, inertia matrix of satellite is perturbed by 40% and 60% during $t = 50$ sec, as shown in Figure 6.51(a) and 6.51(b). From the simulation results it is observed that the designed PD^{β}-SMC is robust enough against inertia uncertainty.

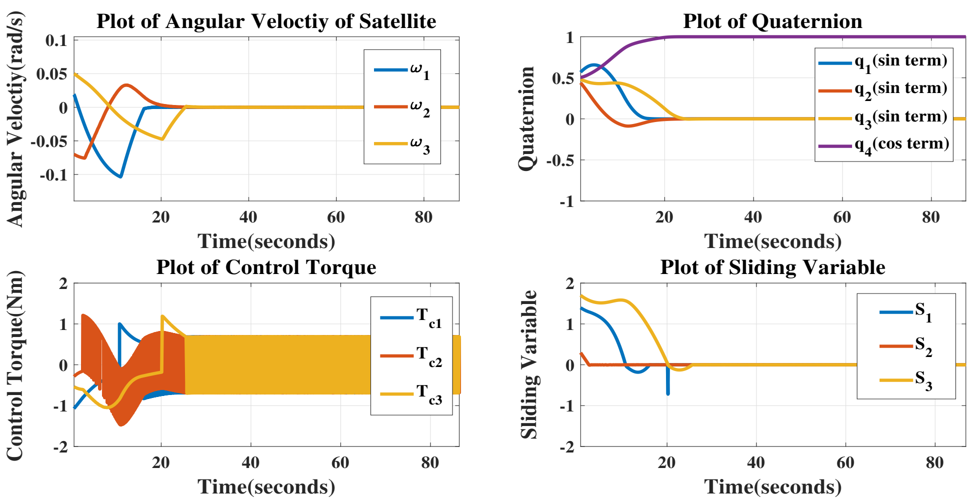

((**a**)) with 40% Perturbation

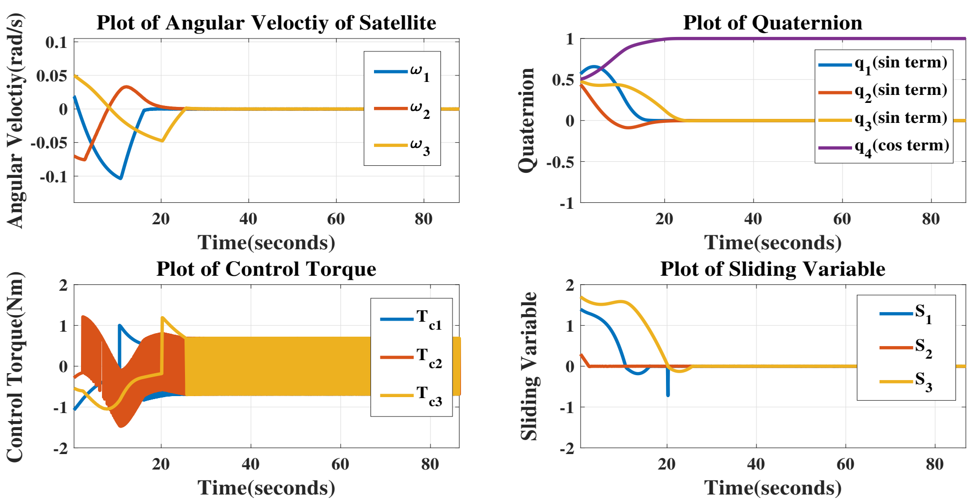

((**b**)) with 60% Perturbation

Figure 6.51: Responses of PD-SMC in presence of Inertia Matrix Perturbation

Case 4: Simulations with Saturation function

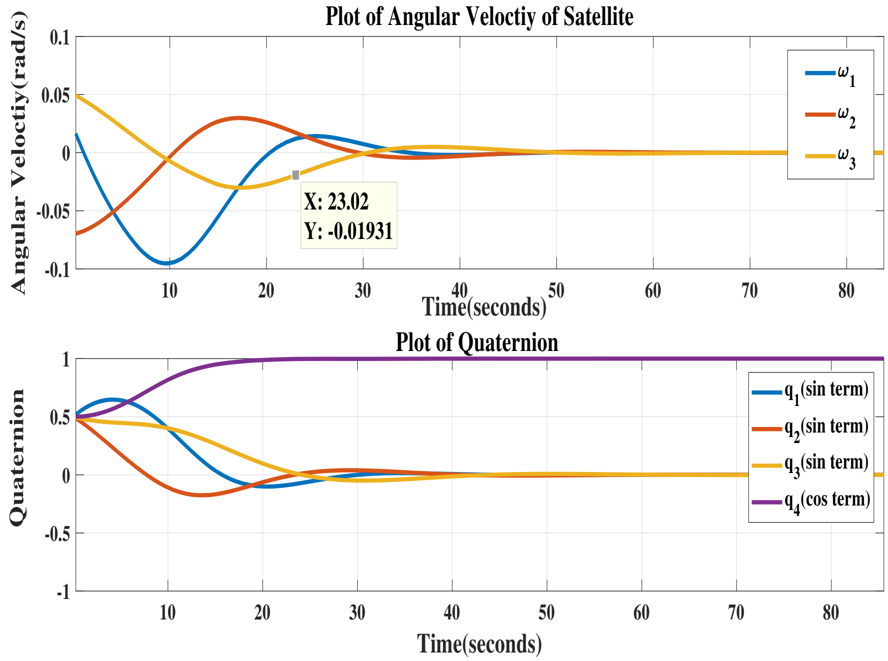

Figure 6.52: Angular Velocity and Quaternion with Saturation Function in PD^{β}-SMC

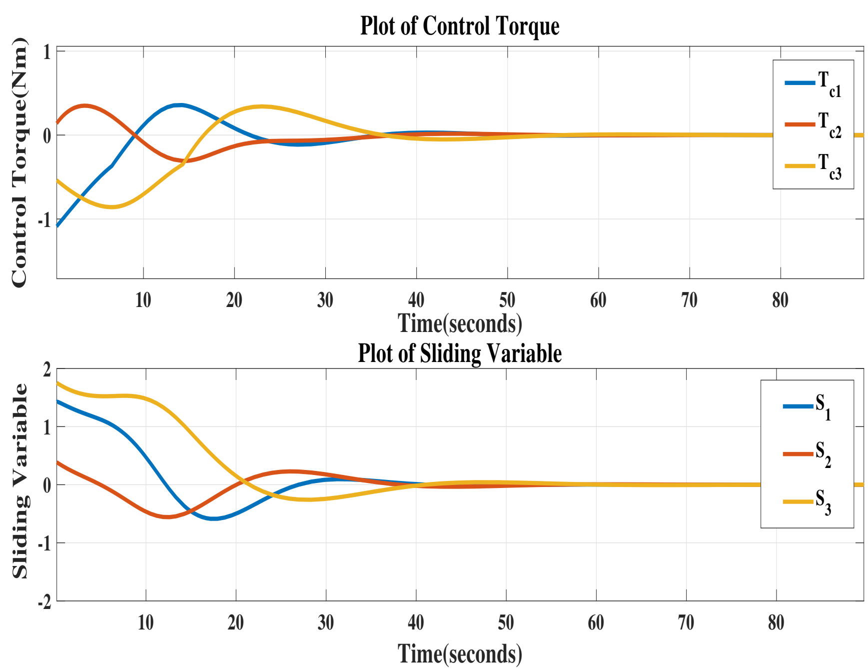

Figure 6.53: Control Torque and Sliding Variable with Saturation Function in PD^{β}-SMC

As signum function (switching operation) causes the high frequency oscillation or chattering, as found in the control torque response of PD^{β}-SMC law.
Hence for chattering avoidance, the signum function used in the control signal is replaced with saturation function and the corresponding results are shown in Figure 6.52 and Figure 6.53. The results shows that the chattering effect is completely eliminated due to the introduction of saturation function.

Case 5 : Simulations with Control Input saturation

Even though chattering is removed by using saturation function, but range of control torque signal is not in the limits of reaction wheel.

Hence, the output of controller is saturated(saturation level $\pm$ 1 Nm) before providng the signal to the reaction wheel.

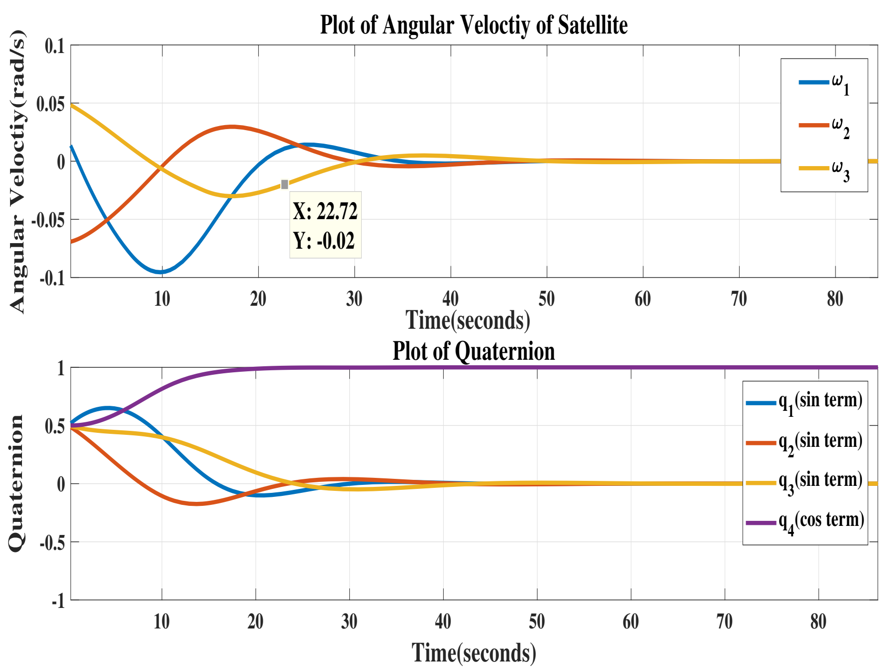

Figure 6.54: Angular Velocity and Quaternion with Control Input Saturation

From the simulation Figure 6.54 to Figure 6.55, it can be noticed that the settling time for the quaternion, angular velocity and control torque has changed to 25.29 sec due to the introduction of saturation in the control torque.

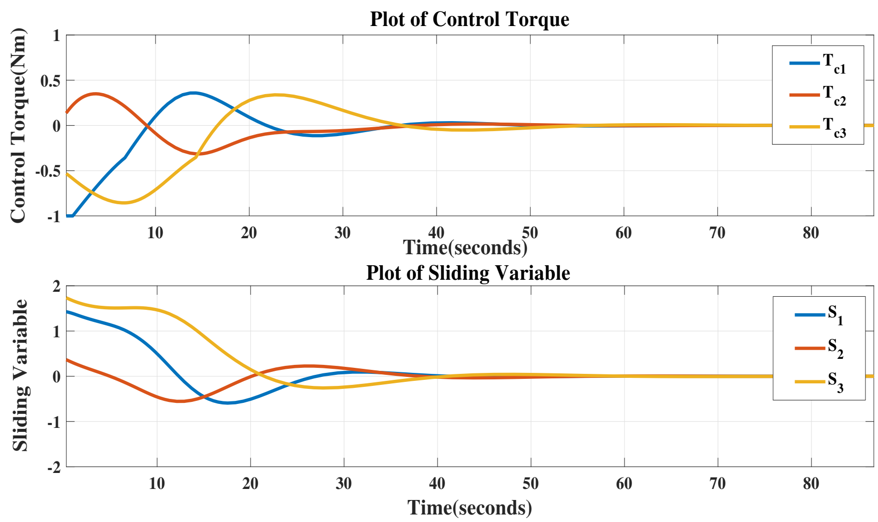

Figure 6.55: Control Torque and Sliding Variable with Control Input Saturation

6.4.2.4 Response of PD^{β}-SMC Controller with Modified Reaching Law

As the boundary layer control (for example, saturation function used in this work) method has the disadvantage of reducing the robustness property of the controller. Hence power rate type reaching law is considered as an alternative to alleviate chattering.

Parameters	**Value**
Initial quaternion	$[0.5 \quad 0.5 \quad 0.5 \quad 0.5]$
Initial angular velocity	$[0.02 \quad -0.07 \;\; 0.05]$
Desired quaternion	$[0 \;\; 0 \;\; 0 \;\; 1]$
Desired angular velocity	$[0 \;\; 0 \;\; 0]$
Inertia matrix of the satellite	$diag[50, 75, 100]$
Inertia matrix of reaction wheel	$0.7259 \times 10^{-4} I_{3\times3}$
Time constant of the reaction wheel	$100ms$
Value of K$_P$	2.2807
Value of K$_D$	25.0744
Value of β	0.001
Positive scalar, K_{mf}	0.5374

Table 6.8: Parameters for PD^{β}-SMC Controller with modified Reaching Law

Case 1: Simulations without Disturbance

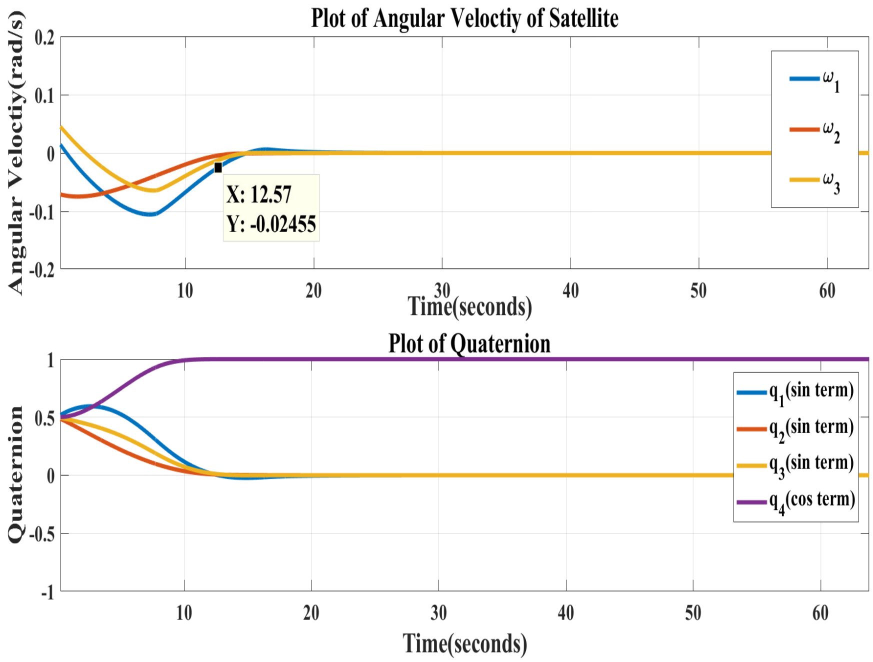

Figure 6.56: Angular Velocity and Quaternion Responses of Modified PD^{β}-SMC

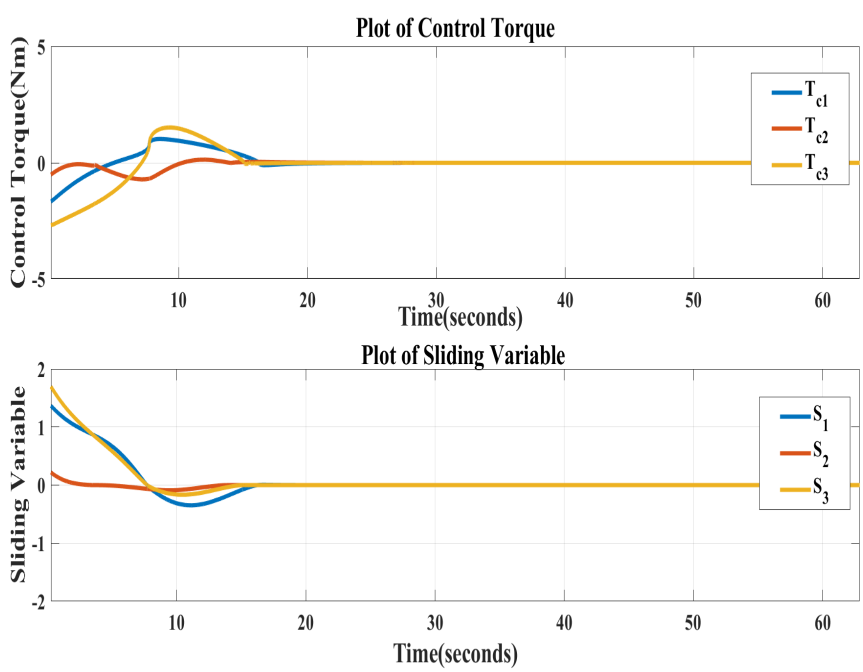

Figure 6.57: Control Torque and Sliding Variable Responses of Modified PD^{β}-SMC

The simulation results of PD^{β}-sliding mode controller with modified reaching law, is shown in Figure 6.56 and Figure 6.57. The results shows that the desired attitude and angular velocity is attained within 12.57 seconds. Most importantly, Chattering problem is solved here.

Case 2: Simulations with Disturbance

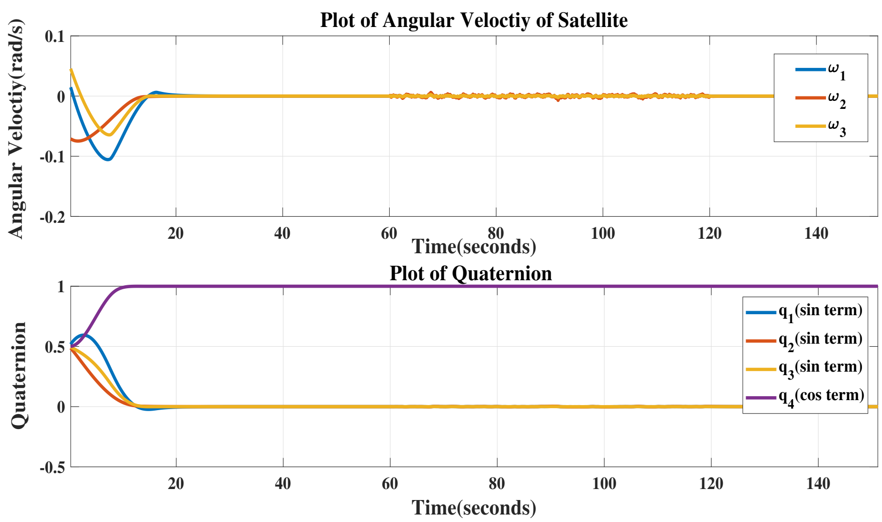

Figure 6.58: Angular Velocity and Quaternion Responses of Modified PD^{β}-SMC

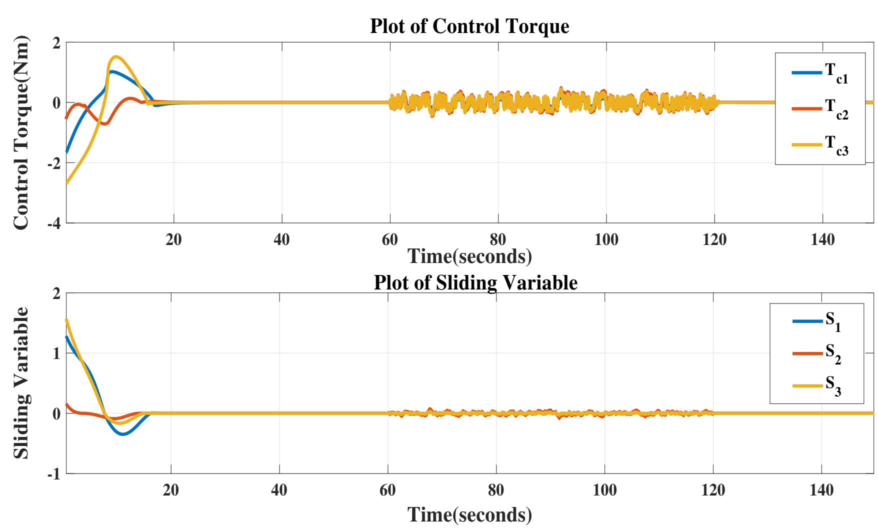

Figure 6.59: Control Torque and Sliding Variable Responses of Modified PD^{β}-SMC

Like all previous controller cases, here also random disturbance is introduced to the system in between 60 sec to 120 sec to check disturbance rejection capability of the system. The simulation results given in Figure 6.58 and Figure 6.59, shows that effect of disturbance is negligible in angular velocity and quaternion responses.

Case 3: Simulations with Inertia Matrix Perturbation

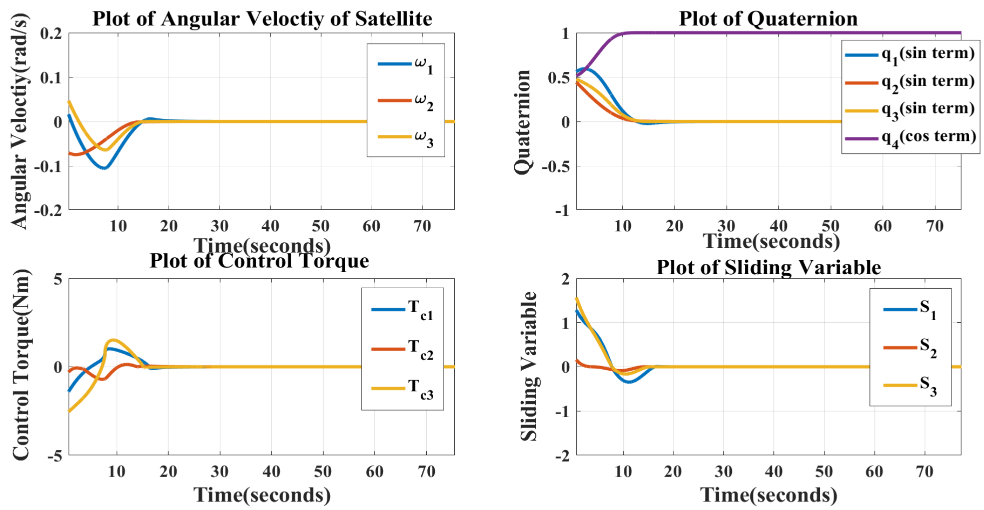

((a)) with 40% Perturbation

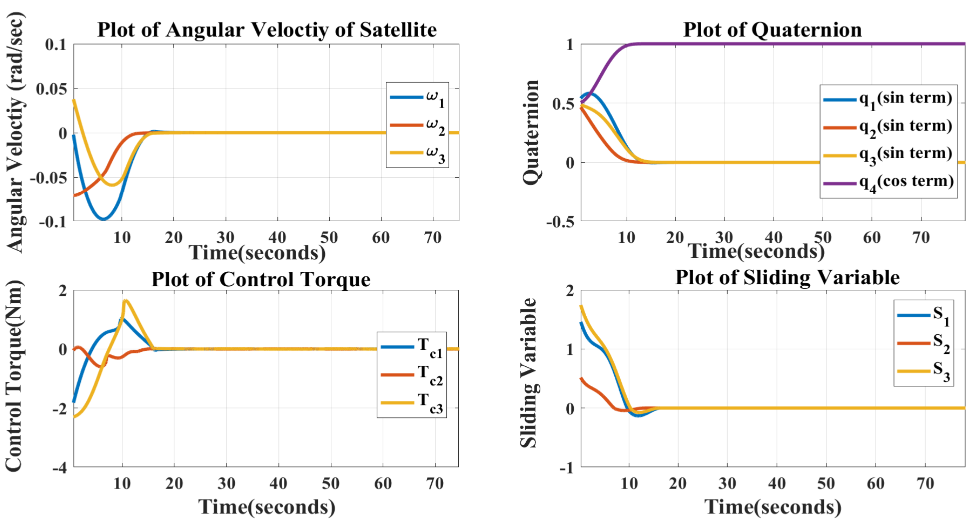

((b)) with 60% Perturbation

Figure 6.60: Responses of Modified PD^{β}-SMC in presence of Inertia Matrix Perturbation

To examine the robustness of the controller, inertia matrix of satellite is perturbed by 40% and 60% during $t = 50$ sec, as shown in Figure 6.60(a) and 6.60(b). From the simulation results it can be concluded that the designed Controller shows robustness property against inertia perturbation.

Case 4 : Simulations with Control Input saturation

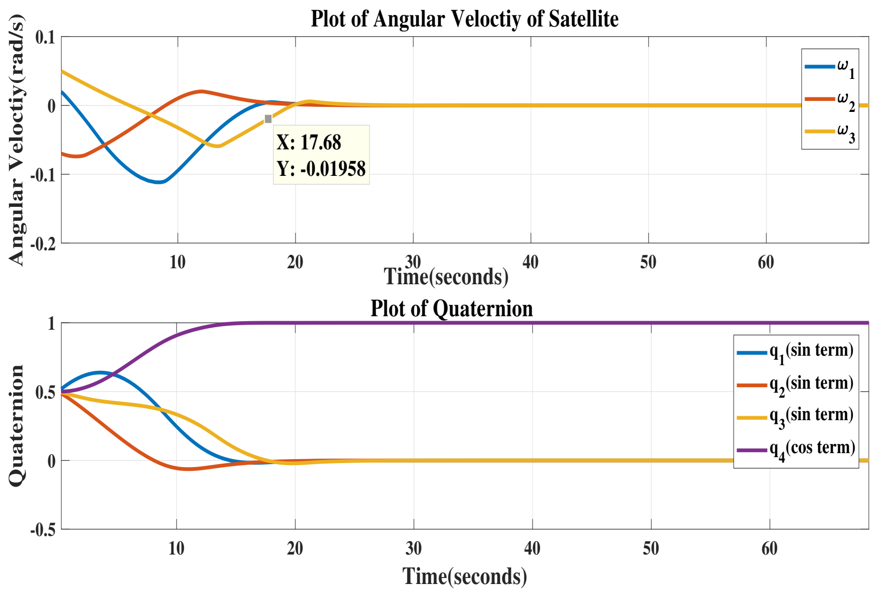

Figure 6.61: Angular Velocity and Quaternion Responses with Modified PD^{β}-SMC

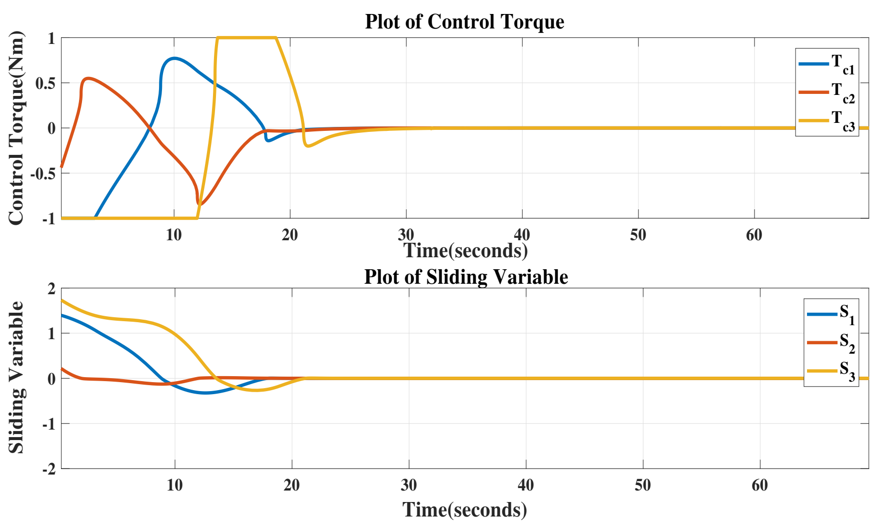

Figure 6.62: Control Torque and Sliding Variable Responses with Modified PD^{β}-SMC

Again in case of Modified PD^{β}-SMC, range of control torque as seen in Figure 6.57, is far above the capability of the reaction wheel. To solve this problem, output of the controller is passed thorugh saturation block with saturation level of $\pm$ 1 Nm.
From Figure 6.61 to Figure 6.62, it can be observed that, controller output torque signal is saturated between $\pm$ 1 Nm but it happens in cost of increment of settling time for the quaternion, angular velocity and control torque from 12.57 second to 17.68 seconds .

6.5 Comparison of different Control Laws

Controller Name	Performance Index				
	$ITAE_{\omega}$	Control Effort	ISE_{ω}	$ITAE_q$	Reaching Time (T_{reach}, in seconds)
Linear Controllers					
PD	7.582	403.1	0.1382	22.657	Not Applicable
PD^{β}	‘18.86	455.7	0.1381	102.81	Not Applicable
Non Linear Controllers					
PD -SMC	21.24	314.4	0.1082	137.27	23.74
PD-SMC modified	11.64	39.18	0.1159	43.639	15.93
PD^{β} SMC	20.96	284.8	0.1216	120.09	23.315
PD^{β} SMC modified	12.230	42.53	0.1214	43.829	15.8

Table 6.9: Comparison of Performance of Different Controllers

For the comparison of controllers, 5 performance indices are considered in this work namely, $ITAE_{\omega}$, Control Effort, ISE_{ω}, $ITAE_q$ and Reaching Time (T_{reach}) [only for non linear controllers case].

Here T_{reach} means the maximum of the reaching time towards sliding surface, among the all 3 axes.

Simulation has been carried out for 200 seconds and performance indices of each controllers have been evaluated respectively.

From table 6.9 it can be noticed that, PD controller has the least $ITAE_\omega$, Control effort and $ITAE_q$ indices in case of linear controllers. Where as, PD^β has the minimum ISE_ω index. Comparing among the non linear controllers, it can be observed that $PD - SMC$ controller with Modified Reaching Law has the least $ITAE_\omega$, Control Effort, $ITAE_q$. Simple PD-SMC law provides the least ISE_ω among all non linear controllers. The reaching phase towards sliding surface is minimum in case of PD^β-SMC controller with Modified Reaching Law.

Controller	$ITAE_\omega$		
	Normal Condition	With Saturation Function	With Control Input Saturation
Linear Controllers			
PD	7.582	Not Applicable	22.05
PD^β	18.86	Not Applicable	29.08
Non Linear Controllers			
PD-SMC	21.24	24.25	25.51
PD-SMC modified	11.64	Not Applicable	18.54
PD^β-SMC	20.96	25.28	35.31
PD^β-SMC modified	12.23	Not Applicable	17.19

Table 6.10: Effect of Control Law Modification on $ITAE_\omega$

Table 6.9 only gives idea of controllers performance under normal condition i.e. without any disturbance or saturation. As discussed earlier, all the controllers proposed in this work have been modified by adding saturation at the output, to restrict the torque signal from controller within the limit of reaction wheel. Also to alleviate chattering effect in case of PD-SMC and PD^β-SMC laws respectively, boundary layer control technique has been implemented by using saturation function instead of signum function. Effect of these modifications over each of these performance indices are investigated from Table 6.10 to 6.14 .

Controller	Control Effort		
	Normal Condition	With Saturation Function	With Control Input Saturation
Linear Controllers			
PD	403.1	Not Applicable	40.03
PD^{β}	455.7	Not Applicable	41.36
Non Linear Controllers			
PD-SMC	314.4	18.37	17.09
PD-SMC modified	39.18	Not Applicable	27.56
PD^{β}-SMC	284.8	14.19	14.06
PD^{β}-SMC modified	42.53	Not Applicable	29.04

Table 6.11: Effect of Control Law Modification on Control Effort

Table 6.10 shows that $ITAE_{\omega}$ increases with saturation of torque input to the reaction wheel and also when signum function is replaced by saturation function for non linear SMC controllers case.

Controller	ISE_{ω}		
	Normal Condition	With Saturation Function	With Control Input Saturation
Linear Controllers			
PD	0.1381	Not Applicable	0.1304
PD^{β}	0.09043	Not Applicable	0.08752
Non Linear Controllers			
PD-SMC	0.1082	0.0915	0.09308
PD-SMC modified	0.1159	Not Applicable	0.1158
PD^{β}-SMC	0.1216	0.1272	0.1273
PD^{β}-SMC modified	0.1214	Not Applicable	0.1265

Table 6.12: Effect of Control Law Modification on ISE_{ω}

Also from Table 6.11 it can be observed that, non linear controllers have reduction in control effort compared to normal condition when saturation function is used instead of signum function. This clearly indicates removal of chattering. Control effort of both linear and non linear controller cases reduce with saturation of control torque input to reaction wheel compared to normal condition.

Table 6.12 shows that ISE_ω reduces with the control input saturation of reaction wheel compared to normal condition for all the controllers except fractional sliding mode controller. An opposite trend is seen in case of fractional sliding mode controller (both $PD^\beta - SMC$ and $PD^\beta - SMC$ with modified reaching law case). In fractional sliding mode case ISE_ω increases for the case when signum function is replaced by saturation function and also when control input of reaction wheel is saturated.

Controller	$ITAE_q$		
	Normal Condition	With Saturation Function	With Control Input Saturation
Linear Controllers			
PD	22.657	Not Applicable	103.428
PD^β	102.81	Not Applicable	102.9
Non Linear Controllers			
PD-SMC	137.27	162.75	175.59
PD-SMC modified	43.639	Not Applicable	76.868
PD^β-SMC	120.09	196.58	196.78
PD^β-SMC modified	43.829	Not Applicable	77.56

Table 6.13: Effect of Control Law Modification on $ITAE_q$

Like $ITAE_\omega$ case, $ITAE_q$ also shows the trend of increment as given in Table 6.13, when control input to the reaction wheel saturated and also in the case when signum function of non linear controller is replaced by saturation function.

Reaching time comparison is done in Table 6.14 and it shows that reaching time increases when control input to reaction wheel is saturated. Also it has been already seen that replacement of signum function by saturation fuction causes reduction of control effort for both PD-SMC and PD^β case. But from the table 6.14 it is clear that replacement of signum function by saturation function leads to increment in reaching time, which directly effects the robustness property of the controllers.

Controller	Reaching Time (T_{reach})		
	Normal Condition	With Saturation Function	With Control Input Saturation
PD-SMC	23.74	44	44.78
PD-SMC modified	15.93	Not Applicable	21.11
PD^{β}-SMC	23.315	54.5	54.607
PD^{β}-SMC modified	15.8	Not Applicable	20.756

Table 6.14: Effect of Control Law Modification on Reaching Time

It is clear that, controller with one of the performance indices as minimum, may not have other performance indices also minimum. For example, Modified PD-SMC controller has the least control effort among all non linear controllers, where as modified PD^{β}-SMC has minimum reaching time among them. Therefore a trade off needs to be maintained when choosing a control law among all the controllers proposed.

6.6 Summary

In this chapter, gain values of both linear (PD, PD^{β}) and non linear (PD-SMC,PD^{β}-SMC and their modified versions) are designed by solving the optimization problems formulated in chapter 4 and 5. Thereafter designed controllers are tested against disturbance condition and inertia matrix perturbation. Based on the requirement, modification in controller (addition of torque saturation or replacement of signum function by saturation function in case of SMC based controllers) has also been carried out in this chapter. Finally results of different controllers are compared on the basis of performance indices chosen. Analysis of the variation of performance indices with modifications of control law is also exercised in this chapter.

Chapter 7

Conclusion & Recommendations

In this work, attitude control system of satellite had been investigated. Various frame of reference and attitude representation schemes were studied. Quaternion based attitude representation was considered from the existing attitude representation methods. Non linear model of satellite was developed, which consists of Kinematics and Dynamics. Reaction wheel had been incorporated as an actuator, with the satellite model. Control algorithms, which were developed in this work include both linear and non linear controllers. PD and PD^{β} were among the linear control laws proposed. Non linear control laws described in this work were sliding mode based. The control laws were: PD Sliding Mode Control (PD-SMC), PD^{β} Sliding Mode Control (PD^{β}-SMC), PD Sliding Mode Control with Modified reaching Law and PD^{β} Sliding Mode Control with Modified Reaching Law.

For the design of linear controllers, linearized model of satellite had been used. Optimization method was applied to tune the parameters of the controller. Frequency domain constraints were used for the optimization purpose. Thereafter designed linear controllers were tested in a non linear satellite model in presence of disturbance, inertia perturbation. Simulation results shows that desired response was achieved by both of the controllers and it was also found that control effort provided by PD controller was less than PD^{β} controller. Both the controllers were found to be robust against 40% 60% parameter variation applied although they showed poor disturbance rejection capability.

Non linear control laws namely PD Sliding Mode Control (PD-SMC), PD^{β} Sliding Mode Control (PD^{β}-SMC), PD Sliding Mode Control with Modified reaching Law and PD^{β} Sliding Mode Control with Modified Reaching Law, were developed to enhance both the disturbance rejection property and robustness towards system parameter uncertainty. Simulation results proves that all the non linear controllers had better disturbance rejection property and robustness towards parameter uncertainty as compared to linear controllers. However chattering effect was present in the responses of PD-SMC and PD^{β}-SMC. To remove chattering, saturation function had been used instead of signum function in the formulation of PD-SMC and PD^{β}-SMC (Boundary layer control technique). Simulation results shows that chattering effect had been completely removed by boundary layer technique but in cost of reduction in robustness, as reaching time had significantly increased when signum function was replaced with saturation function. Power rate type reaching law had been proposed as an alternative solution to the chattering problem . This law had been used in PD-SMC with Modified reaching Law and PD^{β}-SMC with Modified reaching Law and the simulations show that chattering had been completely removed by power rate type reaching laws without effecting the robustness property. Again reduction of chattering ensures reduction in control effort. It can be observed from the simulations of SMC based controllers that control effort provided by controllers with modified reaching law namely PD-SMC with Modified reaching Law and PD^{β}-SMC with Modified reaching Law had been significantly less compared to PD-SMC and PD^{β}-SMC . Comparing various controllers on the basis of performance indices, it was found that PD-SMC with modified reaching law, provided minimum integral time absolute error both in case of angular velocity error and quaternion error (i.e. minimum $ITAE_{\omega}$ and $ITAE_{q}$) . It also provided minimum control effort among all the non linear control laws considered. Minimum integral square error of angular velocity (ISE_{ω}) was achieved by PD-SMC. PD^{β}-SMC with modified reaching law had the the minimum reaching time towards the sliding surface among all the non linear control laws proposed. It indicates PD^{β}-SMC with modified reaching law had shown more robustness compared to other non linear sliding mode based controllers.

Future Work

The present study considered only PD-SMC and PD^{β}-SMC laws. Considering the superiority of $(PD)^{\beta}$ controller over PD^{β} controller, another modification of this work can be $(PD)^{\beta}$ SMC and $(PD)^{\beta}$ SMC with modified reaching law, where $(PD)^{\beta}$ law will be used as sliding surface.

Another improvement of this work can be the development of terminal sliding mode control. While normal sliding mode based control (where sliding surface is linear) assures asymptotic stability where states reaches the origin in infinite time, terminal sliding mode assures convergence in finite time, therefore it is desirable to develop terminal sliding based control for faster convergence of states towards origin. Terminal sliding mode control has two variants: non singular terminal sliding mode and fast terminal sliding mode. Both control laws can be implemented as future work.

Although sliding mode based controllers provide good robustness towards system parameter uncertainty. Robustness can be further enhanced by applying adaptivity in the control law .

Effect of disturbances like solar radiation pressure, gravity effect due to geoid shape of Earth, effect of Earth's magnetic field etc are not considered in this work. But they have significant impact on satellites attitude in practical situation. All these disturbances can be modelled in equation and designed controllers can be tested against these disturbances.

All the above suggestions can be the leading point for future progress on the problem of satellite attitude control.

Bibliography

[1] M. D. Griffin, *Space vehicle design*. Aiaa, 2004.

[2] D. A. Vallado, *Fundamentals of astrodynamics and applications*. Springer Science & Business Media, 2001, vol. 12.

[3] R. Raveendran, "Adavanced control algorithms for satellite attitude control," 2017.

[4] M. J. Sidi, *Spacecraft dynamics and control: a practical engineering approach*. Cambridge university press, 1997, vol. 7.

[5] E. Bekir, *Introduction to modern navigation systems*. World Scientific, 2007.

[6] K. Devika and S. Thomas, "Improved sliding mode controller performance through power rate exponential reaching law," in *2017 Second International Conference on Electrical, Computer and Communication Technologies (ICECCT)*. IEEE, 2017, pp. 1–7.

[7] J. R. Wertz, *Spacecraft attitude determination and control*. Springer Science & Business Media, 2012, vol. 73.

[8] J. B. Kuipers *et al.*, *Quaternions and rotation sequences*. Princeton university press Princeton, 1999, vol. 66.

[9] A. E. Bryson Jr, *Control of spacecraft and aircraft*. Princeton university press, 2015.

[10] S. Vadali, "Variable-structure control of spacecraft large-angle maneuvers," *Journal of Guidance, Control, and Dynamics*, vol. 9, no. 2, pp. 235–239, 1986.

[11] M. Blanke and M. B. Larsen, "Satellite dynamics and control in a quaternion formulation," Technical University of Denmark, Department of Electrical Engineering, Tech. Rep., 2010.

[12] R. Froelich and H. Papapoff, "Reaction wheel attitude control for space vehicles," *IRE Transactions on Automatic Control*, vol. 4, no. 3, pp. 139–149, 1959.

[13] A. Siahpush and J. Gleave, "A brief survey of attitude control systems for small satellites using momentum conceptsm, aiaa 1990," 1988.

[14] D. Hagen, "Spacecraft attitude control: modeling and controller design considering actuator dynamics," *Norway Narvik University College*, vol. 18, no. 4, pp. 73–86, 2006.

[15] T.-V. Chelaru, C. Barbu, and A. Chelaru, "Mathematical model for small satellites, using attitude and rotation angles," *Int. J. Syst. Appl. Eng. Dev, 2011*, vol. 5, no. 4, 2011.

[16] A. Shirazi and A. Mazinan, "Mathematical modeling of spacecraft guidance and control system in 3d space orbit transfer mission," *Computational and Applied Mathematics*, vol. 35, no. 3, pp. 865–879, 2016.

[17] B. D. Anderson and J. B. Moore, *Optimal control: linear quadratic methods*. Courier Corporation, 2007.

[18] W. Kwon and A. Pearson, "A modified quadratic cost problem and feedback stabilization of a linear system," *IEEE Transactions on Automatic Control*, vol. 22, no. 5, pp. 838–842, 1977.

[19] S. Boyd, C. Baratt, and S. Norman, "Linear controller design: limits of performance via convex optimization," *Proceedings of the IEEE*, vol. 78, no. 3, pp. 529–574, 1990.

[20] R. Wisniewski, "Satellite attitude control using only electromagnetic actuation," Ph.D. dissertation, Citeseer, 1996.

[21] Y. Shtessel, C. Edwards, L. Fridman, and A. Levant, *Sliding mode control and observation*. Springer, 2014.

[22] V. I. Utkin, "Sliding mode control design principles and applications to electric drives," *IEEE Transactions on Industrial Electronics*, vol. 40, no. 1, pp. 23–36, 1993.

[23] J. L. Crassidis and F. L. Markley, "Sliding mode control using modified rodrigues parameters," *Journal of Guidance, Control, and Dynamics*, vol. 19, no. 6, pp. 1381–1383, 1996.

[24] Y. P. Chen and S. C. Lo, "Sliding-mode controller design for spacecraft attitude tracking maneuvers," in *1993 American Control Conference*, 1993, pp. 195–196.

[25] C. Pukdeboon and A. S. I. Zinober, "Optimal sliding mode controllers for attitude tracking of spacecraft," in *2009 IEEE Control Applications, (CCA) Intelligent Control, (ISIC)*, 2009, pp. 1708–1713.

[26] J. Liu and X. Wang, *Advanced sliding mode control for mechanical systems: design, analysis and MATLAB simulation*. Springer Science & Business Media, 2012.

[27] B. Bandyopadhyay, S. Janardhanan, and S. K. Spurgeon, "Advances in sliding mode control, springer, 2013."

[28] E. Abdulhamitbilal and E. M. Jafarov, *Design of Sliding Mode Attitude Control for Communication Spacecraft*. INTECH Open Access Publisher, 2012.

[29] Abdulhamitbilal and E. M. Jafarov, "Sliding mode attitude controller design for nonlinear flexible geosynchronous satellite with thrust jets," pp. 221–226, 2008.

[30] "Sliding mode attitude tracking of rigid spacecraft with disturbances," *Journal of the Franklin Institute*, vol. 349, no. 2, pp. 413 – 440, 2012.

[31] S. M. Mirhassani, J. Ahmadian, M. J. Ghorbanian, and M. A. Hassan, "Stability of geostationary flying satellite under combined sliding mode and pid control," in *2013 IEEE Business Engineering and Industrial Applications Colloquium (BEIAC)*, 2013, pp. 115–119.

[32] S. Eshghi and R. Varatharajoo, "Sliding mode control techniques for combined energy and attitude control system," *Applied Mechanics and Materials*, vol. 629, pp. 310–317, 2014.

[33] X. Zheng, X. Jian, D. Wenzheng, and C. Hongjie, "Nonlinear integral sliding mode control for a second order nonlinear system," *Journal of Control Science and Engineering*, vol. 2015, p. 2, 2015.

[34] S. Seshagiri and H. K. Khalil, "On introducing integral action in sliding mode control," in *Proceedings of the 41st IEEE Conference on Decision and Control, 2002.*, vol. 2, 2002, pp. 1473–1478.

[35] İ. Eker and Ş. A. Akınal, "Sliding mode control with integral augmented sliding surface: design and experimental application to an electromechanical system," *Electrical Engineering (Archiv fur Elektrotechnik)*, vol. 90, no. 3, pp. 189–197, 2008.

[36] Z. Chen, B. Cong, and X. Liu, "Robust control of spacecraft eigenaxis maneuver via integral sliding mode," in *2013 25th Chinese Control and Decision Conference (CCDC)*, 2013, pp. 1758–1763.

[37] E. Abdulhamitbilal and E. M. Jafarov, "Performances comparison of linear and sliding mode attitude controllers for flexible spacecraft with reaction wheels," in *International Workshop on Variable Structure Systems, 2006. VSS'06.*, 2006, pp. 351–358.

[38] R. Hull, C. Ham, and R. Johnson, "Systematic design of attitude control systems for a satellite in a circular orbit with guaranteed performance and stability," *in Proc. AIAA/USU Conf. Small Satellite, Logan, UT, Aug. 2000*.

[39] R. Kristiansen and P. J. Nicklasson, "Satellite attitude control by quaternion-based backstepping," in *Proceedings of the 2005, American Control Conference, 2005.*, 2005, pp. 907–912 vol. 2.

[40] D. Xue, Y. Chen, and D. P. Atherton, *Linear feedback control: analysis and design with MATLAB*. SIAM, 2007.

[41] D. Valério, "Introducing fractional sliding mode control," *Proceedings of The Encontro de Jovens Investigadores do LAETA FEUP, 2012*, 2012.

[42] D. Liwei and S. Shenmin, "Attitude control of pico-satellite using flywheel based on fractional order sliding mode," in *Proceedings of 2013 2nd International Conference on Measurement, Information and Control*, vol. 01, 2013, pp. 756–761.

[43] Z. Tianyi, R. Xuemei, and Z. Yao, "A fractional order sliding mode controller design for spacecraft attitude control system," in *2015 34th Chinese Control Conference (CCC)*, 2015, pp. 3379–3382.

[44] A. Kailil, N. Mrani, M. Abid, S. Choukri, M. Touati MLIHA, and N. Elalami, "Fractional regulators for spacecraft attitude stabilization," in *22nd AIAA International Communications Satellite Systems Conference & Exhibit 2004 (ICSSC)*, 2004, p. 3117.

[45] “Fractional order sliding mode control for tethered satellite deployment with disturbances,” *Advances in Space Research*, vol. 59, no. 1, pp. 263 – 273, 2017.

[46] A. Tepljakov, E. Petlenkov, and J. Belikov, “Fomcon: Fractional-order modeling and control toolbox for matlab,” in *Proceedings of the 18th International Conference Mixed Design of Integrated Circuits and Systems - MIXDES 2011*, 2011, pp. 684–689.

[47] C. Yin, Y. Chen, and S.-m. Zhong, “Fractional-order power rate type reaching law for sliding mode control of uncertain nonlinear system,” *IFAC Proceedings Volumes*, vol. 47, no. 3, pp. 5369–5374, 2014.

[48] D. Matignon, “Stability results for fractional differential equations with applications to control processing,” in *Computational engineering in systems applications*, vol. 2. Lille, France, 1996, pp. 963–968.

[49] S. Dadras, S. Dadras, H. Malek, and Y. Chen, “A note on the lyapunov stability of fractional-order nonlinear systems,” in *ASME 2017 International Design Engineering Technical Conferences and Computers and Information in Engineering Conference*. American Society of Mechanical Engineers, 2017, pp. V009T07A033–V009T07A033.

[50] M. Blanke and M. B. Larsen, “Satellite dynamics and control in a quaternion formulation,” 2010.

[51] W. Xinsheng and Z. Huaqiang, “Fractional order controller for satellite attitude control system with pwpf modulator,” in *2015 34th Chinese Control Conference (CCC)*. IEEE, 2015, pp. 5758–5763.

[52] C. A. Monje, Y. Chen, B. M. Vinagre, D. Xue, and V. Feliu-Batlle, *Fractional-order systems and controls: fundamentals and applications*. Springer Science & Business Media, 2010.

[53] C. Edwards and S. Spurgeon, *Sliding mode control: theory and applications*. Crc Press, 1998.

[54] S. H. Strogatz, *Nonlinear Dynamics and Chaos with Student Solutions Manual: With Applications to Physics, Biology, Chemistry, and Engineering*. CRC Press, 2018.

Appendix A

Plagiarism Report

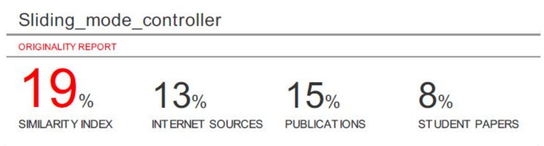
Sliding_mode_controller

ORIGINALITY REPORT

19%	13%	15%	8%
SIMILARITY INDEX	INTERNET SOURCES	PUBLICATIONS	STUDENT PAPERS

Figure A.1: Plagiarism Result

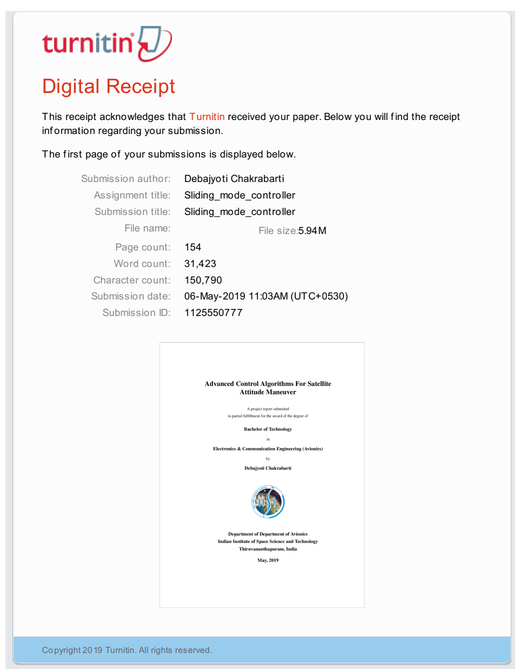
turnitin

Digital Receipt

This receipt acknowledges that Turnitin received your paper. Below you will find the receipt information regarding your submission.

The first page of your submissions is displayed below.

Submission author:	Debajyoti Chakrabarti
Assignment title:	Sliding_mode_controller
Submission title:	Sliding_mode_controller
File name:	File size: 5.94M
Page count:	154
Word count:	31,423
Character count:	150,790
Submission date:	06-May-2019 11:03AM (UTC+0530)
Submission ID:	1125550777

Advanced Control Algorithms For Satellite Attitude Maneuver

A project report submitted
in partial fulfillment for the award of the degree of

Bachelor of Technology

in

Electronics & Communication Engineering (Avionics)

by

Debajyoti Chakrabarti

Department of Department of Avionics
Indian Institute of Space Science and Technology
Thiruvananthapuram, India

May, 2019

Figure A.2: Receipt